VACUUM REFINING MOLTEN STEEL

by

© Ralph Lloyd Harris

A thesis submitted to the Faculty of Graduate Studies and Research in partial fulfilment of the requirements for the degree of Doctor of Philosophy.

Department of Mining and
Metallurgical Engineering,
McGill University,
Montreal,
Canada.

August, 1980.

To

Lisa

and

Troy

But, when we've settled all that, how far ahead are we ?

Henry Lawson.
19th. Century, Australia.

ABSTRACT

Pilot plant scale experiments (15-60 kg melt mass; 1870 - 2020 K; 3 - 16 pascals) have shown that:

(a) 40 to 90 % of initial copper,

(b) 30 to 75 % of initial tin,

(c) 60 to 100 % of initial manganese

and,

(d) 20 to 40 % of initial sulphur

can be eliminated in 30 minutes of vacuum distillation. These elimination rates indicate that refining of scrap steel by vacuum distillation is a viable industrial process.

The elimination rates obtained in this work are considerably better than those of previous pilot plant scale studies. The improvement is due to the higher melt temperatures, cleaner melt surfaces and lesser degree of condensate refluxing of this work.

A theoretical model has been developed to describe vacuum distillation in terms of melt phase mass transport, evaporation at the melt surface and gas phase mass transport. The model predicts that refining of steel will be rapid as long as pressure in the vacuum chamber is less than the total vapour pressure of the liquid surface. Similarly, it predicts negligible rates of elimination at higher chamber pressures.

Both of these predictions are confirmed quantitatively by the experiments and qualitatively by photographs of the vapour flow in the vacuum chamber. They indicate that metal vapour streams rapidly from the melt surface when chamber pressure is less than surface vapour pressure, and that, it flows slowly away at higher chamber pressures.

RESUME

Les expériences précedentes effectuées à grande échelle (15-60 kg de masse fondue; 1870-2020 k; 3-16 Pascals) ont démontré que:

(a) 40 à 90 % du cuivre initial,

(b) 30 à 75 % de l'étain initial,

(c) 60 à 100 % du manganèse initial,

et

(d) 20 à 40 % du soufre initial

peuvent être éliminés en 30 minutes de distillation sous vide. Ces pourcentages d'élimination indiquent que le raffinage de la feraille par distillation sous vide est un procédé industriel efficace.

Les pourcentages d'élimination obtenus dans ce travail, sont considérablement plus élevés que ceux obtenus dans les expériences précédentes. Cette amélioration est attribuée à une température de fusion plus élevée, à une propreté plus grande de la surface du bain de fusion et un degré moindre de reflux condensé pendant l'expérience.

Un modèle théorique a été deéveloppé pour décrire la distillation sous vide en terme de transport de masse en phase

liquide, d'évaporation à la surface du bain de fusion et de transport de masse en phase gazeuse. Le modèle prédit que le raffinage de l'acier sera d'autant plus rapide que la pression de la chambre sous vide sera inférieure à la pression de vapeur totale de la surface liquide du bain de fusion.

D'une façon indentique, il prédit un pourcentage d'élimination négligeable pour une pression plus élevée dans la chambre sous vide.

Ces deux prédictions sont confirmées quantitativement par les expériences et qualitativement par des photographies de l'évaporation dans la chambre sous vide. Ils indiquent que l'évaporation du métal s'effectue rapidement de la surface du bain de fusion lorsque la pression de la chambre sous vide est inférieure à la pression de vapeur de cette surface, et s'effectue lentement pour une plus haute pression de la chambre.

ACKNOWLEDGEMENTS

I extend my deepest thanks to Professor Bill Davenport for his ideas, enthusiasm and most of all his sincerity in his approach to my studies.

I also wish to thank Eric Partelpoeg for his thoughts which, though not always in agreement with my own, were abundant and caused valuable reflection.

All other staff, both technical and academic, of the Department of Metallurgical engineering, McGill University receive my appreciation for making the time I spent with them most enjoyable.

Scholarships from Quebec Iron and Titanium Ltd. and the Horace Young Fellowship, as well as funds from the National Research Council of Canada and McGill University, provided financial assistance and enabled my undertaking these studies.

TABLE OF CONTENTS

CHAPTER ONE

INTRODUCTION

SECTION 1.1 : GENERAL

The steel industry has developed a general goal of reducing energy and resource consumption as a consequence of rising costs of energy and diminishing supplies of raw materials. One means of attaining this goal is by increasing the utilization of scrap steel.

A factor which limits the quantity of steel scrap which can be recycled is the residual element content of the scrap, specifically the levels of copper and tin. The development and implementation of a process which can remove this copper and tin from the steel cycle would fulfil the demands of both producer and consumer by removing an important restriction on the quantity of steel scrap which can be recycled.

It will be shown that one such process is vacuum distillation of melted steel scrap. This process removes copper and tin from the liquid steel and it may provide the key which will unlock the barrier to comprehensive scrap utilization.

SECTION 1.2 : THE THESIS

The first part of this thesis examines the steelmaking cycle with particular emphasis on the recycling of scrap steel. It reviews previous evaluations of potential methods for increasing scrap utilization and concludes that vacuum distillation is the most promising possibility.

Previous vacuum distillation studies are then summarized and a new theoretical model of vacuum distillation of liquid steel is developed.

Experimental measurements of copper, tin, manganese and sulphur elimination rates during vacuum distillation are described and evaluated. A comparison between the predicted theoretical elimination and the experimantally observed vacuum distillation rates is made.

Photographs of metal vapour flow in vacuum, gas bubble eruption under vacuum and violent induction stirring turbulence are presented to give visual meaning to the experiments and the manner in which the photographic observations relate to the theoratical model is discussed.

Finally, future work is suggested and conclusions are formed.

CHAPTER TWO

BACKGROUND

SECTION 2.1. : THE STEEL CYCLE

Figure 2.1.1 shows the flow of iron units around the three major processes and operations which make up the steel cycle. Iron units enter the cycle as pig iron whilst they are bled out in the form of steel which is never recycled, for example, steel that has been used in bridges, dams etc. There exists a relatively fast flow of iron units between the steelworks and fabricators in the form of 'tied' and 'home' scrap. Also, there exists a longer term flow of iron units around the whole production/consumption cycle in the form of 'obsolete' scrap.

Figure 2.1.2 shows typical iron unit flows for 1978 in the U.S.A.(1). It can be seen that 70 million tonnes of pig iron, 30 million tonnes of scrap from the scrap stockpile and 50 million tonnes of home and tied scrap went into steelmaking processes such as open hearth, BOF and electric furnace steelmaking. These operations produced 40 million tonnes of home scrap which was immediately recycled and 110 million tonnes of raw steel which continued on to fabrication.

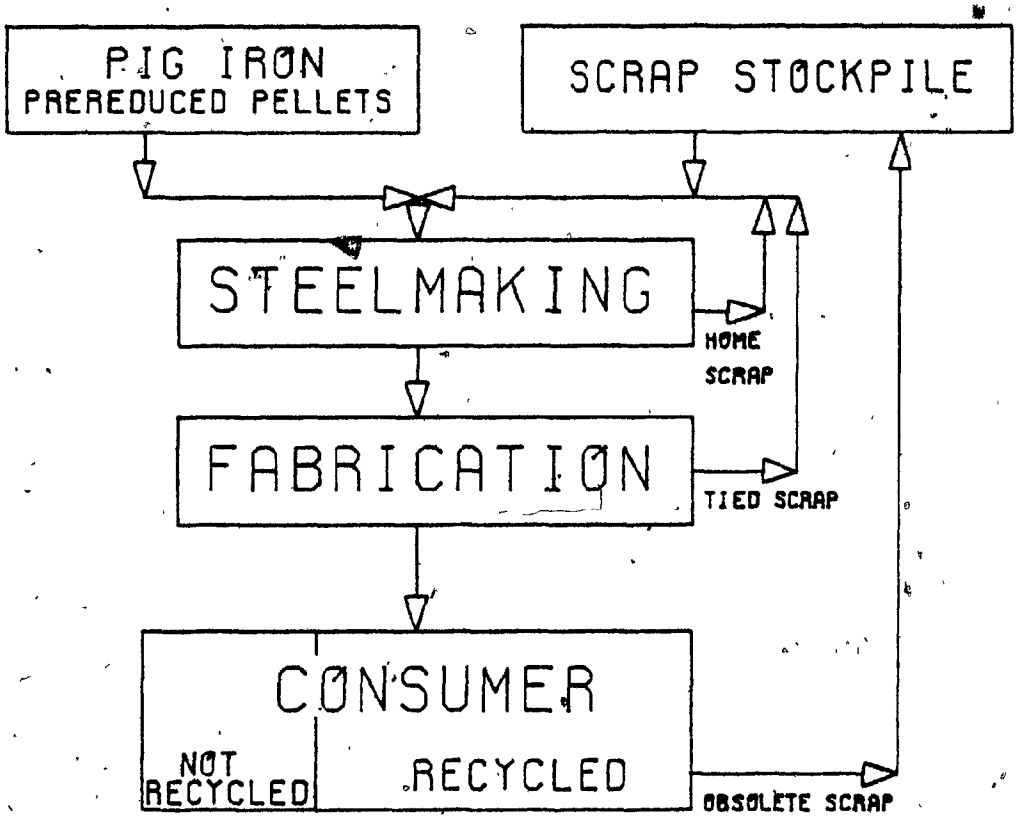

Figure 2.1.1. The steel cycle showing the flow of iron units the steelmaking, product fabrication and consumption operations making up the cycle (1).

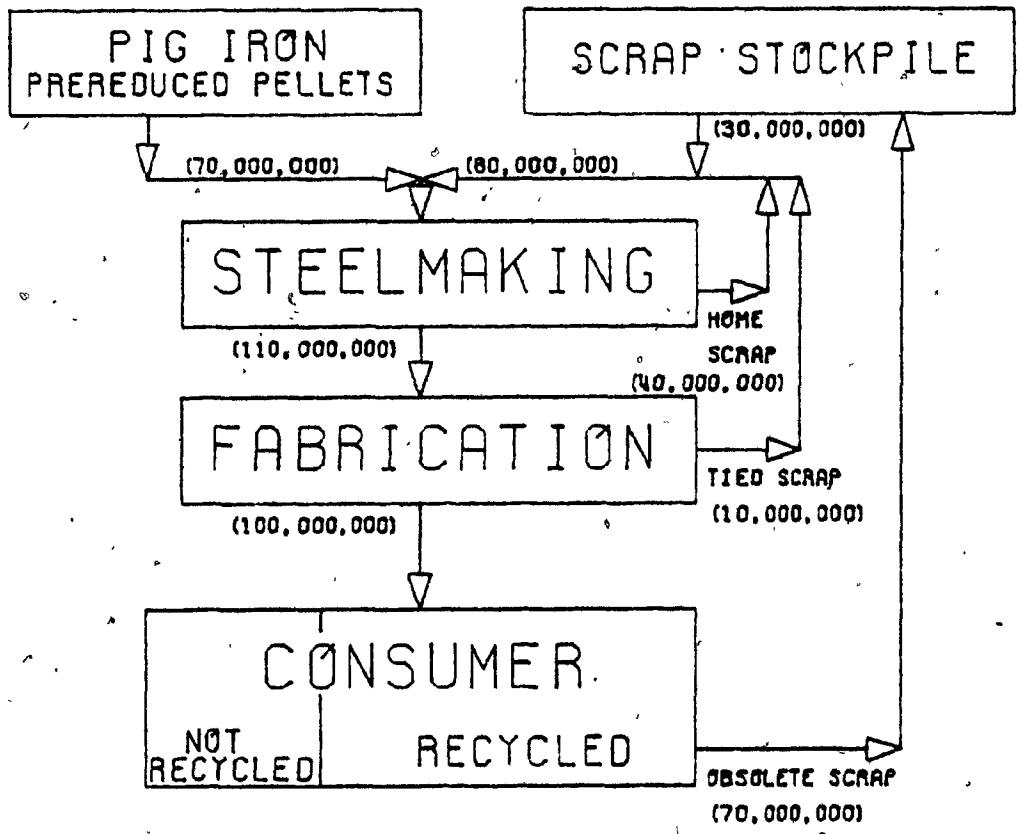

Figure 2.1.2. The iron unit flow cycle showing metric tonnages of iron units flowing between operations and the scrap stockpile. The values are for the United States of America for 1978 (1).

Fabrication methods such as rolling, pressing and punching inadvertently produced 10 million tonnes of tied scrap which was also directly recycled. The remaining 100 million tonnes of finished product went to consumers. About 30 million tonnes of this consumption went into in applications such as bridges, dams, roads and consequently, it is not likely to be recycled in the foreseeable future. The balance of the finished product (70 million tonnes) will find its way onto the scrap stockpile in a relatively small number of years, for example, 10 years for automobiles and 19 years for railroad stock (2). In 1978, the scrap stockpile contained an estiminated 700 million tonnes (1) of iron and from this stockpile 30 million tonnes of selected steel scrap, low in copper and tin, were recycled in that year.

In 1978, 70 million tonnes of pig iron input were balanced by 30 million tonnes not recycled and 40 million tonnes accumulated on the srcap stockpile. It can be seen that for a steady consumption of steel any increase in scrap utilization will directly reduce the pig iron input. Scrap utilization could be increased to 70 million tonnes a year while maintaining a steady level of scrap stockpile. The result would be an equivalent reduction in pig iron consumption. This would contribute significantly towards lowering energy and raw material consumption, and thereby, achieve the general goal of the steel industry. This is shown in table 2.1.1.

	Blast furnace, B.O.F.	Electric furnace
Raw materials consumed, /tonne Fe	1.5 tonnes ore 0.5 tonnes carbon 21×10^3 m^3 blast	1.2 tonnes scrap
Energy required, /tonne Fe	6.4 mJoules	1.3 mJoules
Energy savings, /year	4×10^8 mJoules (mainly in the form of carbon)	

Table 2.1.1. Raw material and Energy requirements for (i) blast furnace - BOF (30% scrap charge) steel making, and (ii), electric furnace (100% scrap charge) steelmaking (3). Estimated yearly energy saving for the U.S.A. is also shown.

SECTION 2.2. : COPPER AND TIN IN STEEL AND SCRAP

Copper and tin enter the steel cycle in fabrication processes which prepare steel for use by consumers. Both elements may be in the form of massive metallic additions (example copper wire and tin solder), in the form of coatings (tin plate), or dissolved in the steel (in high copper corrosion resistant alloys). Table 2.2.1 shows copper and tin concentrations in various types of steel scrap.

ELEMENT	No.1 Heavy Melting Scrap	No.2 Bundle Scrap
Cu	0.06 - 0.36	0.34 - 0.74
Ni	0.02 - 0.13	0.08 - 0.15
Cr	0.0 - 0.05	0.02 - 0.06
Mo	0.01 - 0.05	NA
Sn	0.006 - 0.019	0.0 - 0.14
S	0.021 - 0.054	0.045 - 0.064
Fe	99% +	73 - 84

Figure 2.2.1. Residual element concentration range in two grades of steel scrap (4). No.1 heavy melting scrap is usually home scrap and No.2 bundle scrap is generally purchased obsolete scrap. The latter has a cost of about 1/3 to 1/2 that of No.1 heavy melting scrap.

Once copper and tin enter the steel cycle, they are not eliminated during oxidation steelmaking because of their high oxidation potential with respect to iron. Consequently, they contaminate newly produced steel. This steel is then further contaminated during the fabrication process before being put into service by consumers. At the end of its useful life, most of this steel finds its way to the scrap stockpile and, as a result of the snow-balling effect of recycling, this material as scrap, the copper and tin levels in steel will rise over the years unless corrective action is taken.

To date, the action has been to not recycle poor quality (high Cu, Sn) steel scrap in the United States and Canada. This corrective action has not been used to such a great extent in the United Kingdom due to a less extravagant economy, and, the resultant rise in copper and tin levels in steel products can be seen over the years 1970 to 1974 which are shown in Figure 2.2.1. This figure is testimony to the North American producers containing the situation to date, but as pressure develops in the U.S.A. and Canada to increase scrap utilization, the same increase in residual copper and tin contents will be seen unless new technology is developed which will eliminate copper and tin from the steel cycle.

Another significant point demonstrated by Figure 2.2.1 is, the difference in residual copper content in steel according to the type of furnace in which it was produced. Electric steelmaking furnaces typically use 100% steel scrap charge, and

consequently, the copper concentrations of the steel they produce is appreciably higher than that produced by the open hearth or basic oxygen steelmaking furnaces.

Copper and tin in steel are of great concern. Their presence in steel can cause serious problems of edge and surface cracking due to copper penetrating the grain boundaries during hot rolling of ingot cast steel (8-19). This problem is so severe that it has been given the name 'copper hot shortness'.

In summary, copper and tin are an intrinsic component of today's ferrous scrap, and as a result, methods of eliminating them from the steel cycle need to be developed.

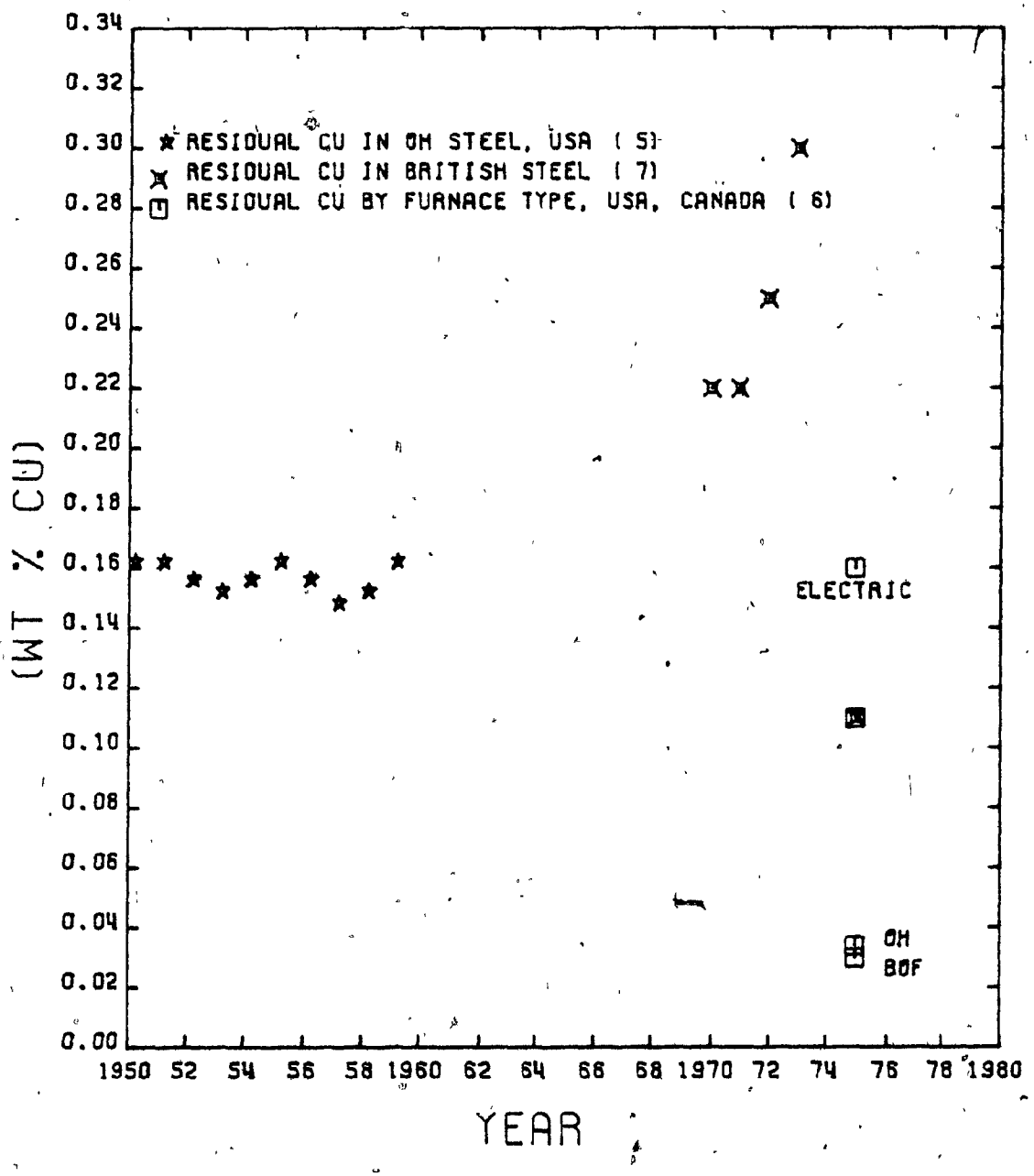

Figure 2.2.1. Residual copper in steel over the last 30 years (5-7). In U.S.A. steels, the residual copper content remained roughly constant in the period 1950 to 1962, whereas, in the period 1970 to 1974 the residual copper in British steel rose dramatically. A low level of low grade scrap utilization is responsible for the U.S.A. experience, and conversely, a high level of low grade scrap utilization was responsible for the experience of the British. In each case, the levels of scrap utilization are a reflection of economic pressures at play in that country.

SECTION 2.3. : PROCESSES FOR REMOVING COPPER AND TIN FROM THE STEEL CYCLE

Massive metallic copper and tin alloys are currently removed from steel scrap by shredding and magnetic separation (20). This method does not eliminate copper and tin which is physically combined with the scrap, either as coatings, or as contaminates dissolved in the scrap steel. A pilot plant study of heating steel scrap to a temperature between the melting point of copper and iron (21) ie., preferential melting overcame the problem of bonded copper and tin. This process used a fused salt bath to heat the scrap and has not been further investigated because (i) the separation was poor and (ii) it does not overcome the problem of dissolved residuals. Any other physical method of scrap processing, such as heavy media separation of shredded scrap automobiles, has the same drawback of not removing impurities dissolved in the steel.

Copper can be eliminated from liquid steel by treatment with sodium sulphate (22,23). Copper in the liquid metal combines with sulphur to form the sulphide, and then, enters the slag while carbon monoxide and sodium vapour are evolved from the melt. Unfortunately, the steel picks up sulphur, the rate of reaction is low and the process does not remove tin. Due to these deficiencies, research on the process was abandoned after extensive investigations in the 1960's.

An alternative process for removing copper and tin from liquid steel is vacuum distillation. In this operation, impure liquid steel is exposed to vacuum which enhances the evaporation of volatile solutes such as copper, tin and manganese. The industrial technology for producing the required vacuum levels exists. The costs of producing the vacuum levels required for vacuum distillation refining are expected to be about the same as those for vacuum degassing.

In summary, this survey of the art reveals that vacuum distillation refining of liquid steel appears to be the only method which has potential industrial application for eliminating copper and tin from the steel cycle. As the previous section indicated that electric furnace steelmaking utilizes the largest amount of low grade scrap, it is concluded that vacuum distillation will find most acceptance with these producers.

CHAPTER THREE

VACUUM DISTILLATION

SECTION 3.1 : INTRODUCTION

Vacuum distillation of liquid steel is a process in which a bath or stream of liquid steel is exposed to vacuum in the range 1 to 15 pascals. Distillation is most rapid (i) at high melt superheats, (ii) when the surface of the liquid steel is clean free from slags or films and (iii) when the vapour which evolves from the melt flows without resistance to condensation sites remote from the liquid metal.

SECTION 3.2 : PREVIOUS STUDIES

Previous studies (24-33) on vacuum distillation of liquid steel have, with one exception, been conducted on systems in which molten steel was contained in crucibles. The one exception was a levitation study of elimination of copper from very small drops (28).

Table 3.2.1 summarizes previous work on vacuum distillation of liquid steel to remove copper and tin. The bench scale studies (21,22,24-27,29) consistently attained sufficiently high elimination rates for the process to be a viable industrial operation. However, the pilot plant scale feasibility studies (23,28,30) showed that vacuum distillation would not be a viable process, because, 90 to 150 minutes were required to eliminate 80% of the copper and tin from the liquid steel. For this reason, the present study was initiated with the goal to discover the causes for these low rates and to investigate means of achieving appreciably higher rates.

The following sections of this chapter comment on previous models which were developed for vacuum distillation of liquid steel. Expressions for maximum rates and for rates of vacuum distillation into imperfect vacuums follow. The last sections present a model for vacuum distillation and a numerical method for its simulation.

Investigator	Year	Chamber Volume m^3	Melt Mass kg	Area/Volume cm^{-1}	Copper concentration Initial %	Copper concentration Final %	Process Time min	% Elimination
Gill[24]	1959	10^{-3}	0.1	0.5	0.32	0.01	90	99
Olette[25]	1961	10^{-3}	0.5	0.1	0.12	0.001	40	100
Ward[26]	1963	1.5	12	0.08	1.0	0.1	120	90
Fischer[27]	1964	10^{-3}	0.03	0.5	0.17	< 0.001	<60	100
Ward[28]	1966	10^{-5}	0.001	5	0.55	0.1	0.2	80
Ohno[29]	1968	10^{-3}	0.15	0.6	1.0	0.1	15	90
Fischer[30]	1974	NA	5	0.11	1.9	0.1	50	95
Salomon De-Friedberg[31]	1976	3	26	0.08	0.5	0.1	150	80
Ohno[32]	1977	10^{-3}	0.15	0.6	2.1	0.3	15	85
Harris[33]	1979	3	22	0.1	2.0	0.1	180	95

Table 3.2.1.A. Summary of previous vacuum distillation studies showing COPPER elimination.

Investigator	Year	Chamber Volume m^3	Melt Mass kg	Area/Volume cm^{-1}	Tin concentration Initial %	Tin concentration Final %	Process Time min	% Elimination
Gill[24]	1959	10^{-3}	0.1	0.5	0.04	0.005	90	90
Olette[25]	1961	10^{-3}	0.5	0.1	0.12	0.001	40	100
Fischer[27]	1964	10^{-3}	0.03	0.5	0.88	0.15	60	85
Ohno[29]	1968	10^{-3}	0.15	0.6	0.95	0.30	15	70

Table 3.2.1.B. Summary of previous vacuum distillation studies showing TIN elimination.

SECTION 3.3. : VACUUM DISTILLATION OF LIQUID STEEL - THEORY

Ward described the transfer of solute atoms from the bulk of liquid steel to a remote condensation site in terms of a six step process (26):

(a) transport of a solute atom through the melt to the neighbourhood of the free metal surface,

(b) transport of the atom across a non-turbulent boundary layer to the free metal surface,

(c) evaporation of the atom,

(d) transport of the atom across a stagnant boundary layer on the gas side of the free metal surface,

(e) transport of the atom through the gas phase to a condensation site,

and

(f) condensation of the atom.

Later work (34) showed that not all of Ward's steps are required to develop a vacuum distillation model. Three steps fully describe the mechanism of vacuum distillation:

(a) transport of a solute atom across a non-turbulent boundary layer in the liquid to the free metal surface,

(b) evaporation of the atom,

and

(c) transport of the atom in the gas phase away from the free metal surface.

SECTION 3.4. : MASS TRANSFER TO THE LIQUID STEEL SURFACE

Machlin (35) modelled mass transfer of solute elements from the bulk melt to the liquid steel surface during vacuum distillation by applying surface renewal theory. Davenport, Wakelin and Bradshaw (36) developed a similar model which also predicted the change in bulk solute concentration with respect to time. The resulting expression for the flux of solute atoms to the surface is:

$$\dot{n}_i'' = (n_{i,b}''' - n_{i,s}''') \cdot \left[\frac{8\ D\ v}{\pi\ r}\right]^{1/2} \qquad \ldots\ 3.1$$

where:

$\dot{n}_i''$ = molar flux of solute atoms of species i to the surface, kgmole/m2.s

n_i''' = concentration of solute element, kgmoles/m3.

b,s = bulk and surface respectively

D = solute diffusion coefficient, m2/s

v = melt surface velocity, m/s

r = melt radius, m.

Use of this expression as part of an overall model for predicting solute elimination requires that D, v and r be known. The melt radius is known or can be quickly measured and the diffusion coefficient, D, is known quite accurately for most metallurgical systems ($\simeq$ 1 x 10**-8 m2/s for metallic solutes in liquid steel (35)).

The velocity of the melt surface, v, is less well known and not easily measured. It has two contributing components, natural convection and induction stirring.

Natural convection is caused by cooling at the crucible walls and by radiation from the melt surface. Any additional contribution to convection caused by cooling due to evaporation at the surface is thought to be insignificant.

Induction stirring gives rise to a radial melt surface velocity. Irons (37) measured this velocity by graphite tracer techniques and found it to be about 0.2 m/s for an induction melting furnace identical to the unit used in the present study. Induction stirring increases as furnace power input increases. Szekely (38), for example, reported a two fold increase in average melt surface velocity with a four fold increase in furnace power input on a 12 tonne inductively stirred melt.

A further component of the melt surface velocity may be due to evaporation of surface active solutes which increases melt surface turbulence, and in turn, alters the magnitude of the surface velocity (39). This effect is also thought to be quite small.

SECTION 3.5. : EVAPORATION

Evaporation is the transition of atoms from the liquid state to the gaseous state. It is the response of the system attempting to attain an equilibrium distribution of atoms between those in the liquid surface and those in the vapour phase above it. The transition from the liquid to the gaseous state is extremely rapid. Consequently, the concentration of atoms in a very thin layer of space immediately above the liquid surface is always very nearly in equilibrium with the liquid surface.

The gaseous atoms in this thin layer have translational velocities and if they are not restricted in any way to this region ie., if there exists a perfect vacuum above the surface, they will flow out of the surface at a rate predicted by the Hertz-Knudsen-Langmuir expression (40-44):

$$\dot{q}_i'' = \frac{q_{i,s}}{V} \cdot \left[\frac{k \cdot T}{2 \cdot \pi \cdot m_i}\right]^{1/2} \quad \ldots\ldots 3.2$$

where:

$\dot{q}_i''$ = atom flux of evaporating species away from the liquid surface, atom/m2.s

(q_i/V) = atom concentration of evaporated species i at the surface, atom/m3

k = boltzman's constant, 1.3805 x 10**-23 joules/atom.K

T = temperatute of the vapour, K

m_i = atom mass, kg/atom

This equation specifies the flux of atoms across a unit plane in space when (i) there is a gas of a particular atomic density on one side of the plane and (ii) a perfect vacuum on the other side of the plane.

In the case of evaporation from a liquid metal surface, the density of the gas in the layer of space immediately adjacent to the liquid metal (below the 'Langmuir plane') is very nearly in equilibrium with the liquid metal. The concentration of this gas can be obtained from measured values of the equilibrium vapour pressure for the system by use of the ideal gas law (45):

$$\frac{q_{i,s}}{V} = \frac{p^{\phi}_{i,s}}{k \cdot T} \qquad \ldots. 3.3$$

where:

(q_i/V) = equilibrium atomic concentration of gaseous species i at the surface, atom/m3

P_i = equilibrium vapour pressure of species i in the surface, pascals

k = Boltzman's constant, 1.3805 x 10**-23 joules/atom.K

T = temperature, K

Combining Equation 3.2 and 3.3, the atom flux from a liquid metal surface into a perfect vacuum is given by the expression:

$$\dot{q}_i'' = p_{i,s}^{\phi} \cdot \left[\frac{1}{2.\pi.m_i.k.T}\right]^{1/2} \quad \ldots. 3.4$$

(where the terms have the meanings defined in the above two equations).

This equation can be rewritten (making its application simpler) in terms of (i) a molar flux of evaporating atoms, (ii) the equilibrium vapour pressure of the pure species and (iii), the molar concentration of the species in the liquid surface, ie.:

$$\dot{n}_i'' = \frac{\gamma_i.P_i^{\phi}.M_b}{\rho_b} \cdot \left[\frac{1}{2.\pi.M_i.R.T}\right]^{1/2} \quad \ldots. 3.5$$

where:

$\dot{n}_i''$ = molar flux of species i evaporating, kgmole/m2.s

n_i''' = molar concentration of species i in the surface, kgmole/m3

γ_i = Raoultian activity coefficient of species i in the liquid surface $\simeq \gamma_i^{\phi}$, the Raoultian activity coefficient at infinite dilution of species i

P_i^{ϕ} = equilibrium vapour pressure of pure species i, pascals

M_b = molar mass of bulk material in the surface $\simeq$ molar mass of iron, $\simeq$ 55.9 kg/kgmole

ρ_b = density of bulk material in the surface $\simeq$ density of liquid iron, $\simeq$ 7.8 x 10**3 kg/m3

M_i = molar mass of evaporating species i, kg/kgmole

R = gas constant, 8.314 x 10**3 joules/kgmole.K

T = temperature, K

This is the form of the Hertz-Knudsen-Langmuir expression as it is usually presented (25,26,29,31-33). It predicts the molar flux of atoms of species i evaporating from a liquid surface; at certain temperature and particular molar concentration of species i in the surface.

SECTION 3.6. : COMBINED LIQUID PHASE TRANSPORT AND EVAPORATION

Equations 3.1 and 3.5 can be combined to give an expression for the rate of vacuum distillation when there is resistance to transport from melt diffusion and evaporation. This overall expression has the form:

$$\dot{n}''_i = K_i \cdot n'''_{i,b} \qquad \ldots\ldots 3.6$$

where:

$\dot{n}''_i$ = total molar flux, kg moles/m2.s

K_i = overall rate constant, m/s

$n'''_{i,b}$ = molar concentration of species i in the bulk liquid phase, kg moles/m3

The overall rate constant as defined by Equation 3.6 can be obtained by combining the rate constants for each step, Equations 3.1 and 3.5 ie.,

$$K_i = \left[\frac{1}{Kl} + \frac{1}{\Psi_i . K2_i} \right]^{-1} \quad \ldots\ldots 3.7$$

where:

K_i = overall rate constant for vacuum distillation, m/s

Kl = melt phase rate constant = $(8Dv/\pi r)^{\frac{1}{2}}$, m/s (Eqn. 3.1)

$K2_i$ = evaporation rate constant = $(1/2\pi M_i RT)^{\frac{1}{2}}$, m/s (Eqn. 3.5)

Ψ_i = constant = $(\gamma_i^{\phi} P_i^{\phi} M_b / \rho_b)$, kg.m2/kgmole.s2

Equation 3.7 can be used to predict the maximum theoretical rate of solute elimination by vacuum distillation. The maximum rate can be attained only when there is no return of atoms to the liquid steel, ie., when the gas space behaves as a perfect vacuum. In practice, vacuum distillation pressure levels are never quite this low, and as a result, there is always some small resistance to atom transport in the gas phase. This is described in the next section.

SECTION 3.7. : EVAPORATION INTO AN IMPERFECT VACUUM

The flow of a gas in a system may be characterized by the frequency of interactions between the gas atoms or molecules. When there is an extremely low probability of atom/atom collisions, the flow is said to be 'molecular' and under such circumstances the atoms move in straight paths until they meet some bounding surface (46). Under these conditions, the maximum rate of distillation should be observed as there is very little chance of atom/atom collisions bouncing atoms back into the liquid.

When there are many atom/atom collisions in the gas, the flow is called 'viscous' and the gas demonstrates characteristics of gases at normal pressures (46). Under these conditions, atom/atom collisions in the vicinity of the liquid can cause atoms to be bounced back into the liquid or they can cause them to coalesce (if they have cooled sufficiently) into tiny droplets which may fall back into the liquid. The return of atoms or very small droplets to the liquid can be envisaged as a gas of a certain pressure over the liquid, ie., a back pressure of the evaporating species.

The flux of atoms back into the liquid can be obtained by applying the Hertz-Knudsen-Langmuir expression. The plane in space is immediately above the liquid surface and the source of atoms is now the gas phase side of the plane. The flux of atoms due to the back pressure is then:

$$\dot{n}''_{i,back} = P_i^{bp} \cdot \left[\frac{1}{2.\pi.M_i.R.T}\right]^{1/2} \quad \ldots\ldots 3.8$$

where all terms have the meanings previously defined.

Consequently the net flux of atoms across this plane in terms of moles is the difference of Equations 3.5 and 3.8, ie.,

$$\dot{n}''_i = (P^{\phi}_{i,s} - P_i^{bp}) \cdot K2_i \quad \ldots\ldots 3.9$$

where:

$\dot{n}''_i$ = net molar flux away from the liquid surface, moles/m2.s

P^{ϕ}_i = equilibrium vapour pressure of species i in the surface, pascals

P_i^{bp} = back pressure of species i at the gas side of the liquid surface, pascals

$K2_i$ = evaporation rate constant, m/s

Equation 3.9 is the form of the equation previously presented (29,31-33) and it can be applied to all evaporating species in the liquid metal surface.

In real terms, Equation 3.9 predicts a flux of vapour across the Langmuir plane away from the liquid surface whenever the back pressure is less than the equilibrium vapour pressure of the surface. The back pressure of a particular species is the result of the inability of the evaporated atoms of that

species to move away from the liquid metal surface, ie., gas phase mass transport resistance.

The next section examines the concentration profiles of the atoms present in the gas space above the melt surface. It also develops a quantitative model for predicting the flux of the evaporating species away from the melt surface.

SECTION 3.8. : GAS PHASE MASS TRANSPORT

Mass transport across the gas space during vacuum distillation involves convective flow and diffusion of the various species present in the vacuum chamber. Figure 3.8.1 schematically depicts the concentration profiles of the metallic vapours evolving from the melt as well as that for argon which is assumed to be the only non-condensible species present in the chamber.

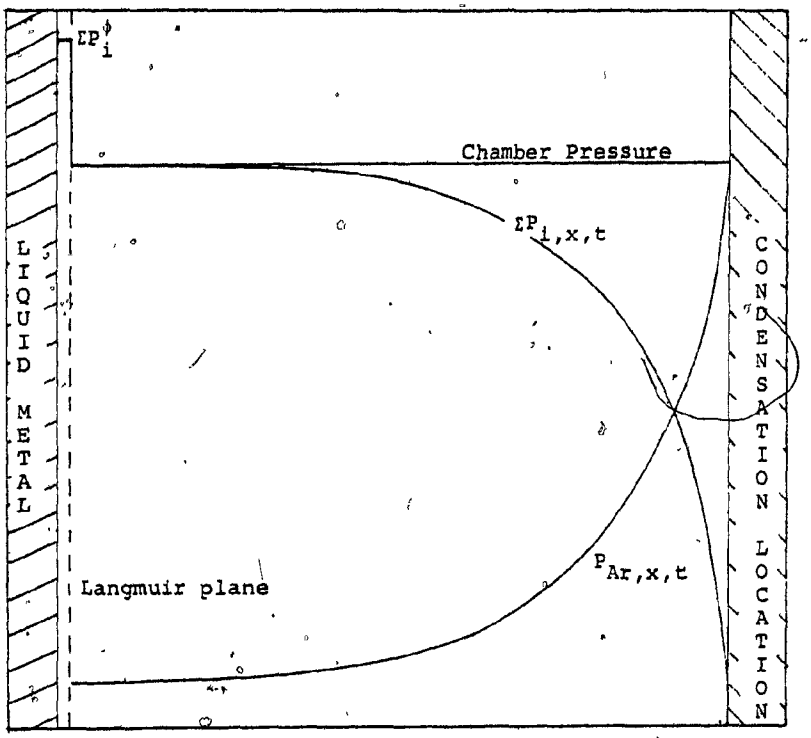

Figure 3.8.1. Schematic diagram of vapour pressures in the region between the liquid metal surface and the condensation site. Pressure profiles for both the evaporating vapour and argon are drawn. They demonstrate the very low value for the argon pressure at the liquid surface. At chamber pressures less than the total equilibrium partial pressure, there is a bulk flow of evaporating vapour away from the liquid surface towards the condensation site.

To obtain an expression for the fluxes of the various vapour species across the gas space, it is necessary to make five assumptions and to establish the boundary conditions for the system. The asumptions are: (i) the cross-sectional area of the gas space is constant and equal to the surface area of the liquid metal, (ii) the temperature throughout the gas space is uniform and equal to the melt temperature, (iii) all evaporated atoms which reach the condensation location condense immediately, (iv) the total pressure is roughly constant

everywhere above the Langmuir plane (Section 3.7) and (v) there is no consumption or generation of vapour species in the gas space.

The first assumption is made to place a simplifying constraint on the geometry of the system. The second assumption enables cooling of the vapour to be neglected until it reaches the condensation location, at which point, the evaporated vapours cool and condense, from assumption (iii). The fourth assumption is valid because, in systems having large dimensions (for example 2 m as in the present case), and operating at pressures in the range of the present experiments (ie., 3 to 100,000 pascals) there is no possibility of pressure gradients within the chamber. The final assumption implies that all evaporation takes place at the liquid surface, and that, all condensation takes place at the condensation site.,

The boundary conditions for argon are (i) at x = s, (the condensation location) the pressure of argon is equal to the total chamber pressure (from the third and fourth assumptions) at all time, and (ii), at x = 0, the flux of argon is zero at all time because the argon is insoluble in liquid steel.

Fick's first law (47) can be used to express the value of various fluxes in terms of diffusion and convection of the atoms present at a given position and time. For the case of argon, Fick's first law is:

$$\dot{n}''_{Ar,x,t} = \frac{-D}{R.T} \cdot \frac{\partial P_{Ar,x,t}}{\partial x} + \frac{v}{R.T} \cdot P_{Ar,x,t} \quad \ldots\ 3.10$$

where:

$\dot{n}''_{Ar,x,t}$	=	flux of argon in the gas space, kgmole/m2.s
D	=	diffusion coefficient of argon in metal vapour, m2/s
$\delta P_{Ar,x,t}/\delta x$	=	pressure gradient of argon, pascals/m
v	=	velocity of bulk flow, m/s
R	=	gas constant, 8.314 x 10**3 joules/kgmole.K
T	=	temperature, K
t	=	elapsed vacuum exposure time, seconds

Equation 3.10 may be substituted into the equation of continuity (48a) to give the relationship between the flux of argon at a particular point and the accumulation of argon at that same point, ie.:

$$\frac{-\partial\left[\frac{-D}{R.T} \cdot \frac{P_{Ar,x,t}}{x} + \frac{v}{R.T} \cdot P_{Ar,x,t}\right]}{\partial x} = \frac{1}{R.T} \cdot \frac{\partial P_{Ar,x,t}}{\partial t} \quad 3.11$$

where the left hand side is the change of the flux in the x direction at a particular x and t, and, the right hand side is the rate of change in the concentration with respect to time at the same x and t.

The consumption/generation term which appears in the complete form of the equation of continuity (48a) has been

dropped from the expression on the basis of assumption v.

Under vacuum distillation conditions, the rate of change of argon pressure at any particular location is very small with respect to time and its term can also be dropped from the expression. As a result, the equation can be rewritten as:

$$D \cdot \frac{\partial P_{Ar,x,t}}{\partial x} = v \cdot P_{Ar,x,t} \qquad \ldots\ldots 3.12$$

where all terms have the meanings defined in Equation 3.10.

In Equation 3.12, the velocity of the bulk flow is the only term which has yet to be defined precisely. Intuitively it can be seen, that when chamber pressure is less than sum of the equilibrium vapour pressures of the species present in the liquid surface (the general mode of vacuum distillation operation), there will be a flux of each species across the Langmuir plane, Equation 3.9. The evaporating species move away from the liquid surface by convection and diffusion. It is this convection of evaporating vapours away from the liquid surface which is responsible for the bulk flow. An equation for the velocity of the bulk flow is presented shortly.

The pressure profile for argon across the gas space (Figure 3.8.1) can be developed precisely as a function of x and the bulk velocity by solving Equation 3.12 with the substitution of the first boundary condition for argon:

$$P_{Ar,x,t} = P_{ch} \cdot e^{v(x-s)/D} \quad \ldots. 3.13$$

The value of s is about one meter in the experimental apparatus used in this investigation and the value of the argon diffusion coefficient at 10 pascals is about 0.6 m2/s (48b). Using these values, Equation 3.13 shows that the pressure of argon is negligible across the gas space for all values of x, almost up to the value of s, whenever the bulk gas velocity is greater than zero, ie., vacuum distillation conditions.

At first glance, Equation 3.13 suggests that argon pressure at any point in the chamber is independent of time. This is not correct. The velocity of the bulk flow changes with time because the concentration of volatile impurities in the melt decreases during refining. This dependence is demonstrated in the next few paragraphs.

Equation 3.13 indicates that at any particular time, the pressure of argon is negligible for almost all x less than s under the normal conditions of vacuum distillation. This means that, the pressure of evaporated species which make up the balance of the chamber pressure must be roughly equal to chamber pressure across the gas space. Consequently, pressure of the evaporated species must be roughly constant across the gas space. Therefore, the bulk velocity of evaporating vapour can be obtained quite precisely by considering the net flux of

vapour across the Langmuir plane, and the total pressure of the vapours (from the conservation of mass equation at constant pressure (49)) ie.:

$$v = \frac{\Sigma \dot{n}_i'' \cdot R.T}{P_{ch}} \quad \ldots\ldots 3.14$$

where:

- v = bulk velocity, m/s
- $\Sigma \dot{n}_i''$ = sum of the flux of all evaporating species, kgmole/m2.s
- P_{ch} = chamber pressure, pascals
- R = gas constant, 8.314 x 10**3 joules/kgmole.K
- T = temperature, K

Equation 3.14 shows that the bulk velocity of vapour away from the liquid steel surface is a function of the total net flux crossing the Langmuir plane.

The value of the bulk velocity is a maximum at commencement of refining, at which time, there is the largest flux of vapour away from the liquid surface. It has a minimum value equal to zero, when the chamber pressure exceeds the total equilibrium vapour pressure of the liquid surface (no bulk flow), or it has a minimum value given by the flux of iron vapour when chamber pressure is less than the equilibrium vapour pressure of iron (all other volatile solutes having been eliminated from the melt).

Now, the expression for the bulk velocity can be substituted into Fick's first law to express the flux of a particular species of metal vapour (47) ie.:

$$\dot{n}''_{i,x,t} = \frac{-D}{R.T} \cdot \frac{\partial P_{i,x,t}}{\partial x} + \frac{v}{R\,T} \cdot P_{i,x,t} \quad \ldots\ldots 3.15$$

where all terms have the meanings previously defined.

The diffusive term in Equation 3.15 can be dropped because pressure of evaporating species is roughly constant across the gas space.

Therefore, flux of metal vapour across the gas space can be written as:

$$\dot{n}''_{i,x,t} = \frac{v}{R.T} \cdot P_{i,x,t} \,. \quad \ldots\ldots 3.16$$

The vapour pressure of species i is constant for all x across the gas space at any particular time. As a result, its value must be equal to its back pressure just above the Langmuir plane. This, and the substitution of Equation 3.14 for the bulk velocity, give the final form of the expression for the flux of species i across the gas space at that particular time:

$$\dot{n}''_{i,t} = \frac{\Sigma \dot{n}''_{i,t} \cdot p_i^{bp}}{P_{ch}} \quad \ldots\ldots 3.17$$

Equation 3.17 is used as part of an overall model for vacuum distillation which is presented in the next section.

SECTION 3.9. : COMBINED MELT PHASE MASS TRANSPORT, EVAPORATION AND GAS PHASE MASS TRANSPORT

Equations 3.1, 3.9 and 3.17 can be rewritten and combined to give an overall expression for the rate of vacuum distillation refining as follows:

Equation 3.1 gives:

$$\dot{n}''_{i,melt} = Kl \cdot (n'''_{i,b} - \frac{p^{\phi}_{i,s}}{\psi_i}) \quad \ldots\ldots 3.18$$

Equation 3.9 gives:

$$\dot{n}''_{i,evap} = K2_i \cdot (p^{\phi}_{i,s} - p_i^{bp}) \quad \ldots\ldots 3.19$$

And Equation 3.17 gives:

$$\dot{n}''_{i,gas} = K3 \cdot p_i^{bp} \quad \ldots\ldots 3.20$$

As there is negligible accumulation of vapour in the gas space, the flux of atoms to the liquid steel surface is at all times very nearly equal to the net flux of atoms across the Langmuir plane and to the flux of atoms away from the liquid metal in the gas phase, ie.:

$$\dot{n}''_{i,melt} = \dot{n}''_{i,evap} = \dot{n}''_{i,t,gas} \quad \ldots\ldots 3.21$$

Equation 3.21 can be used to combine Equations 3.18, 3.19 and 3.20 to give an overall expression for the flux of solute atoms from the melt in terms of the bulk concentration of solute atoms. The resulting expression is:

$$\dot{n}''_{i,t} = \left[\frac{1}{K1} + \frac{1}{\psi_i . K2_i} + \frac{1}{\psi_i . K3} \right]^{-1} \cdot n'''_{i,b} \quad \ldots 3.22$$

where:

$$K1 = \left[\frac{8.D.v}{\pi.r}\right]^{1/2} \quad \ldots\ldots 3.22a$$

$$K2_i = \left[\frac{1}{2.\pi.M_i.R.T}\right]^{1/2} \quad \ldots\ldots 3.22b$$

$$K3 = \frac{\Sigma \dot{n}_i''}{P_{ch}} \quad \ldots\ldots 3.22c$$

$$\Psi_i = \frac{\gamma_i.P_i.M_b}{\rho_b} \quad \ldots\ldots 3.22d$$

Equation 3.22 is a new model for vacuum distillation refining. In this model, K1 (the melt phase mass transport rate coefficient) is a function of (i) the diffusion coefficient of metallic solute atoms in liquid steel, (ii) the velocity of the liquid steel surface during induction heating and (iii) the radius of the melt surface, Equation 3.1. $K2_i$ (the evaporation rate coefficient) is a function of the molecular mass of the evaporating species and the temperature

of the Langmuir plane, Equation 3.9. K3 (the gas phase rate coefficient) is a function of the total flux evaporating from the liquid steel surface and the total pressure of the vacuum chamber, Equation 3.19. has the value defined by Equation 3.24d and is fixed when K2 is fixed.

K3 is not constant with respect to time. It is directly proportional to the bulk vapour velocity away from the liquid surface. As a result, it decreases from a maximum value at the commencement of the vacuum distillation when there is a large flux of vapour across the Langmuir plane to a minimum value when all of the volatile solutes have been eliminated from the melt, at which time, the flux of vapour across the Langmuir plane is mainly that of iron vapour. As K3 is dependent on time, it is not possible to find a simple analytical solution to Equation 3.22. Therefore, for Equation 3.22 to be applied to vacuum distillation predictions, it is expedient to use a numerical solution.

A computer program was developed to serve this purpose. It predicts the bulk concentration of copper, tin, manganese and iron as a function of time under various conditions of simulated vacuum distillation refining. The next section presents the details of the computer program which simulates vacuum distillation and suggests an optimum operating range for vacuum distillation refining based on the model described by Equation 3.22.

SECTION 3.10. : COMPUTER SIMULATION OF VACUUM DISTILLATION REFINING

The computer program described in this section simulates vacuum distillation by iteratively calculating melt composition on the basis of the flux of material away from the melt, Equation 3.22. The values of all constant parameters appearing in Equation 3.22a to 3.22d are stored within the program, while, the values of the other variable parameters need to be supplied for each simulation by the operator. A complete list of the variable parameters appears on Figure 3.10.1 along with values of the parameters during a typical vacuum distillation experiment.

The computer program simulates vacuum distillation by first calculating the flux from the melt surface for the initial conditions, assuming there is a perfect vacuum, ie., Equation 3.5. It uses this value of flux to calculate an initial value for the gas phase mass transport rate coefficient (Equation 3.22c). The program then calculates the flux of metal vapour for the initial time interval (Equation 3.22), and using the melt area, calculates individual an total masses evaporating during that interval. These values are utilized to calculate the change in the melt volume which then allows an evaluation of new melt composition.

Once adjustment of the melt composition has been performed, the program goes to the start of the loop and

calculates a flux for the next time interval on the basis of the melt composition at this time, and, the flux during the previous time interval, ie., for the gas phase rate coefficient.

The program continues iteration in this manner until some predetermined simulation time elapses. This method assumes that the magnitude of the flux does not change very much from one time interval to the next. Accuracy of this assumption was checked by trying various iteration time intervals. Time intervals of 10 seconds or less gave consistent predictions of the final melt composition, and as a result, the program employs a 10 second iteration interval for the simulation. A listing of the program appears in Appendix 1.

The computer program output is successive, 100 second interval predictions of the bulk liquid composition. Figure 3.10.1 is a plot of the simulation when the input variables have the values shown on the figure.

A factorial screening test was performed using the computer model to simulate vacuum distillation refining. The parameters which were found to effect the simulated elimination rate are listed below in decreasing order of effect:

(a) melt diameter (0.1 to 0.4 m),

(b) melt mass (15 to 60 kg),

(c) melt temperature (1850 to 2000 K),

(d) chamber pressure (1 to 50 pascals),

(e) velocity of the melt surface (0.05 to 0.5 m/s),

(f) diffusion coefficient in liquid steel (5 x 10**-9 to 5 x 10**-8),

and

(g) melt composition (0.1 to 1.0 wt% Cu, Sn, or Mn).

The first two parameters effect the elimination rate by simply altering the geometry of the melt, thereby, changing the melt area to volume ratio.

The remaining important experimental variables are then melt temperature, chamber pressure and the velocity of the melt surface (as the diffusion coefficient is fixed). The effects of these variables are demonstrated on Figures 3.10.1 to 3.10.7. They indicate that the best operating range of controllable variables is (i) melt temperature 1950 - 2050 K and (ii) chamber pressure 1 to 10 pascals.

The effect of melt composition, with respect to a certain starting level of a particular element, was very small for the range simulated in the above factorial test. However, changing the initial manganese concentration from 0.1 to 5 wt%, does in fact, lower the copper concentration at six thousand seconds of simulated vacuum distillation, Figure 3.10.7.

The computer program was also used to calculate the bulk velocity of the vaporizing species (Equation 3.14). The result is presented in Figure 3.10.8. It confirms that the assumption of, bulk velocity always greater than zero (Section 3.9), is valid for normal vacuum distillation conditions.

Primed with this information, the remainder of this thesis covers the experimental study of pilot plant scale vacuum distillation and makes comparison between measured experimental results and predictions of the computer model developed here.

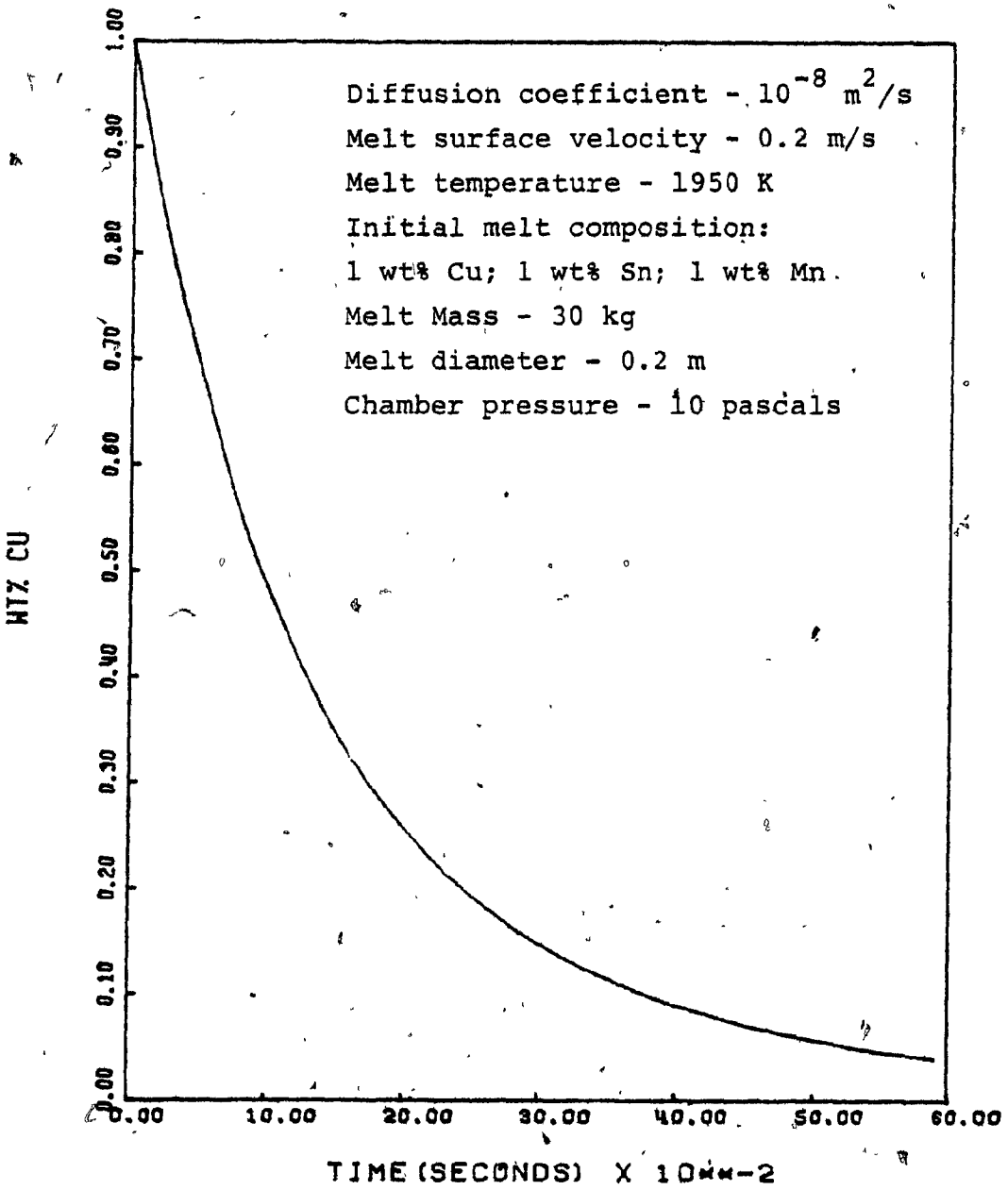

Figure 3.10.1. Computer simulation of copper concentration in liquid steel during vacuum distillation. Inset shows values of the parameters taken for this base case.

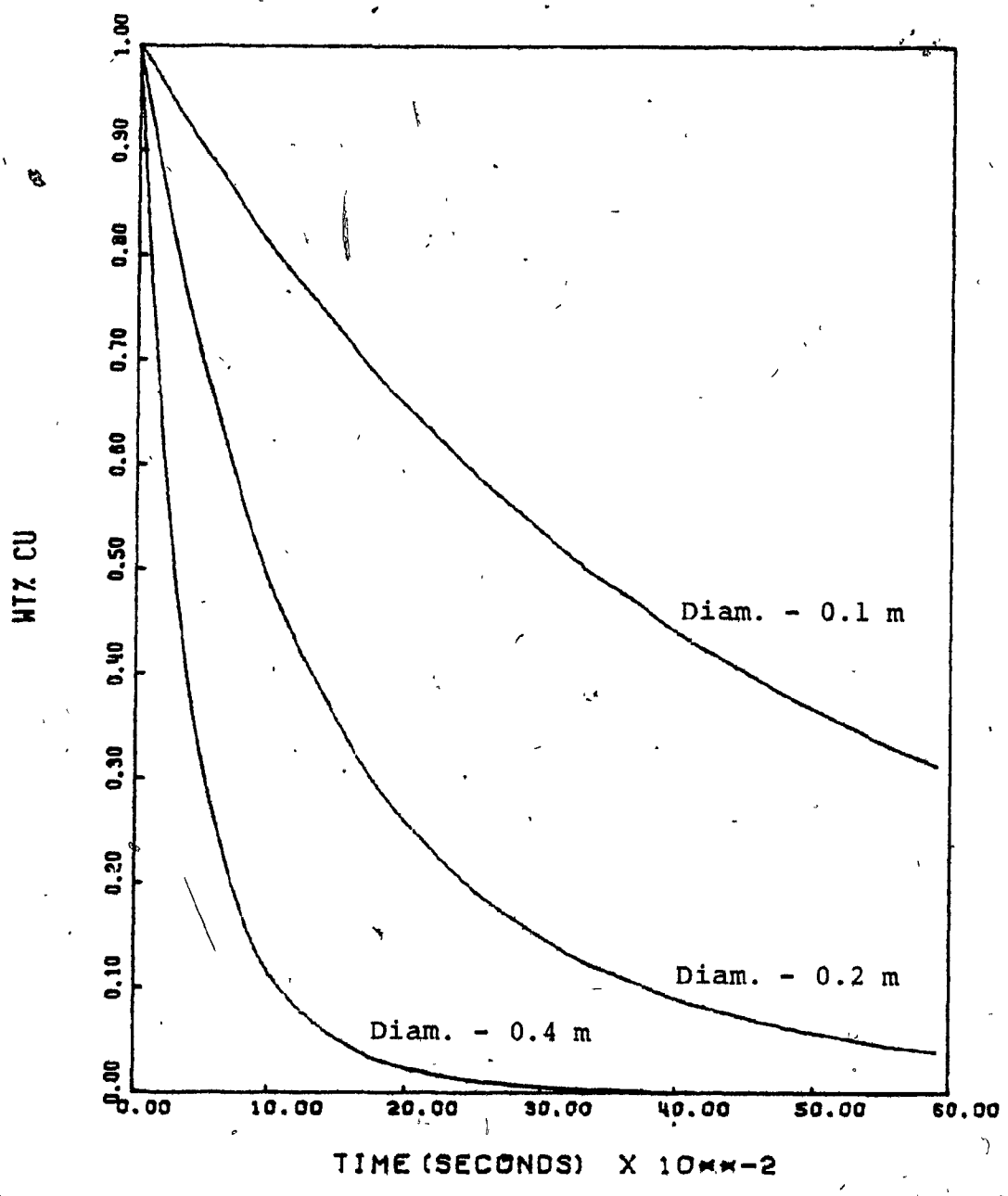

Figure 3.10.2. Computer simulation of copper concentration in liquid steel during vacuum distillation showing the effect of changing melt radius. Values of all other parameters are the same as for the base case, Figure 3.10.1.

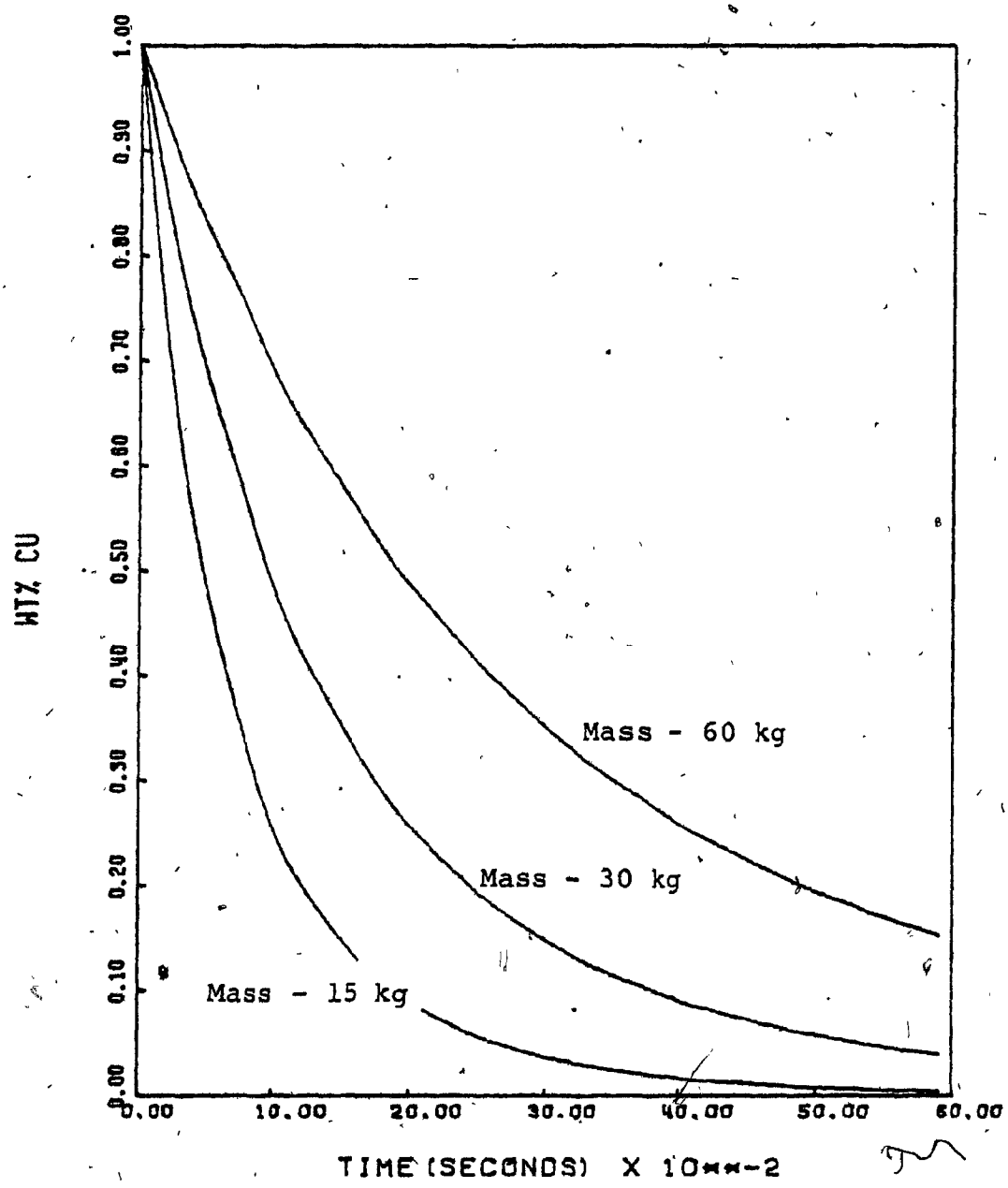

Figure 3.10.3. Computer simulation of copper concentration in liquid steel during vacuum distillation showing the effect of changing melt mass. Values of all other parameters are the same as for the base case, Figure 3.10.1.

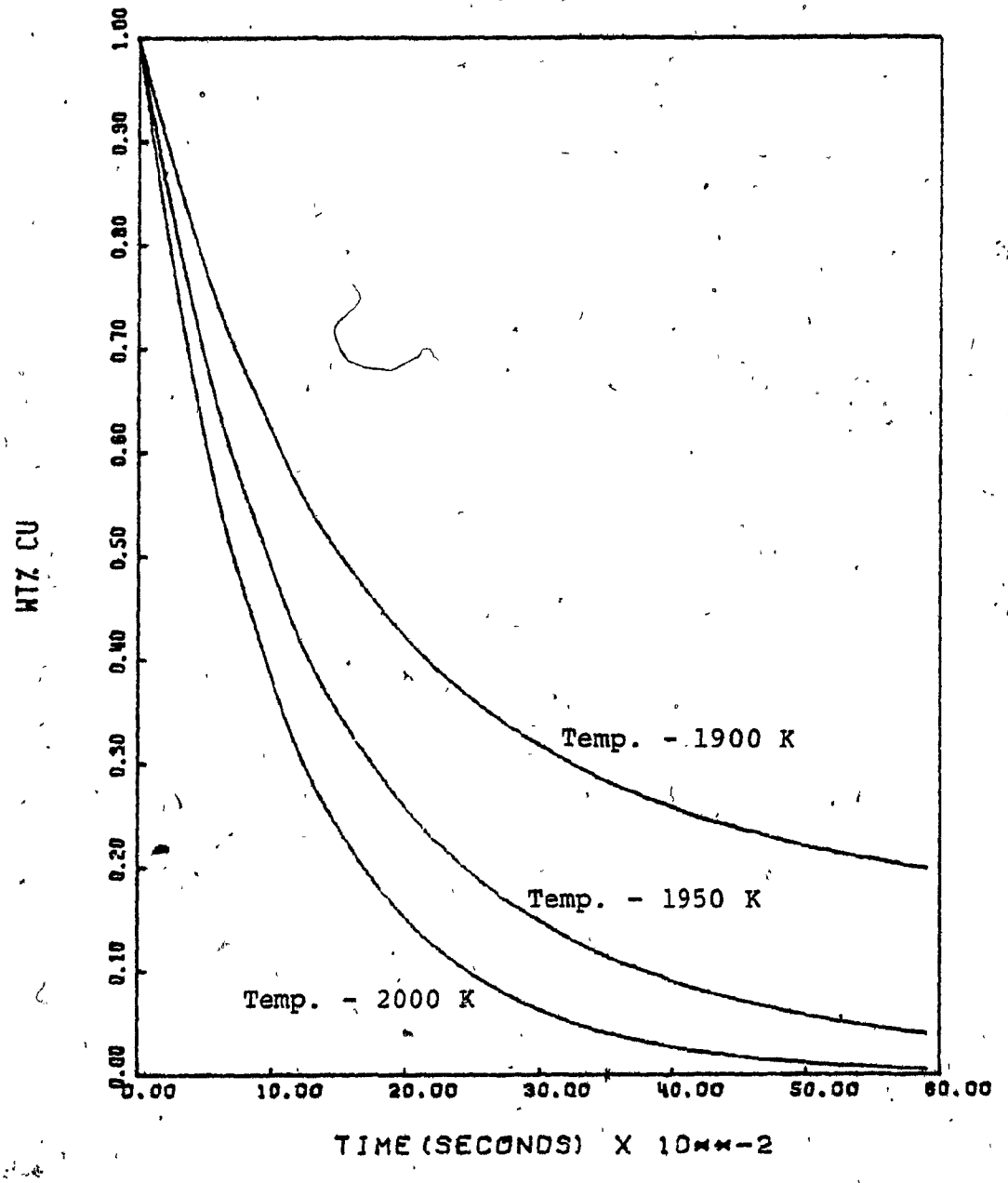

Figure 3.10.4. Computer simulation of copper concentration in liquid steel during vacuum distillation showing the effect of changing melt temperature. Values of all other parameters are the same as for the base case, Figure 3.10.1.

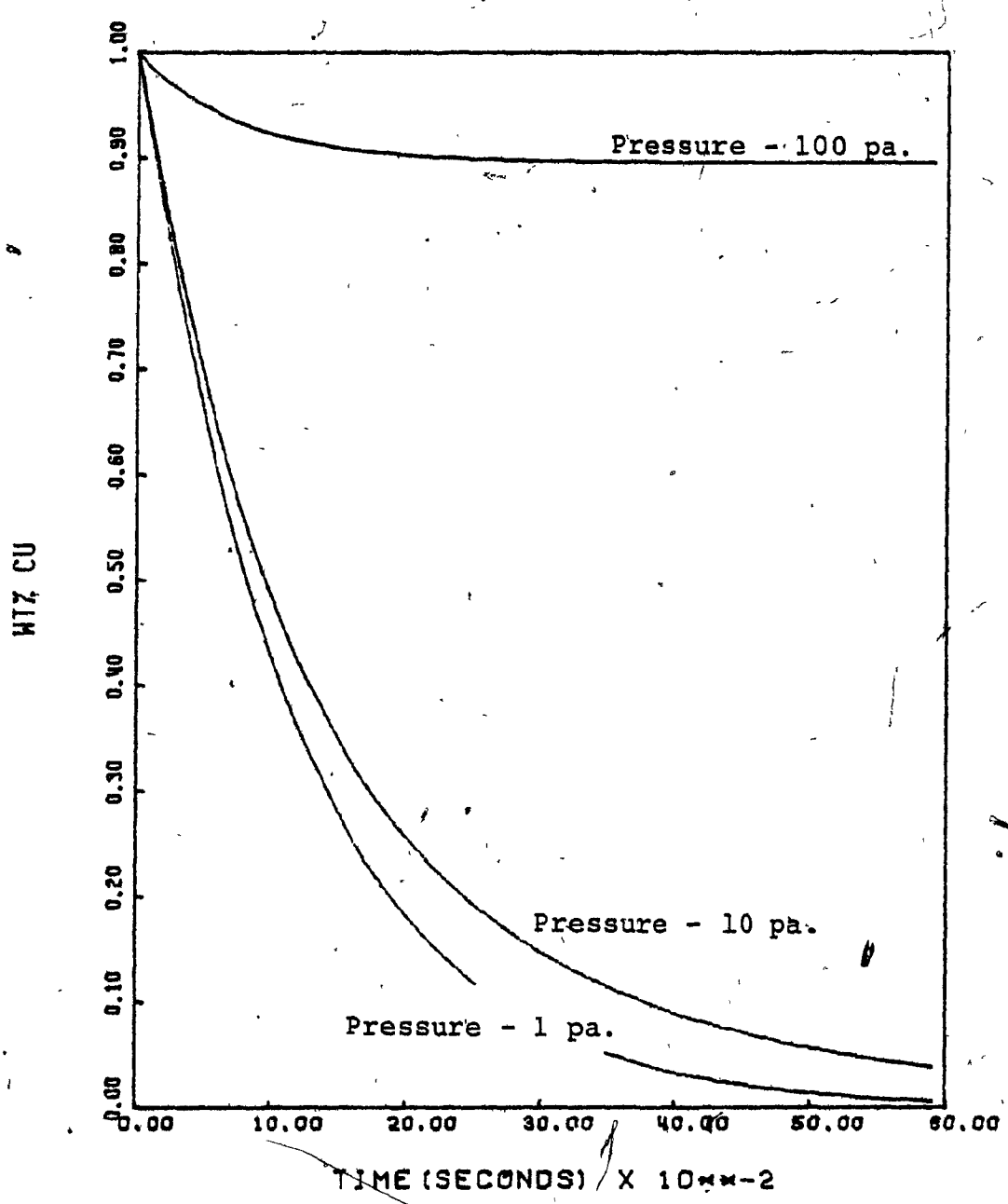

Figure 3.10.5. Computer simulation of copper concentration in liquid steel during vacuum distillation showing the effect of changing chamber pressure. Values of all other parameters are the same as for the base case, Figure 3.10.1.

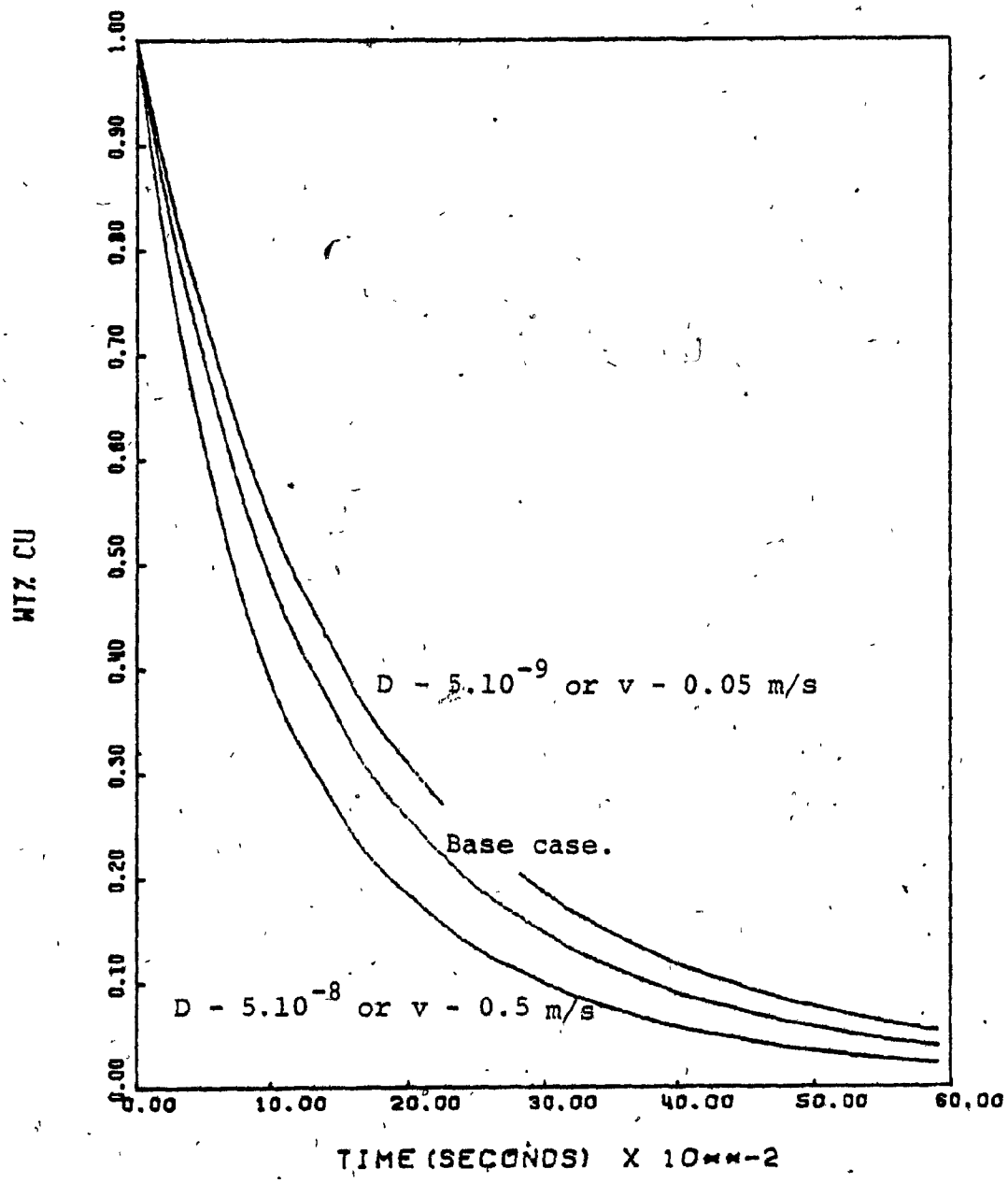

Figure 3.10.6. Computer simulation of copper concentration in liquid steel during vacuum distillation showing the effect of changing melt surface velocity or the diffusion coefficient of the solute atoms in liquid steel. Values of all other parameters are the same as for the base case, Figure 3.10.1.

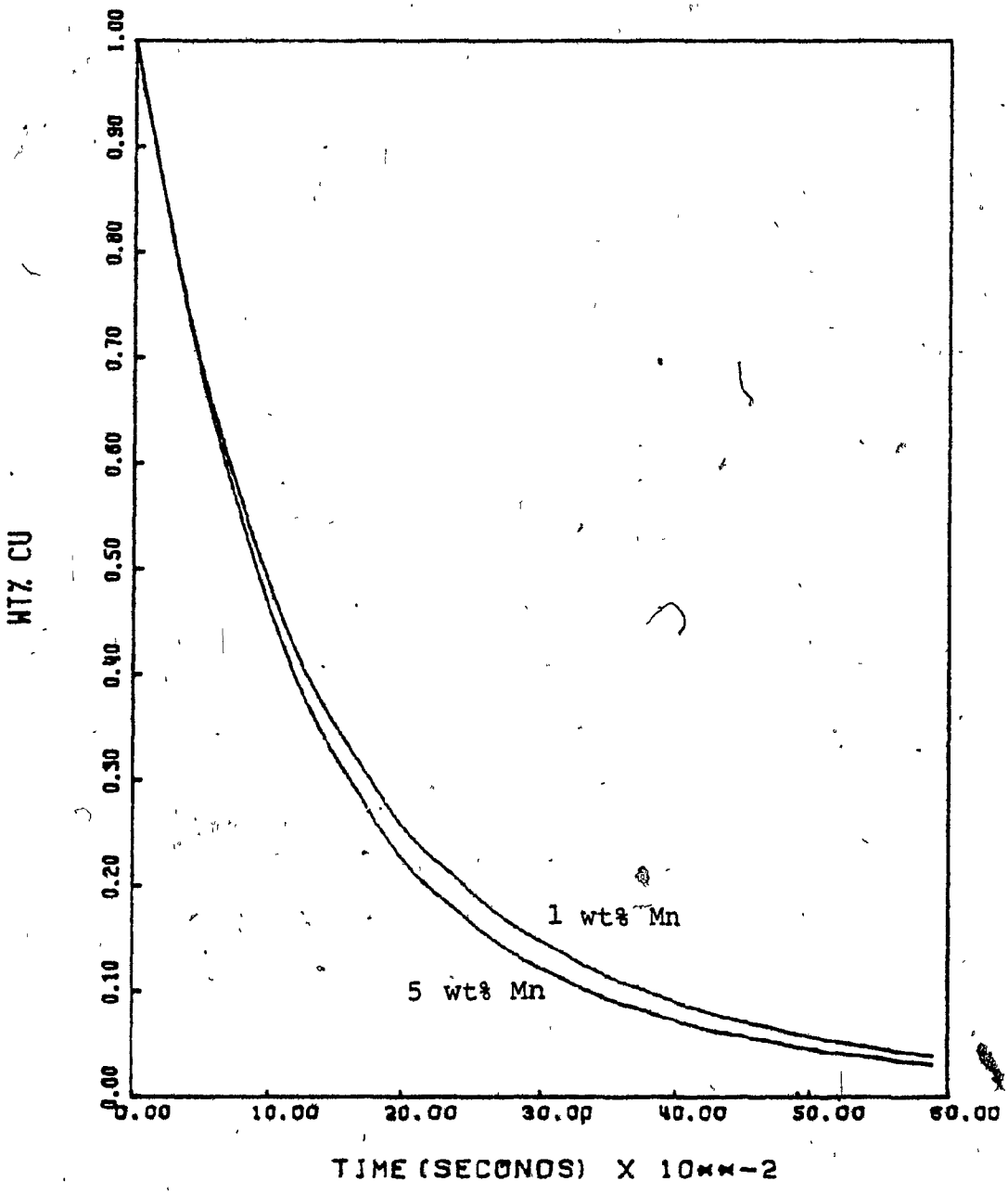

Figure 3.10.7. Computer simulation of copper concentration in liquid steel during vacuum distillation showing the effect of changing initial manganese concentration. Values of all other parameters are the same as for the base case, Figure 3.10.1.

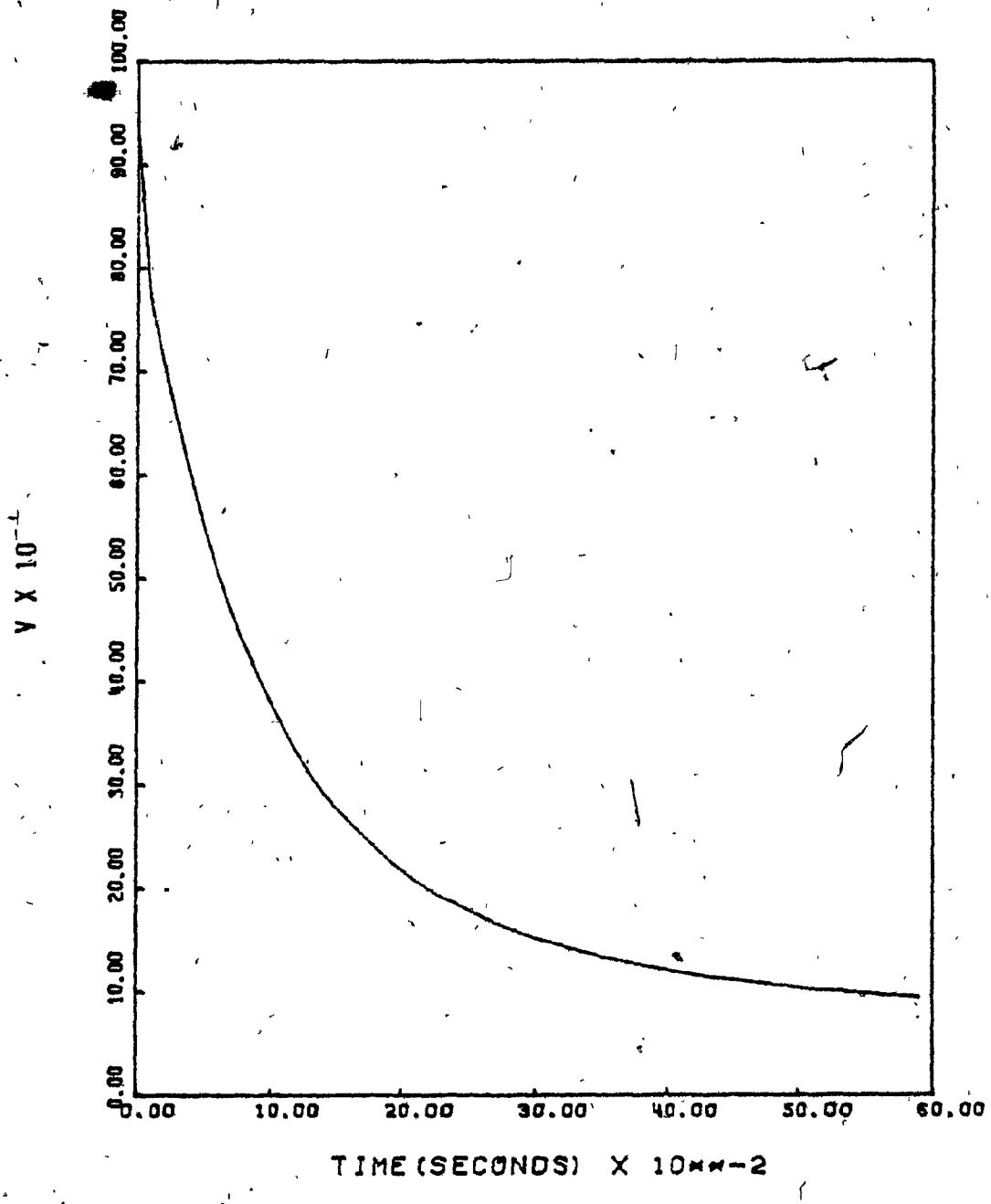

Figure 3.10.8. Computer simulation of bulk vapour velocity during vacuum distillation. Values of all parameters are the same as for the base case, Figure 3.10.1.

CHAPTER FOUR

EXPERIMENTAL

SECTION 4.1. : INTRODUCTION

The principal aim of the experimental program was to measure rates of copper, tin, manganese and sulphur elimination from liquid steel when it is exposed to vacuum. Copper and tin elimination were studied by adding metallic copper and tin to the liquid steel without breaking vacuum. This was followed by melt sampling at regular intervals. Later, these samples were chemically analysed. Manganese and sulphur elimination were studied simultaneously with the copper and tin elimination, however, neither was added to the liquid steel and their initial concentrations were those of the steel charge.

Gas phase and melt surface behaviour were studied by cine and still frame photography of the melt surface and gas space above the crucible. The resulting films greatly aided in understanding the quantitative experimental results.

SECTION 4.2. : EXPERIMENTAL VARIABLES

Previous studies (24-33) have suggested that the following experimental variables influence the rate of residual element elimination by vacuum distillation:

(a) melt temperature,
(b) pressure of the vacuum chamber,
(c) melt area to volume ratio,
(d) initial residual element concentration,
(e) melt oxygen content,
(f) melt sulphur content,
(g) slag on the melt surface,
(h) pumping rates of the vacuum pumps,
(i) inert gas bubbling,
(j) inert gas jetting,
(k) distance from melt surface to condensation site, and
(l) location of the vacuum outlet.

The importance of the first three parameters has been shown in the previous chapter, and as a result, considerable effort was invested to ensure that values of these parameters were known accurately throughout the experimental investigation.

Of the remaining parameters, only g, (surface slags) was considered to cause a potentially large reduction in the elimination rate and, as a result, experimental procedure was established with this in mind.

The parameters which were controlled during the experimental investigation were:

(a) melt temperature,

(b) melt area to volume ratio,

(c) chamber pressure

and

(d) location of outlet from the chamber to the vacuum pumps.

The ranges of these parameters were:

MELT TEMPERATURE:

1780 K to 2030 K as fixed by the melting points of the steel and of Pt - Pt 13% Rh thermocouples used for temperature measurement.

MELT AREA TO VOLUME RATIO:

6 m-1 to 60 m-1. The limits were set by the maximum and minimum depths and diameters of melts which could be held in the induction coils.

CHAMBER PRESSURE:

The lower limit was the minimum pressure the vacuum pumps could attain, about 3 pascals. The upper limit was chosen to be the pressure at which there was negligible evaporation, about 2000 pascals.

LOCATION OF PUMPING OUTLET:

This was a discreet variable. The outlet was either 100 cm away from the melt surface, or it was 15 cm away with an extension into the chamber (Figure 4.3.2).

The parameters which were not controlled are listed below, and in each case, there is a brief note concerning the importance of the variable and reasons for its omission from direct study. In some cases however, it was still possible to collect data which showed the effect of the variable on solute elimination rate. An example of this was the influence of slag on the melt surface.

Initial residual element concentration:

It is thought that this variable would not have a large effect on solute elimination rate (Section 3.10). In these experiments, it was not possible to precisely control the initial value of solute concentration as there was variable recovery due to melt splashing when the addition of the solute was made to the melt under vacuum.

Melt oxygen and sulphur:

The effect of these variables is unknown. Melt oxygen was at a low level in all experiments as a consequence of aluminium killing of the liquid steel. It was planned to control melt sulphur with additions of calcium carbide. This was not feasible as any excess CaC2 floated on the top of the melt and blocked metal evaporation.

Slags:

The effect of a coherent slag on the surface of the melt is to fully block evaporation of metal from the bath. It was thought that calcium fluoride could be used to modify any slag which formed. However, very little slag formed and it was difficult to add CaF2 to liquid steel under vacuum since the CaF2 was in powder form which sprayed everywhere upon introduction into the vacuum.

Pumping rate:

Metallic vapours evolving from the melt condensed to powder before they reached the vacuum pumps. For this reason, pumping rate, per se, has no effect on solute elimination rate.

Inert gas bubbling and jetting:

It is thought that inert gas could be used to increase mass transfer rates in the melt by bubbling, and in the chamber space by jetting. The concept was dropped because of the mechanical problem of maintaining a gas outlet deep beneath the surface of the liquid steel. Also the pumping system was inadequate to cope with increased volumes of gas.

Melt to condenser distance:

A condenser placed at a distance less than the mean free path of the metal vapour away from the liquid steel surface should enhance the rate of solute element elimination (50). This was not experimentally viable as the melt-condenser distance would have had to have been less than 1 cm (50). Also a condenser would have interfered with visual observation and melt sampling.

SECTION 4.3. : EXPERIMENTAL APPARATUS

A coreless 3000 Hz, 150 kW Tocco induction furnace* (* - see Appendix 2) was used to melt and hold at temperature 10 to 65 kg steel charges (Figure 4.3.1). The charge was either 4x4 cm A36 grade hot rolled steel bar* or scrap steel*. The induction furnace was mounted inside a 2.6 m3 (1.8 m diameter x 1.6 m long) vacuum chamber. Ports were located on the top of the chamber allowing sampling and temperature probing without breaking vacuum. Vacuum-tight windows permitted observation and photography of the chamber interior.

The liquid steel was contained in 19.5 cm diameter "Hycor" alumina crucibles* which were used for all experiments, except 5A to 6C, where 35.5 cm diameter "Hycor" crucibles were used.

The pumping system consisted of two stages, a Roots blower* followed by a Stokes mechanical pump*. The outlet from the chamber to the pumps was extended inwards towards the crucible in some experiments (Figure 4.3.2A), and in other experiments, it was not modified (Figure 4.3.2B). A tilting type McLeod vacuum gauge* provided pressure readings. It was mounted just outside the chamber on the vacuum line to the pumps.

Norton type "R" "DIP TIP" thermocouple* assemblies mounted on a temperature probe were used to determine melt temperature. Thermocouple EMF was measured with a Fluke 8600A digital potentiometer*. Temperature measurements were taken with these instruments, without breaking vacuum, by inserting the probe through a vacuum seal on top of the vacuum chamber.

Graphite cups* were used for sampling in all experiments as they consistently produced a sound sample. Quartz cups* were tried in an attempt to avoid melt and sample contamination by carbon. They were unsuccessful as the steel always splashed out of the cup before it froze.

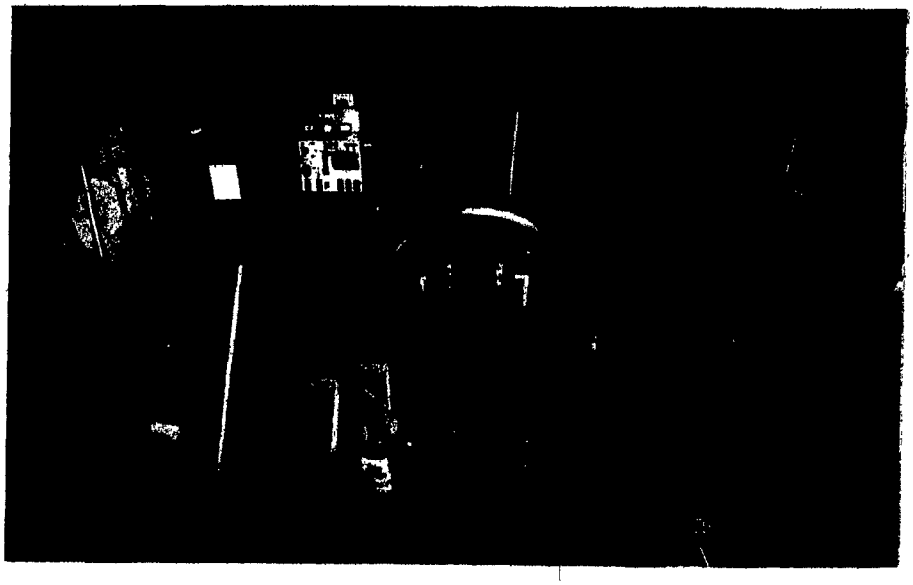

Figure 4.3.1. Overview of experimental apparatus. The vacuum chamber and its door can be seen in the center of the photograph. Controls for furnace power are on the left with vacuum pump controls next to them. The vacuum pumps are located behind the chamber and can not be seen here. Melt sampling and temperature probing ports are located on top of the chamber along with two observation ports. A third observation port is located in the center of the door.

A B

Figure 4.3.2. Details of the chamber interior. Figure A shows the outlet extension in place just above, and to the right of, the furnace (center foreground) and Figure B shows the apparatus without the extension in place. A furnace tilting mechanism is located in the top of the chamber and a radiation shield can be seen to the left of the furnace.

A Perkin Elmer Model 403 atomic absorption spectrometer* was used initially for copper and manganese analyses. Later, a Baird Atomic Model DV-2 Spectrovac* spectrometer was used to analyse the samples for copper, tin, manganese and sulphur.

Motion picture films were taken with a Locam 16 mm* variable frame speed camera fitted with a Cosmicar 22.5-95 mm F 1.5 television zoom lens. Still frame pictures were taken with a Minolta SRT 100 35 mm camera fitted with, either a 300 mm F 3.5 Tokina lens for photographing the melt surface or, a 55 mm F 2.0 Rokkor lens for photographing the gas space.

SECTION 4.4. : EXPERIMENTAL PROCEDURE

Crucibles used in this study were cut down with a diamond saw, from an internal wall height of 35 cm, to a height of about 20 cm for experiments which had 30 or 60 kg steel charges, and, to about 10 cm for those with 10 kg charges. The crucible was placed high in the furnace coils, and tightly packed with clean refractory* (* - see Appendix 2).

Great care was taken in all experiments to ensure that there was no contamination of the refractory packing with either previously splashed metal droplets or with refractory cement which had been used to hold the packing in place during

the previous experiment. This was essential because any contamination of the refractory lowered its melting point, thereby, rendering it unsuitable for high temperature experiments. Even with this precaution, the packing was observed to fuse beneath the crucible during prolonged high temperature experiments.

The 4x4 cm A 36 grade steel was surface ground to remove oxide which could contaminate the melt surface. The scrap steel was charged as received. Charge mass was adjusted so that when molten, it almost filled the crucible. Aluminium, 0.2 to 0.4 wt% of the steel charge weight, was added to the cold charge. The aluminium reacted with oxygen which was present in the steel when it melted and almost completely eliminated splashing and bubbling due to carbon monoxide evolution during pumpdown.

The chamber was sealed once the crucible and charge were in place and evacuated to about 7 pascals using both the mechanical pump and the roots blower. By this means, chamber oxygen potential was lowered to about 1 to 2 pascals. Commercial grade argon* was then admitted until the chamber pressure was just slightly less than 1 atmosphere which helped to reduce splashing during melt-down. The low oxygen potential minimized excessive oxidation of the steel during this time. Melt-down required about 60 to 90 minutes.

As soon as the charge was molten (1770 K), the Stokes mechanical pump was restarted and the chamber was evacuated to about 2000 pascals, at which time, the Roots blower was restarted as well. An initial problem was that the rush of hot gas through the pumping system melted the pumping line foam rubber dust filter. In addition, the filter tended to burn due to the presence of some oxygen in these gases. The problem was overcome by adopting a practice of intermittent pumping during re-evacuation, ie., pressure was lowered in 4000 pascal steps with the mechanical pump until it was around 2000 pascals, at which time, the Root's blower was restarted. Both pumps were then employed to pump continuously for the remainder of the experiment.

Chamber pressure fell quite rapidly from 2000 pascals to 400 pascals and then slowly from about 400 pascals to a steady value in the range 3 to 16 pascals in 15 to 25 minutes. The final steady value of chamber pressure depended upon the amount of air inleakage from a number of minor leaks in the system.

A thin film was always present on the surface of the steel after melting, but, it tended to dissipate during superheating. In runs at lower melt temperatures, around 1900 K, the rate of film dissipation was low, and in some low temperature experiments (less than 1900 K), the bath had to be held at temperature for a considerable time (60 minutes) before the film began clearing. It was found that superheating the

steel to 2050 K quickly cleared the film. The melt could then be allowed to cool to run temperature, whereupon, the copper or copper and tin were added. This procedure required 15 to 20 minutes.

An experimental run began when copper or copper and tin were added to the melt. Samples of the melt were taken thereafter at regular 5 to 10 minute intervals by means of graphite cups attached to steel rods. These devices were inserted into the chamber without breaking vacuum. The samples were cylindrical and weighed about 80 gms. Depending on how rapidly the samples cooled, they were either gray or white cast iron, the carbon being picked up from the sampling cup.

Temperature measurement was performed each time a sample was taken. The "dip tip" was fixed to a probe which was inserted through the bridge breaker port without breaking vacuum. The probe was introduced into the system as fast as possible to minimize heating of the cold junction 5 cm above the thermocouple bead. The cold junction was insulated with 1 cm of refractory which was sufficient to delay its heating until a reading of melt temperature could be taken. Six minutes were required to allow the assembly to cool before a further reading could be taken.

Droplets of steel sometimes splashed into the sample port during sampling or addition making, preventing it from sealing.

When this occured, the pumps were shut off, the chamber was repressurized with argon and the valve was removed, cleaned and replaced. The chamber was re-evacuated and the experiment continued. The break in the experiment under such circumstances lasted about 15 minutes.

At the finish of a day's experimentation, the charge was allowed to cool in the crucible. It was then removed and weighed to estimate the mass splashed and evaporated from the crucible during the experiments. The difference between final and initial weights was divided by the number of times additions were made. It was assumed that melt mass decreased in a stepwise fashion by this amount each time an addition was made. Melt area to volume ratio was calculated for each run on this basis.

The chamber was cleaned after each experiment. Great care was taken during cleaning because of the pyrophoric nature of condensate which adhered loosely to all surfaces of the chamber interior. This condensate was extremely finely divided and it caught fire on several occasions.

Photographs of the melt surface were taken with cine and still cameras. Exposure was 1/18000 sec and F 2.5 at 500 frames per second on 160 ASA film for the cine films, and, 1/500 sec at F 8 on 64 ASA film for the still photographs. The gas space over the crucible was photographed using 1/80 sec and

F 1.5 at 24 frames per second, and, 1/4 sec to 1/15 sec at F 2.0 on the 64 ASA film respectively. The slow film speeds and large apertures were necessary when photographing the gas space due to low light intensity. This was not the case for photographs of the liquid steel surface.

SECTION 4.5. : EXPERIMENTAL CONTROL

4.5.1. : MELT TEMPERATURE

Melt temperature was controlled by varying the power input to the furnace by manually adjusting the potential applied to the induction furnace coils. Power input variation was based upon measured melt temperature, ie., a feed back loop with a human controller. The smallest adjustment available on the power controller was a 2% change in % rated volts. The control attainable by this means is summarized in Table 4.5.1.

MELT MASS (kg)	TEMPERATURE CONTROL
10	+/- 50 K
30	+/- 20 K
60	+/- 10 K

Table 4.5.1 Temperature control achieved on 10, 30 and 60 kg melts in this study as indicated by a 'dip tip' thermocouple measurements.

A typical thermocouple probe EMF response is shown in Figure 4.5.1.

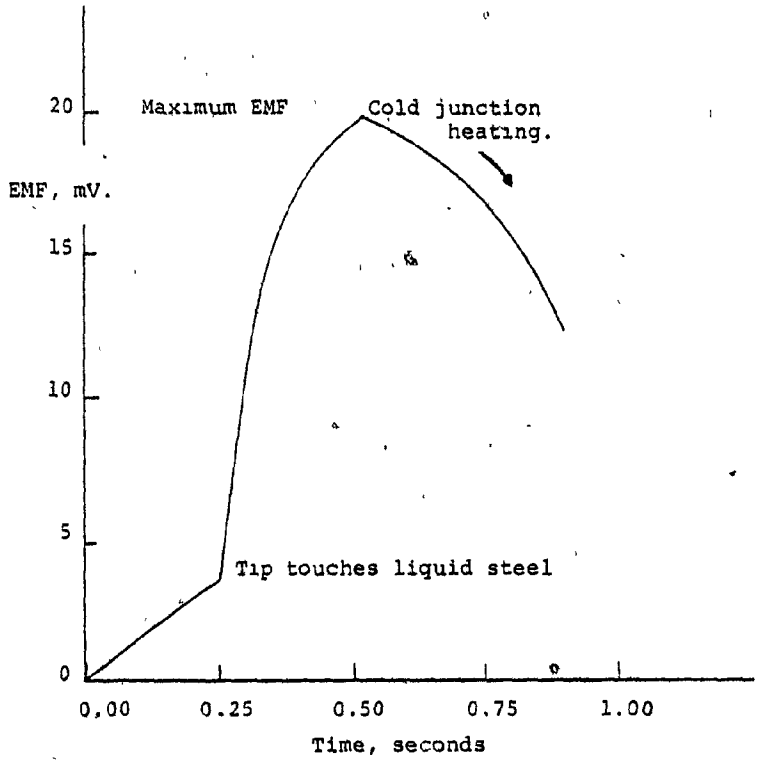

Figure 4.5.1. Melt temperature probe response as a function of time from the moment the port was opened to permit entry of the thermocouple probe to the chamber.

It can be seen that the EMF of the temperature probe changed continuously with time. As the thermocouple junction came to equilibrium with the bath, its EMF rose to a steady value which would have been maintained if the cold junction did not heat up. However, only a fraction of a second elapsed before the EMF began to decay due to warming of the cold junction.

In other words, the reading had to be taken quickly and coupled with the unsteady nature of the digital output, for example, a +/- 0.1 mV change between updates, precision of the reading was limited to +/- 0.1 mV. This corresponds to a +/- 10 K precision in melt temperature in the range 1790 K to 2030 K for Pt / Pt 13% Rh thermocouples. The thermocouple measurements were thought to be accurate to +/- 10 K as they corresponded within +/- 10 K of the liquidus temperature of the steel when a reading was noted just after meltdown.

4.5.2. : CHAMBER PRESSURE

Chamber pressure fell to a steady value at which the rate the vacuum pumps removed gas from the chamber became equal to the rate gas entered the chamber plus the rate gas was generated within the chamber. The gases entering the chamber were either (i) air which accidentally entered the chamber through a number of minor leaks or (ii) argon which was purposefully injected through a port in the center of the rear wall of the chamber. The argon was injected at a controlled rate to maintain the chamber pressure above the value it would have had with full pumping (Figure 4.5.2). The rate air leaked into the chamber varied depending on the condition of the seals of the chamber.

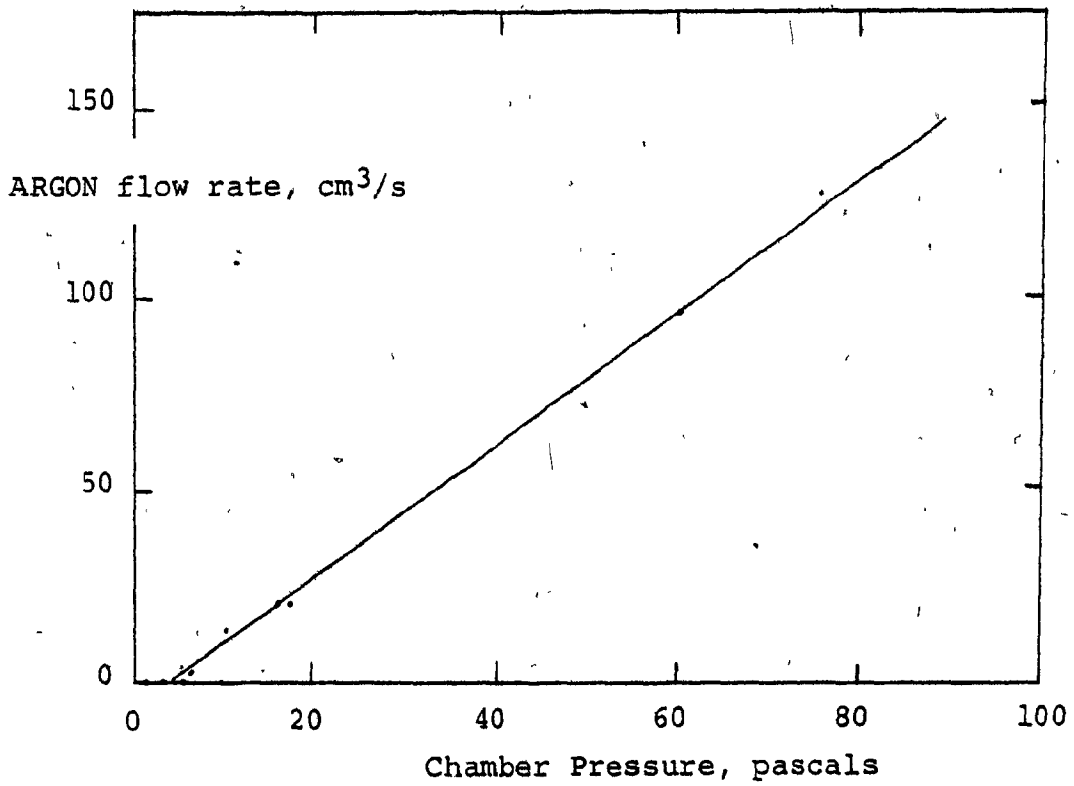

Figure 4.5.2. Chamber pressure as a function of argon flow rate.

The rate gas was generated within the chamber was the sum of outgassing, ie., the evolution of gas from solid surfaces in the chamber, plus the rate gas was evolved from the melt, for example carbon monoxide. Metal evaporation is thought to not influence the chamber pressure measurements, because, the vapours cool and condense either in the chamber itself or in the McLeod vacuum gauge.

In most cases there was no argon injection during the experiments and chamber pressure during the experiments was generally steady. The only control exerted under these circumstances was at times when the chamber pressure accidentally rose above 30 pascals, with full pumping and all

ports closed due to a sealing problem. In such a case, the experiment was stopped to check and clean probable leaks. The most frequent leak source was the sampling port and procedure for its repair was described in Section 4.4.

Argon was used in several experiments to maintain high chamber pressure (16 to 50 pascals). The argon injection rate was controlled by adjusting an argon flow valve setting. At any setting, the argon flow rate varied less than 10 % which resulted in an equivalent percentage variation in chamber pressure.

4.5.3. : MELT AREA TO VOLUME RATIO

The area to volume ratio of a melt in a cyclindrical crucible is equal to the reciprocal of melt depth. It can be determined from the dimensions of the crucible and the mass of the melt. The melt area to volume ratio increased during the course of an experiment, due to melt splashing, metal evaporation and sample taking. At any time during an experiment the melt mass was thought to have been known to within +/- 1 kg. Table 4.5.2 shows approximate values and accuracies of melt area to volume ratio in this study.

MELT MASS (kg)	CRUCIBLE DIAMETER (cm)	A/V (/m)
10+/-1	20+/-1	25 +/- 12.5%
30+/-1	20+/-1	7 +/- 3.5%
60+/-1	36+/-1	7 +/- 1.5%

Table 4.5.2. Precision of reported melt area to volume ratio as a function of melt mass and crucible diameter.

4.5.4. : LOCATION OF PUMPING OUTLET

The location of the chamber pumping outlet was controlled by placing or removing an outlet extension before starting the day's experiments. With the extension in place, the mouth of the outlet was 15 +/- 3 cm from the midpoint of the steel surface, whilst without the outlet extension, it was 100 +/- 3 cm away.

SECTION 4.6. : PRECISION OF MEASURED DATA

4.6.1. : SAMPLING TIME

The time of the first sample following an addition of copper or copper and tin was taken as the initial time for the measurement of solute elimination rate. Vacuum exposure time was then taken as that elapsed from the initial time. Sampling

times were precise to +/- 0.5 minutes.

4.6.2. : CHEMICAL ANALYSIS

Duplicate analyses of melt samples gave an estimate (Table 4.6.1) of the precision of copper and manganese analyses performed using the flame atomic absorption spectrometer. Analyses of melt samples taken simultaneously from the liquid steel generally fell within the accuracy claimed by the manufacturer. This consistency is considered to be a good check for the accuracy of the analytical techniques and the precision with which the melt samples represented the liquid steel at any given time.

ELEMENT	RANGE (wt %)	ACCURACY*	PRECISION
Cu	2 - 0.01	+/- 3%	+/- 1%
Cu	0.01 - 0.001	+/- 10%	+/- 10%
Mn	1 - 0.01	+/- 3%	+/- 3%
Mn	0.01 - 0.001	+/- 10%	+/- 30%

Table 4.6.1. Accuracy and precision for copper and manganese analyses by atomic absorption spectrometry. * Manufacturer's claimed accuracy when their standard technique is followed.

A set of samples analysed by flame atomic absorption was employed to calibrate the vacuum arc spectrometer (Appendix 2) utilized for later experiments. Table 4.6.2 shows the accuracy and precision of the latter method.

ELEMENT	RANGE	ACCURACY*	PRECISION
Cu	2 - 0.001	+/- 3%	+/- 3%
Sn	2 - 0.001	+/- 3%	+/- 3%
Mn	1 - 0.010	+/- 3%	+/- 3%
Mn	0.010 - 0.001	+/- 10%	+/- 30%
S	0.10 - 0.001	+/- 10%	+/- 20%

Table 4.6.2. Accuracy and precision for copper, tin, manganese and sulphur analyses using vacuum arc atomic absorption spectrometry. * Manufacturer's suggested accuracy when their standard technique is followed.

SECTION 4.7. : DEFECTS AND ADVANTAGES OF THE EXPERIMENTS

Two major problems of this experimental work were melt splashing and condensate refluxing. Splashing was a problem because it led to uncertainty in the melt area volume ratio. Condensate refluxing (caused by material which had evaporated from the liquid steel, and condensed on the crucible free wall, being washed back into the melt by melt splashing) was a problem because it led to low apparent rates of elimination. This refluxing was particularly pronounced due to the splashing which occurred whenever an addition or a sample cup was introduced into the melt. It was reduced by ensuring the melt filled the crucible as full as feasible.

Another major problem was that, the metal vapour which evolved from the liquid steel and escaped from the crucible, adhered loosely to all surfaces within the vacuum chamber. The

amount of deposit was greatest on the roof of the chamber directly over the crucible, and when it became too heavy, it detached itself and fell, some falling back into the liquid steel. This also led to low apparent rates of solute elimination. It was significantly reduced by trapping the condensate with a sheet of aluminium gauze which was stretched between two supports in the roof of the chamber (Figure 4.7.1).

As for experimental advantages, the most useful feature of the apparatus was the facility which enabled independent sampling and temperature probing as well as simultaneous visual observations through the chamber windows. In all previous work on vacuum distillation, problems associated with the maintenance of the vacuum seals led to difficulty in either melt sampling or temperature measurement. As a consequence of the visual observations, difficulties with one device could immediately be seen so that it did not interrupt the gathering of data with the other. For example, touching the crucible wall with the sample probe (breaking off the cup) did not stop the measurement of the melt temperature which was essential to good temperature control. The flexibility of this arrangement led to excellent experimental control because it was possible to observe, quickly measure and compensate for changes which occurred during the course of an experiment. It also led to excellent melt sampling because it was possible to observe and ensure that a good sample was obtained.

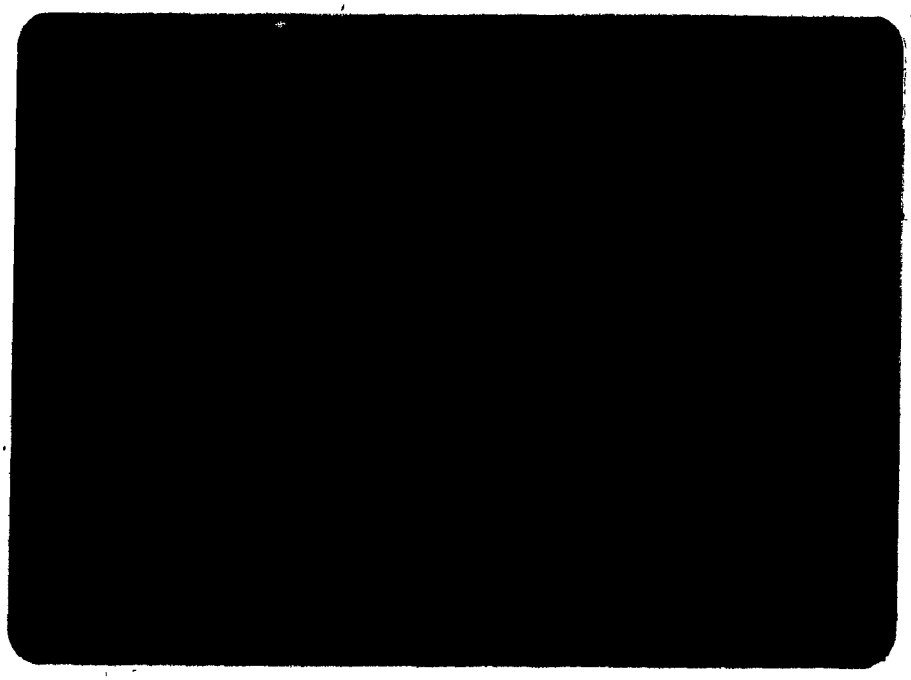

Figure 4.7.1. Aluminum gauze attached to the roof of the vacuum chamber to prevent condensate refluxing. The gauze can be seen to be covered with fine condensate and to have disintegrated directly over the melt. A large build-up of condensate can be seen on the wire that supports the furnace.

SECTION 4.8. : OVERVIEW OF THE PRESENT EXPERIMENTS

The experimental plan was flexible which made it possible to try out new ideas, for example, placing the gauze in the roof of the chamber. The step-wise development of the experimental program can be seen in Table 4.8.1 which shows an overview of the experiments in the order they were performed.

The significant developments and improvements in this program were:

(a) good temperature control,
(b) good pressure control,
(c) wide temperature range,
(d) standard melt surface conditions,
(e) addition of copper or copper and tin to liquid steel without breaking vacuum,
(f) minimum air inleakage,
(g) placing gauze in roof to minimize refluxing

and

(h) simultaneous quantitative and photographic records.

EXPERIMENT NUMBER	DESCRIPTION
1A -1B	Cu added to cold 30 kg charge, poor temperature control
2A	No data, Cu added to liquid steel, poor temperature control
3A - 3D	Good temperature control, vacuum outlet extended towards melt
4A - 4b	Good temperature control, outlet extension in place
5A	No data, entire 10 kg charge, splashed from crucible during melting
6A - 6C	10 kg charge, good temperature control, outlet extension in place
7A - 7D	65 kg charge, good temperature control, outlet extension in place
8A - 8D	Gauze in roof, no outlet extension, good temperature control
9A - 9E	Gauze in roof, no outlet extension, good temperature control
10A - 10B	Gauze in roof, no outlet extension, good temperature control
11A - 11B	Steel scrap charge, outlet extension, gauze in roof, good temperature control
12A - 12B	Steel scrap charge, no outlet extension, gauze in roof, good temperature control, continuous argon injection

Table 4.8.1. Outline of experimental development.

SECTION 4.9. : SUMMARY

In summary, the experiments were aimed at measuring rates of copper, tin, manganese and sulphur elimination from liquid steel under vacuum. Variation in melt surface condition, splashing and refluxing were sources of experimental uncertainty. Photographic observations led to an understanding of gas flow in vacuum and also helped evaluate the influence of the experimental parameters.

CHAPTER FIVE

RESULTS

SECTION 5.1. : MEASUREMENTS

The measurements taken in this investigation were:

(a) melt mass,

(b) crucible diameter and height,

(c) vacuum exposure time,

(d) melt temperature,

(e) chamber pressure,

(f) copper concentration in the liquid steel,

(g) tin concentration in the liquid steel,

(h) manganese concentration in the liquid steel

and

(i) sulphur concentration in the liquid steel.

These measurements are tabulated for each experiment in Tables 5.1.1 to 5.1.4.

Experiment number	Melt mass, kg	Crucible diameter, cm / Crucible depth, cm	Vacuum exposure time, min	Melt temperature, K	Chamber pressure, Pa	Wt % Cu	Wt % Sn	Wt % Mn	Wt % S
1A	31.5	20;20	0	1906	10.7	0.881	-----	0.31	0.037
			30	2009	16.0	0.520	-----	0.10	0.035
			52	----	----	0.304	-----	0.03	0.028
1B	29.5	20;20	0	----	----	0.95	-----	0.02	0.026
			15	----	----	0.43	-----	0.005	0.018
2A	29.5	20;20	0	1973	----	0.805	-----	0.296	-----
			12	----	13.3	0.555	-----	0.131	-----
3A	32.5	20;20	0	1980	20.0	0.579	-----	0.125	-----
			11	1987	16.0	0.409	-----	0.048	-----
			24	----	----	0.278	-----	0.003	-----
			32	----	16.0	0.232	-----	0.002	-----
3B	30.5	20;20	0	2002	26.7	0.697	-----	0.004	-----
			15	2002	21.3	0.428	-----	-----	-----
			27	2002	14.7	0.325	-----	-----	-----
			36	2002	20.0	0.293	-----	-----	-----
3C	28.5	20;20	0	1906	12.0	0.802	-----	-----	-----
			12	1928	8.0	0.581	-----	-----	-----
			21	1921	4.0	0.423	-----	-----	-----
			30	1928	----	0.336	-----	-----	-----
3D	26.5	20;20	0	1943	6.7	0.948	-----	-----	-----
			10	1950	6.7	0.619	-----	-----	-----
			22	1918	6.7	0.457	-----	-----	-----
			36	1870	6.7	0.312	-----	-----	-----
4A	29.5	20;20	0	1856	14.7	0.680	-----	0.501	-----
			8	1885	8.0	0.621	-----	0.317	-----
			17	1870	8.0	0.501	-----	0.130	-----
			27	1885	8.0	0.427	-----	0.084	-----
4B	27.5	20;20	0	1813	4.7	0.743	-----	0.047	-----
			17	1870	3.3	0.659	-----	0.034	-----
			27	----	4.7	0.500	-----	0.016	-----
			37	1885	4.7	0.418	-----	0.010	-----

Table 5.2.1. Measured values of experimental parameters and melt composition for Experiments 1A to 4B.

Experiment number	Melt mass, kg	Crucible diameter, cm Crucible depth, cm	Vacuum exposure time, min	Melt temperature, K	Chamber pressure, Pa	Wt % Cu	Wt % Sn	Wt % Mn	Wt % S
6A	9.2	20;10	0	?1773?	25.3	0.673	-----	0.017	-----
			13	1935	12.0	0.453	-----	0.005	-----
			20	1921	10.7	0.236	-----	0.002	-----
			30	1913	----	0.141	-----	0.001	-----
6B	7.2	20;10	0	1899	6.7	0.629	-----	-----	-----
			9	1890	6.7	0.454	-----	-----	-----
			19	1904	6.7	0.222	-----	-----	-----
			31	1904	6.0	0.108	-----	-----	-----
6C	5.2	20;10	0	----	6.7	0.625	-----	-----	-----
			8	1899	8.0	0.395	-----	-----	-----
7A	62.3	36;20	0	1849	9.3	0.786	-----	0.127	-----
			12	1892	9.3	0.678	-----	0.084	-----
			18	1899	----	0.562	-----	0.052	-----
			37	1899	33.3	0.501	-----	0.038	-----
7B	60.3	36;20	0	1892	6.7	0.836	-----	0.038	-----
			10	1899	6.7	0.692	-----	0.020	-----
			21	1921	13.3	0.533	-----	0.011	-----
7C	60.3	36;20	0	1928	6.7	0.466	-----	0.009	-----
			9	1923	6.7	0.396	-----	0.006	-----
			20	1943	6.7	0.277	-----	0.003	-----
			27	1921	----	0.236	-----	0.002	-----
7D	58.3	36;20	0	1987	13.3	0.429	-----	-----	-----
			12	1993	37.3	0.288	-----	-----	-----
			20	1972	37.3	0.272	-----	-----	-----

Table 5.2.2. Measured values of experimental parameters and melt composition for Experiments 6A to 7D.

Experiment number	Melt mass, kg	Crucible diameter, cm Crucible depth, cm	Vacuum exposure time, min	Melt temperature, K	Chamber pressure, Pa	Wt % Cu	Wt % Sn	Wt % Mn	Wt % S
8A	29.5	20;20	0	1965	13.3	0.150	0.100	0.570	0.048
			10	1972	12.0	0.110	0.080	0.200	0.043
			22	1965	13.3	0.071	0.057	0.010	0.037
			32	1972	8.0	0.048	0.036	0.017	0.028
			41	1972	8.0	0.036	0.029	-----	0.026
8B	27.5	20;20	0	1965	5.3	0.148	0.117	-----	0.016
			11	1965	6.7	0.114	0.102	-----	0.012
			20	1951	4.0	0.081	0.083	-----	0.012
8C	27.5	20;20	0	1958	5.3	0.071	0.082	-----	0.011
			12	1958	4.0	0.054	0.064	-----	0.009
8D	25.5	20;20	0	----	40.0	0.580	-----	-----	0.009
			11	1958	26.7	0.448	-----	-----	0.008
			21	1958	30.7	0.384	-----	-----	0.007
9A	36.4	20;20	0	1958	26.7	0.239	0.088	0.460	0.040
			9	2029	26.7	0.138	0.072	0.056	0.031
			19	2017	26.7	0.078	0.036	0.020	0.022
			34	2028	26.7	0.053	0.020	0.009	0.020
9B	34.4	20;20	0	1999	13.3	0.181	0.106	0.016	0.018
			8	1998	10.7	0.129	0.080	0.004	0.013
			16	2009	10.7	0.082	0.070	0.014	0.013
			26	2018	13.3	0.047	0.046	0.003	0.011
			35	2005	13.3	0.034	0.042	0.008	0.010
9C	32.4	20;20	0	1809	10.7	0.277	0.135	0.009	0.008
			8	1777	8.0	0.272	0.137	0.009	0.009
			16	1784	8.0	0.281	0.140	0.019	0.009
			30	1798	6.7	0.270	0.130	-----	0.008
9D	32.4	20;20	0	1892	6.7	0.266	0.144	0.017	0.009
			10	1892	6.7	0.250	0.148	0.009	0.009
9E	32.4	20;20	0	1939	6.7	0.184	0.132	0.007	0.008
			10	1935	8.0	0.137	0.130	-----	0.006
			20	1935	8.0	0.103	-----	-----	-----
			30	1935	6.7	0.080	0.104	-----	0.006

Table 5.2.3. Measured values of experimental parameters and melt composition for experiments 8A to 9E.

Experiment number	Melt mass, kg	Crucible diameter; Crucible depth, cm	Vacuum exposure time, min	Melt temperature, K	Chamber pressure, Pa	Wt % Cu	Wt % Sn	Wt % Mn	Wt % S
10A	36.4	20;20	0	1921	14.0	0.205	0.098	0.450	-----
			11	1980	13.3	0.154	0.080	0.152	-----
			31	1972	13.3	0.077	0.050	0.019	-----
			41	----	13.3	0.061	0.034	0.025	-----
			46	1965	20.0	0.050	0.029	0.007	-----
10B	34.4	20;20	0	1799	14.7	0.074	0.083	0.003	0.013
			10	1804	13.3	0.075	0.087	0.012	0.014
			23	1764	14.7	0.074	0.082	0.006	0.016
11A	36.4	20;20	0	2005	60.0	0.168	0.067	0.167	0.032
			13	1965	347	0.150	0.064	0.120	0.030
			32	1993	373	0.140	0.056	0.094	0.028
			42	1996	400	0.132	0.056	0.070	0.027
11B	34.4	20;20	0	1968	8.0	0.294	0.034	0.016	0.022
			10	1983	6.7	0.194	0.022	0.005	0.020
			20	1993	6.7	0.140	0.018	0.004	0.017
			30	1991	8.0	0.100	0.013	?0.015?	0.017
12A	36.4	20;20	0	2000	6.7	0.230	0.095	-----	0.029
			15	1985	13.3	0.190	0.088	-----	0.026

Table 5.2.4. Measured values of experimental parameters and melt composition for Experiments 10A to 12A.

SECTION 5.2. : RESULTS

The measured data were used to evaluate:

(a) the experimental conditions,

(b) initial solute concentrations,

(c) percentage solute elimination as a function of vacuum exposure time,

(d) elimination rate coefficients (see Section 7.9) for each solute

and to prepare:

(e) plots of Ln(wt % solute) versus vacuum exposure time.

Figures 5.2.1 to 5.2.29 show this information for each of the experimental runs.

EXPERIMENT NUMBER : 1 A

MELT TEMPERATURE :1970±50K

CRUCIBLE DIAMETER :0.20M

CHAMBER PRESSURE :14.1±2.7PA

CRUCIBLE DEPTH :0.20M

MELT MASS :31.5±0.5KG

MELT AREA TØ VØLUME :7.1±0.3/M

SAMPLE	TIME (MIN)	%CU ELIM'D	%SN ELIM'D	%MN ELIM'D	%S ELIM'D
		% CU INIT:0.881	% SN INIT:######	% MN INIT:0.310	% S INIT:0.037
1	0	0		0	0
2	30	41		68	5
3	52	65		90	24

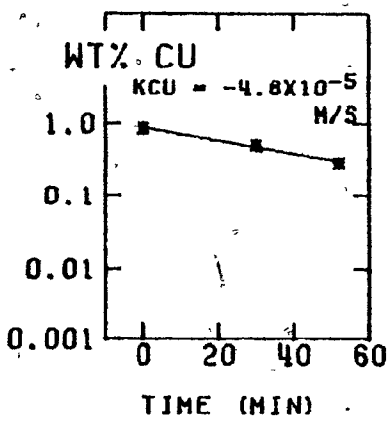

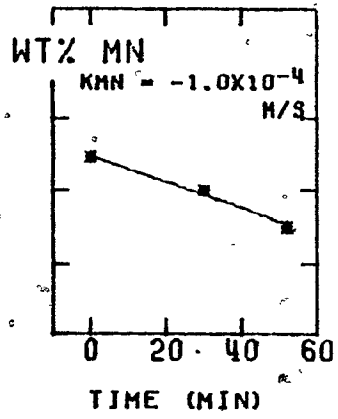

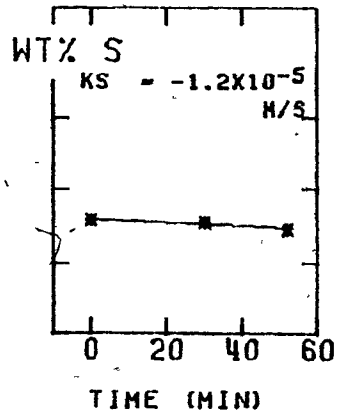

Figure 5.2.1. Values of experimental parameters, percentage copper, manganese and sulphur eliminated at each sampling time and plots of natural logarithm of measured copper, manganese and sulphur concentration against time for experiment 1A. The value of a rate coefficient for each measured solute are also given.

EXPERIMENT NUMBER : 1 B

MELT TEMPERATURE :1970±99K

CHAMBER PRESSURE :14.0±9.9PA

MELT MASS :29.5±0.5KG

CRUCIBLE DIAMETER :0.20M

CRUCIBLE DEPTH :0.20M

MELT AREA TO VOLUME :7.5±0.3/M

SAMPLE	TIME (MIN)	%CU ELIM'D	%SN ELIM'D	%MN ELIM'D	%S ELIM'D
		% CU INIT:0.950	% SN INIT:#####	% MN INIT:0.020	% S INIT:0.026
1	0	0		0	0
2	15	55		75	38
3	25	77		95	31

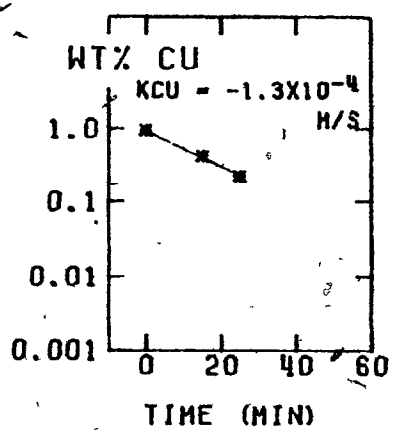

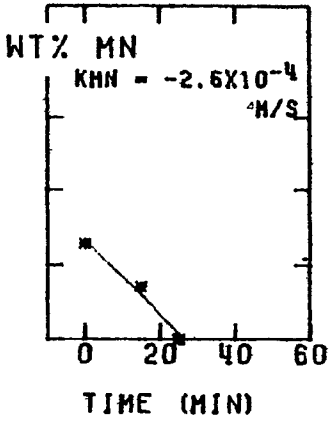

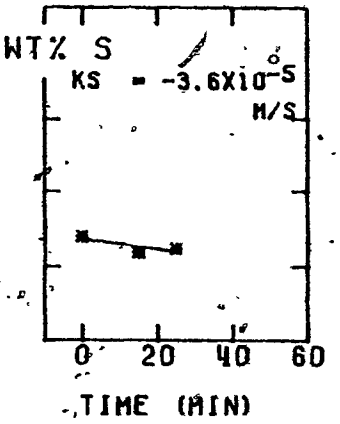

Figure 5.2.2. Values of experimental parameters, percentage copper, manganese and sulphur eliminated at each sampling time and plots of natural logarithm of measured copper, manganese and sulphur concentration against time for experiment 1B. The value of a rate coefficient for each measured solute are also given.

EXPERIMENT NUMBER : 2 A

MELT TEMPERATURE :2000±99K

CHAMBER PRESSURE :13.3±9.9PA

MELT MASS :29.5±0.5KG

CRUCIBLE DIAMETER :0.20M

CRUCIBLE DEPTH :0.20M

MELT AREA TO VOLUME :7.5±0.3/M

SAMPLE	TIME (MIN)	%CU ELIM'D	%SN ELIM'D	%MN ELIM'D	%S ELIM'D
		X CU INIT:0.805	X SN INIT:******	X MN INIT:0.296	X S INIT:******
1	0	0		0	
2	12	31		56	

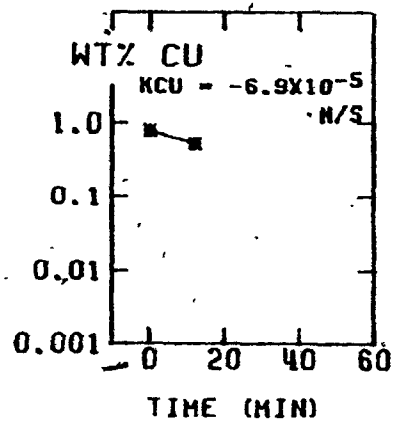

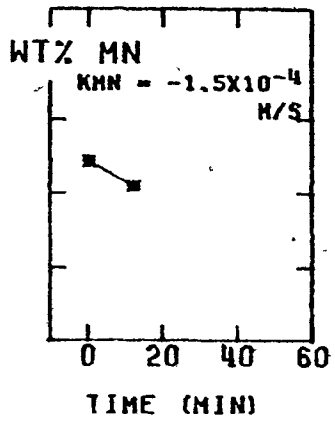

Figure 5.2.3. Values of experimental parameters, percentage copper and manganese eliminated at each sampling time and plots of natural logarithm of measured copper and manganese concentration against time for experiment 2A. The value of a rate coefficient for each measured solute are also given.

EXPERIMENT NUMBER : 3 A

MELT TEMPERATURE : 1985±13K

CHAMBER PRESSURE : 17.2±0.3PA

MELT MASS : 32.5±0.5KG

CRUCIBLE DIAMETER : 0.20M

CRUCIBLE DEPTH : 0.20M

MELT AREA TO VOLUME : 6.8±0.2/M

SAMPLE	TIME (MIN)	%CU ELIM'D	%SN ELIM'D	%MN ELIM'D	%S ELIM'D
		% CU INIT=0.579	% SN INIT=******	% MN INIT=0.125	% S INIT=******
1	0	0		0	
2	11	29		62	
3	24	52		98	
4	32	60		99	

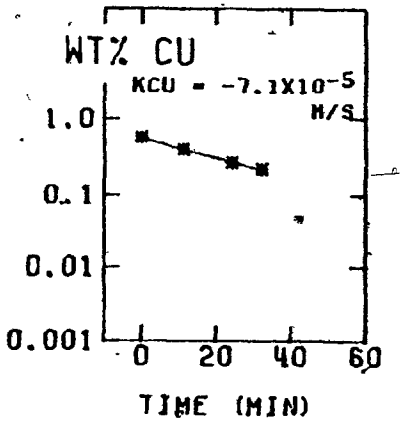

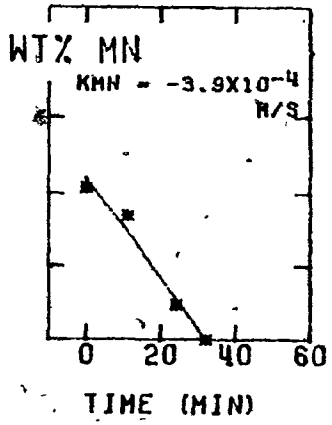

Figure 5.2.4. Values of experimental parameters, percentage copper and manganese eliminated at each sampling time and plots of natural logarithm of measured copper and manganese concentration against time for experiment 3A. The value of a rate coefficient for each measured solute are also given.

EXPERIMENT NUMBER : 3 B

MELT TEMPERATURE : 2002±10K CRUCIBLE DIAMETER : 0.20M

CHAMBER PRESSURE : 21.5±4.0PA CRUCIBLE DEPTH : 0.20M

MELT MASS : 30.5±0.5KG MELT AREA TO VOLUME : 7.3±0.3/M

SAMPLE	TIME (MIN)	%CU ELIM'D	%SN ELIM'D	%MN ELIM'D	%S ELIM'D
		% CU INIT: 0.697	% SN INIT: ******	% MN INIT: 0.004	% S INIT: ******
1	0	0		0	
2	15	39		75	
3	27	53		0	
4	36	58		75	

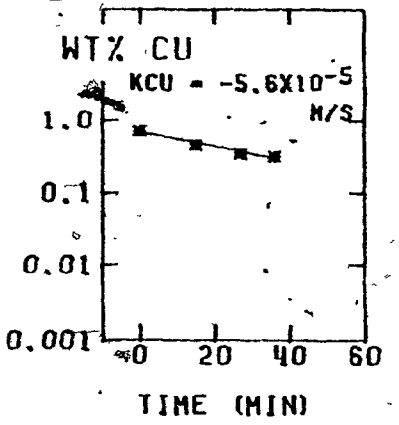

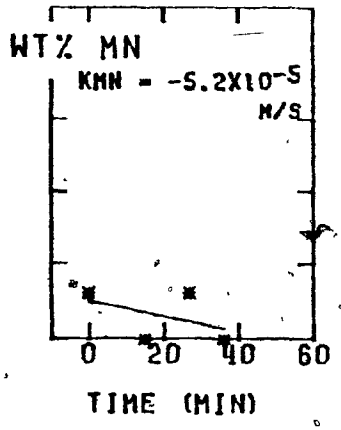

Figure 5.2.5. Values of experimental parameters, percentage copper and manganese eliminated at each sampling time and plots of natural logarithm of measured copper and manganese concentration against time for experiment 3B. The value of a rate coefficient for each measured solute are also given.

EXPERIMENT NUMBER : 3 C

MELT TEMPERATURE : 1920±20K

CHAMBER PRESSURE : 8.2 ±4.0PA

MELT MASS : 28.5±0.5KG

CRUCIBLE DIAMETER : 0.20M

CRUCIBLE DEPTH : 0.20M

MELT AREA TO VOLUME : 7.8±0.3/M

SAMPLE	TIME (MIN)	%CU ELIM'D	%SN ELIM'D	%MN ELIM'D	%S ELIM'D
		% CU INIT:0.802	% SN INIT:*****	% MN INIT:0.001	% S INIT:*****
1	0	0			
2	12	28			
3	21	47			
4	30	58			

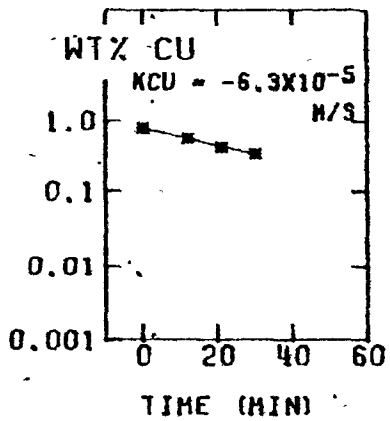

Figure 5.2.6. Values of experimental parameters, percentage copper eliminated at each sampling time and plots of natural logarithm of measured copper concentration against time for experiment 3C. The value of a rate coefficient for each measured solute are also given.

EXPERIMENT NUMBER : 3 D

MELT TEMPERATURE : 1934±20K

CHAMBER PRESSURE : 6.7 ±0.7PA

MELT MASS : 26.5±0.5KG

CRUCIBLE DIAMETER : 0.20M

CRUCIBLE DEPTH : 0.20M

MELT AREA TO VOLUME : 8.6±0.3/M

SAMPLE	TIME (MIN)	%CU ELIM'D	%SN ELIM'D	%MN ELIM'D	%S ELIM'D
		X CU INIT: 0.948	X SN INIT: *****	X MN INIT: *****	X S INIT: *****
1	0	0			
2	10	35			
3	22	52			
4	36	67			

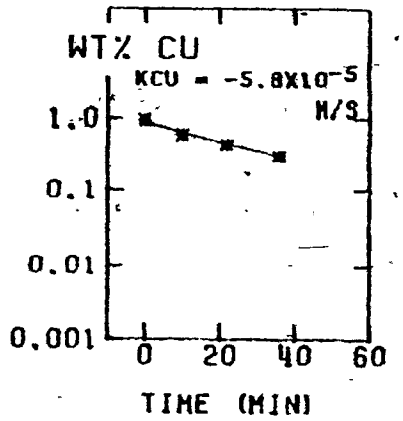

Figure 5.2.7. Values of experimental parameters, percentage copper eliminated at each sampling time and plots of natural logarithm of measured copper concentration against time for experiment 3D. The value of a rate coefficient for each measured solute are also given.

EXPERIMENT NUMBER : 4 A

MELT TEMPERATURE :1874±20K

CHAMBER PRESSURE :9.6 ±2.0PA

MELT MASS :29.5±0.5KG

CRUCIBLE DIAMETER :0.20M

CRUCIBLE DEPTH :0.20M

MELT AREA TO VOLUME :7.5±0.3/M

SAMPLE	TIME (MIN)	%CU ELIM'D	%SN ELIM'D	%MN ELIM'D	%S ELIM'D
		Z CU INIT:0.680	Z SN INIT:*****	Z MN INIT:0.501	Z S INIT:*****
1	0	0		0	
2	8	9		37	
3	17	26		74	
4	27	37		83	

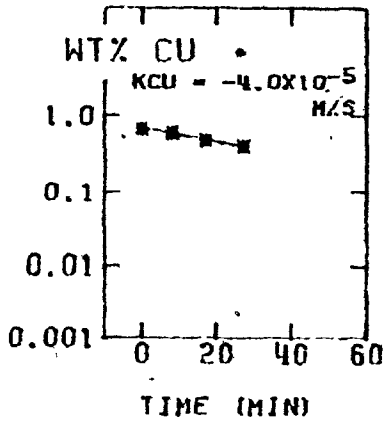

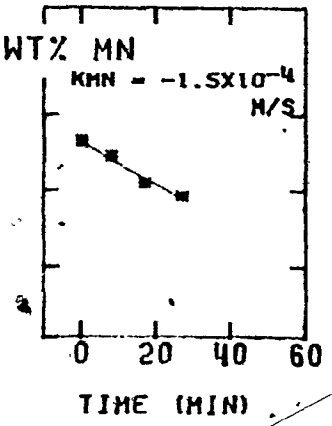

Figure 5.2.8. Values of experimental parameters, percentage copper and manganese eliminated at each sampling time and plots of natural logarithm of measured copper and manganese concentration against time for experiment 4A. The value of a rate coefficient for each measured solute are also given.

EXPERIMENT NUMBER : 4 B

MELT TEMPERATURE : 1858±45K

CRUCIBLE DIAMETER : 0.20M

CHAMBER PRESSURE : 4.3 ±0.4PA

CRUCIBLE DEPTH : 0.20M

MELT MASS : 27.5±0.5KG

MELT AREA TO VOLUME : 8.1±0.3/M

SAMPLE	TIME (MIN)	%CU ELIM'D	%SN ELIM'D	%MN ELIM'D	%S ELIM'D
		% CU INIT: 0.743	% SN INIT: *****	% MN INIT: 0.047	% S INIT: *****
1	0	0		0	
2	17	11		28	
3	27	33		66	
4	37	44		79	

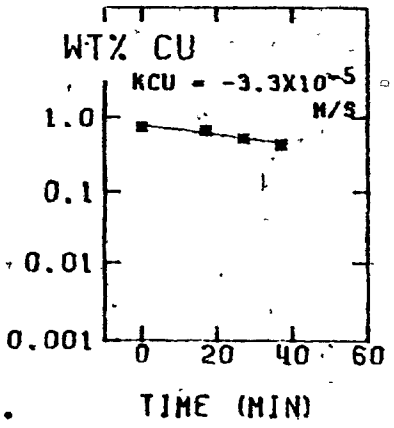

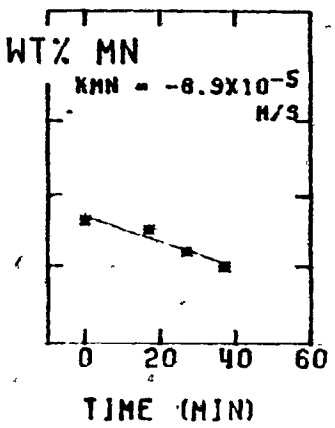

Figure 5.2.9. Values of experimental parameters, percentage copper and manganese eliminated at each sampling time and plots of natural logarithm of measured copper and manganese concentration against time for experiment 4B. The value of a rate coefficient for each measured solute are also given.

EXPERIMENT NUMBER : 6. A

MELT TEMPERATURE :1930±30K CRUCIBLE DIAMETER :0.20M

CHAMBER PRESSURE :14.1±9.0PA CRUCIBLE DEPTH :0.10M

MELT MASS :9.2 ±0.5KG MELT AREA TO VOLUME :24 ±3.0/M

SAMPLE	TIME (MIN)	%CU ELIM'D	%SN ELIM'D	%MN ELIM'D	%S ELIM'D
		% CU INIT:0.673	% SN INIT:««««	% MN INIT:0.017	% S INIT:««««
1	0	0		0	
2	13	33		71	
3	20	65		88	
4	30	79		94	

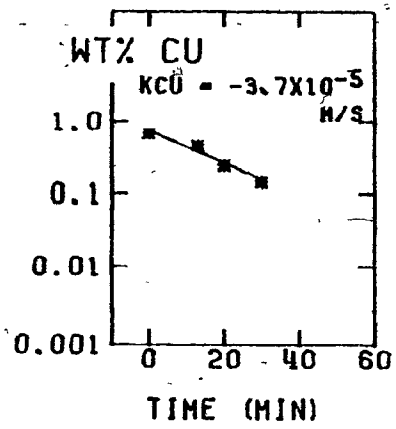

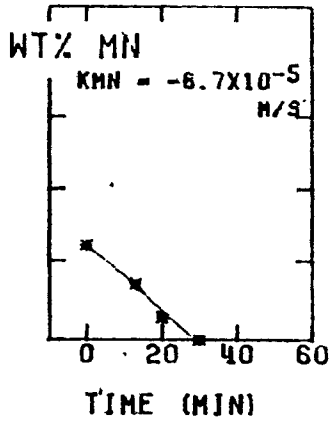

Figure 5.2.10. Values of experimental parameters, percentage copper and manganese eliminated at each sampling time and plots of natural logarithm of measured copper and manganese concentration against time for experiment 6A. The value of a rate coefficient for each measured solute are also given.

EXPERIMENT NUMBER : 6 B

MELT TEMPERATURE : 1899±14K

CRUCIBLE DIAMETER : 0.20M

CHAMBER PRESSURE : 6.7 ±0.7PA

CRUCIBLE DEPTH : 0.10M

MELT MASS : 7.2 ±0.5KG

MELT AREA TO VOLUME : 31 ±3.9/M

SAMPLE	TIME (MIN)	%CU ELIM'D	%SN ELIM'D	%MN ELIM'D	%S ELIM'D
		% CU INIT=0.629	% SN INIT=######	% MN INIT=0.001	% S INIT=######
1	0	0			
2	9	28			
3	19	65			
4	31	83			

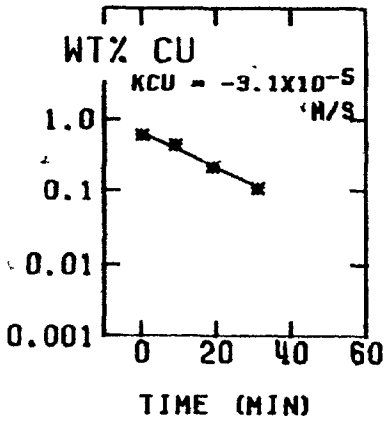

Figure 5.2.11. Values of experimental parameters, percentage copper eliminated at each sampling time and plots of natural logarithm of measured copper concentration against time for experiment 6B. The value of a rate coefficient for each measured solute are also given.

EXPERIMENT NUMBER : 6 C

MELT TEMPERATURE :1899±99K CRUCIBLE DIAMETER :0.20M

CHAMBER PRESSURE :7.4 ±0.7PA CRUCIBLE DEPTH :0.10M

MELT MASS :5.2 ±0.5KG MELT AREA TO VOLUME :43 ±5.4/M

SAMPLE	TIME (MIN)	%CU ELIM'D	%SN ELIM'D	%MN ELIM'D	%S ELIM'D
		% CU INIT:0.625	% SN INIT:######	% MN INIT:######	% S INIT:######
1	0	0			
2	8	43			

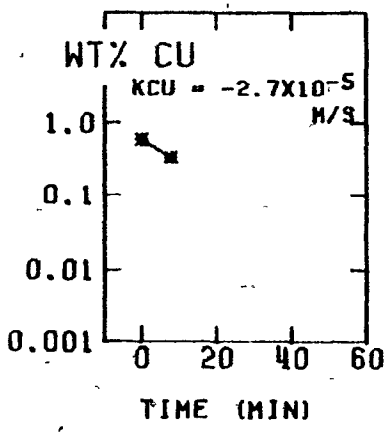

Figure 5.2.12. Values of experimental parameters, percentage copper eliminated at each sampling time and plots of natural logarithm of measured copper concentration against time for experiment 6C. The value of a rate coefficient for each measured solute are also given.

EXPERIMENT NUMBER : 7 A

MELT TEMPERATURE : 1887±32K

CHAMBER PRESSURE : 22.0±10.8A

MELT MASS : 62.3±0.5KG

CRUCIBLE DIAMETER : 0.36M

CRUCIBLE DEPTH : 0.10M

MELT AREA TO VOLUME : 7.1±0.0/M

SAMPLE	TIME (MIN)	%CU ELIM'D	%SN ELIM'D	%MN ELIM'D	%S ELIM'D
		X CU INIT:0.786	X SN INIT:******	X MN INIT:0.121	X S INIT:******
1	0	0		0	
2	12	14		31	
3	18	28		57	
4	37	36		69	

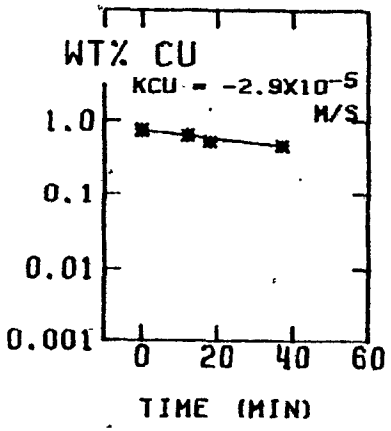

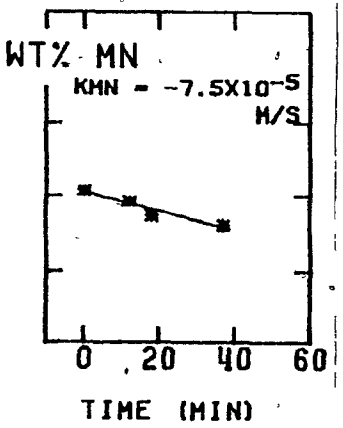

Figure 5.2.13. Values of experimental parameters, percentage copper and manganese eliminated at each sampling time and plots of natural logarithm of measured copper and manganese concentration against time for experiment 7A. The value of a rate coefficient for each measured solute are also given.

EXPERIMENT NUMBER : 7 B

MELT TEMPERATURE :1904±25K

CHAMBER PRESSURE :10.0±3.3PA

MELT MASS :60.3±0.5KG

CRUCIBLE DIAMETER :0.36M

CRUCIBLE DEPTH :0.20M

MELT AREA TO VOLUME :7.4±0.0/M

SAMPLE	TIME (MIN)	%CU ELIM'D	%SN ELIM'D	%MN ELIM'D	%S ELIM'D
		X CU INIT:0.836	X SN INIT:******	X MN INIT:0.038	X S INIT:******
1	0	0		0	
2	10	17		47	
3	21	36		71	

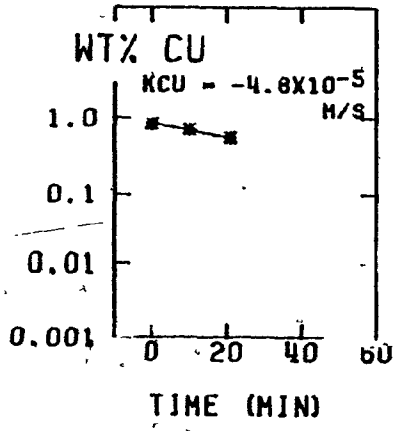

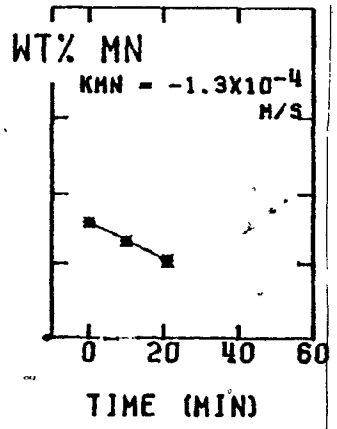

Figure 5.2.14. Values of experimental parameters, percentage copper and manganese eliminated at each sampling time and plots of natural logarithm of measured copper and manganese concentration against time for experiment 7B. The value of a rate coefficient for each measured solute are also given.

EXPERIMENT NUMBER : 7 C

MELT TEMPERATURE :1929±12K

CHAMBER PRESSURE :6.7 ±0.7PA

MELT MASS :60.3±0.5KG

CRUCIBLE DIAMETER :0.36M

CRUCIBLE DEPTH :0.20M

MELT AREA TO VOLUME :7.4±0.0/M

SAMPLE	TIME (MIN)	%CU ELIM'D	%SN ELIM'D	%MN ELIM'D	%S ELIM'D
		% CU INIT:0.466	% SN INIT:*****	% MN INIT:0.009	% S INIT:*****
1	0	0		0	
2	9	15		33	
3	20	41		67	
4	27	49		78	

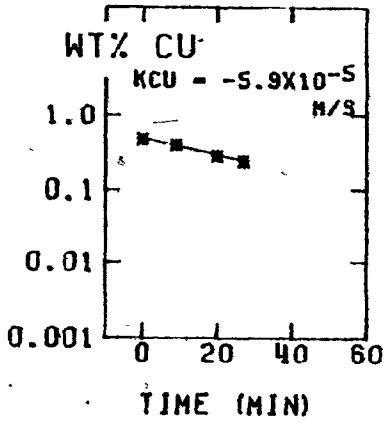

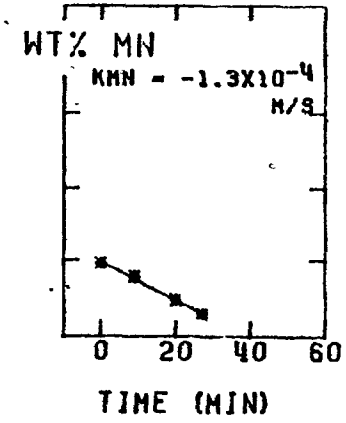

Figure 5.2.15. Values of experimental parameters, percentage copper and manganese eliminated at each sampling time and plots of natural logarithm of measured copper and manganese concentration against time for experiment 7C. The value of a rate coefficient for each measured solute are also given.

EXPERIMENT NUMBER : 7 D

MELT TEMPERATURE : 1951±50K

CHAMBER PRESSURE : 25.3±12.8A

MELT MASS : 58.3±0.5KG

CRUCIBLE DIAMETER : 0.36M

CRUCIBLE DEPTH : 0.20M

MELT AREA TO VOLUME : 7.6±0.0/M

SAMPLE	TIME (MIN)	%CU ELIM'D	%SN ELIM'D	%MN ELIM'D	%S ELIM'D
		% CU INIT: 0.428	% SN INIT: ######	% MN INIT: 0.003	% S INIT: ######
1	0	0		0	
2	12	33		33	
3	20	37		67	

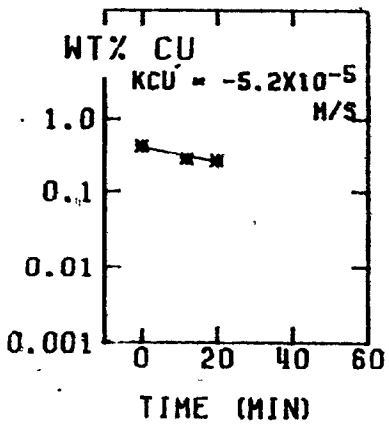

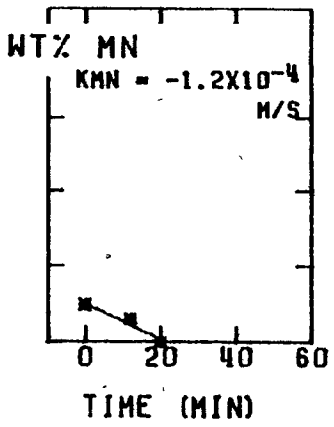

Figure 5.2.16. Values of experimental parameters, percentage copper and manganese eliminated at each sampling time and plots of natural logarithm of measured copper and manganese concentration against time for experiment 7D. The value of a rate coefficient for each measured solute are also given.

EXPERIMENT NUMBER : 8 A

MELT TEMPERATURE : 1969±13K

CRUCIBLE DIAMETER : 0.20M

CHAMBER PRESSURE : 11.0±3.0PA

CRUCIBLE DEPTH : 0.20M

MELT MASS : 29.5±0.5KG

MELT AREA TØ VØLUME : 7.5±0.3/M

SAMPLE	TIME (MIN)	%CU ELIM'D	%SN ELIM'D	%MN ELIM'D	%S ELIM'D
		% CU INIT=0.150	% SN INIT=0.100	% MN INIT=0.570	% S INIT=0.048
1	0	0	0	0	0
2	10	27	20	65	10
3	22	53	43	98	23
4	32	68	64	97	42
5	41	76	71	100	46

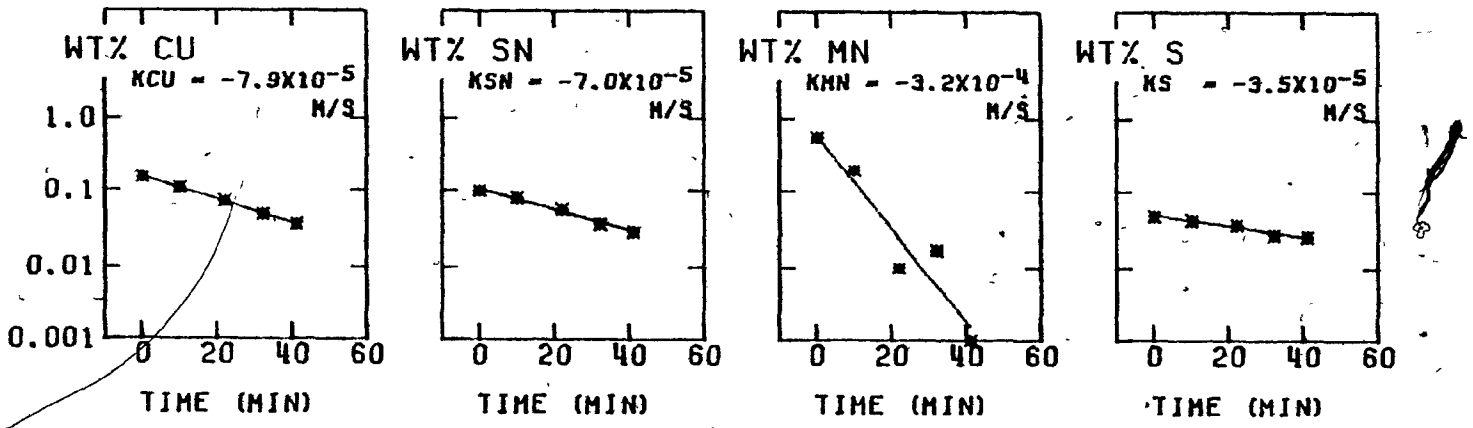

Figure 5.2.17. Values of experimental parameters, percentage copper, tin, manganese and sulphur eliminated at each sampling time and plots of natural logarithm of measured copper, tin, manganese and sulphur concentration against time for experiment 8A. The value of a rate coefficient for each measured solute are also given.

EXPERIMENT NUMBER : 8 B

MELT TEMPERATURE :1960±15K CRUCIBLE DIAMETER :0.20M

CHAMBER PRESSURE :5.3 ±1.3PA CRUCIBLE DEPTH :0.20M

MELT MASS :27.5±0.5KG MELT AREA TO VOLUME :8.1±0.3/M

SAMPLE	TIME (MIN)	%CU ELIM'D	%SN ELIM'D	%MN ELIM'D	%S ELIM'D
		% CU INIT:0.148	% SN INIT:0.117	% MN INIT:******	% S INIT:0.016
1	0	0	0		0
2	11	23	13		25
3	20	45	29		25

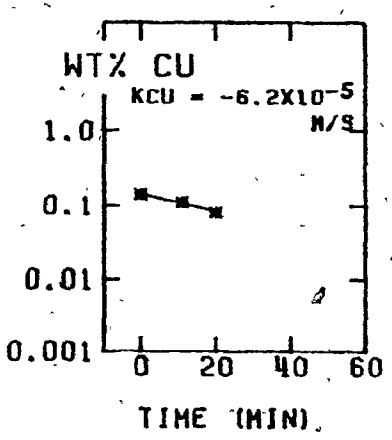

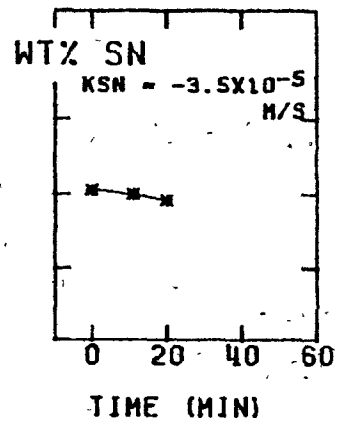

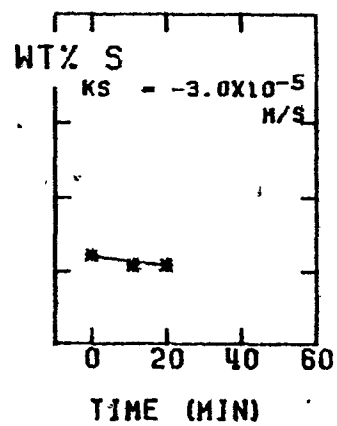

Figure 5.2.18. Values of experimental parameters, percentage copper, tin and sulphur eliminated at each sampling time and plots of natural logarithm of measured copper, tin and sulphur concentration against time for experiment 8B. The value of a rate coefficient for each measured solute are also given.

EXPERIMENT NUMBER : 8 C

MELT TEMPERATURE :1958±10K CRUCIBLE DIAMETER :0.20M

CHAMBER PRESSURE :4.6 ±0.5PA CRUCIBLE DEPTH :0.20M

MELT MASS :27.5±0.5KG MELT AREA TO VOLUME :8.1±0.3/M

SAMPLE	TIME (MIN)	%CU ELIM'D	%SN ELIM'D	%MN ELIM'D	%S ELIM'D
		% CU INIT:0.071	% SN INIT:0.082	% MN INIT:******	% S INIT:0.011
1	0	0	0		0
2	12	24	22		18

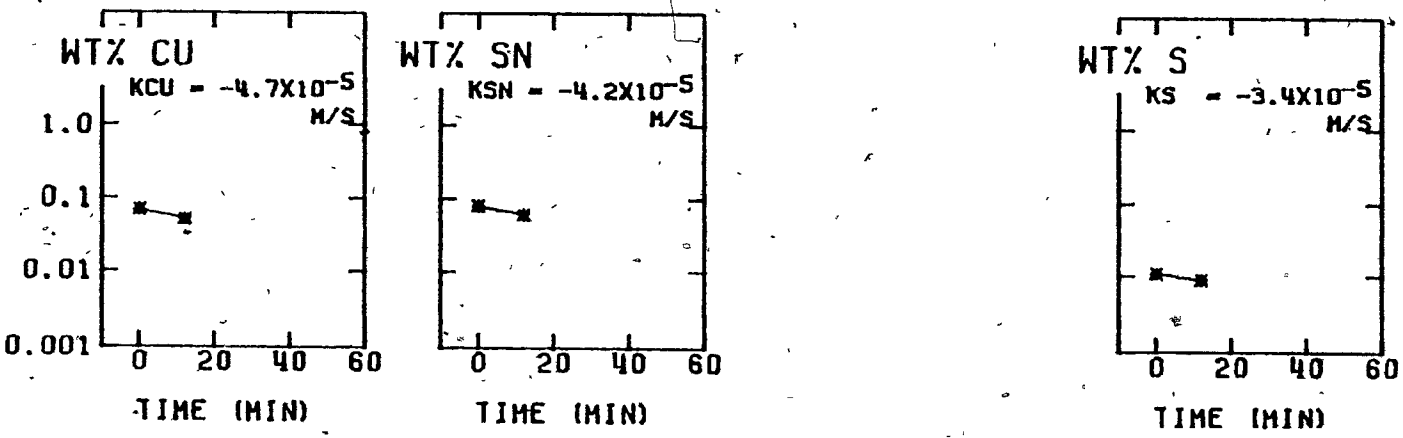

Figure 5.2.19. Values of experimental parameters, percentage copper, tin and sulphur eliminated at each sampling time and plots of natural logarithm of measured copper, tin and sulphur concentration against time for experiment 8C. The value of a rate coefficient for each measured solute are also given.

EXPERIMENT NUMBER : 8 D

MELT TEMPERATURE : 1958±10K

CRUCIBLE DIAMETER : 0.20M

CHAMBER PRESSURE : 32.5±7.5PA

CRUCIBLE DEPTH : 0.20M

MELT MASS : 25.5±0.5KG

MELT AREA TO VOLUME : 8.7±0.3/M

SAMPLE	TIME (MIN)	%CU ELIM'D	%SN ELIM'D	%MN ELIM'D	%S ELIM'D
		% CU INIT:0.580	% SN INIT:******	% MN INIT:******	% S INIT:0.009
1	0	0			0
2	11	23			11
3	21	34			22

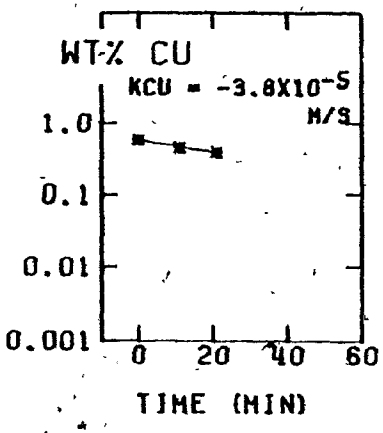

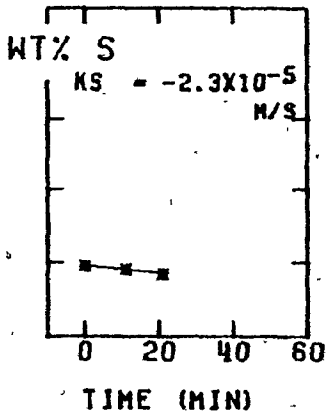

Figure 5.2.20. Values of experimental parameters, percentage copper and sulphur eliminated at each sampling time and plots of natural logarithm of measured copper and sulphur concentration against time for experiment 8D. The value of a rate coefficient for each measured solute are also given.

EXPERIMENT NUMBER : 9 A

MELT TEMPERATURE : 2010±40K

CRUCIBLE DIAMETER : 0.20M

CHAMBER PRESSURE : 26.7±2.7PA

CRUCIBLE DEPTH : 0.20M

MELT MASS : 36.4±0.5KG

MELT AREA TO VOLUME : 6.1±0.2/M

SAMPLE	TIME (MIN)	%CU ELIM'D	%SN ELIM'D	%MN ELIM'D	%S ELIM'D
		% CU INIT:0.239	% SN INIT:0.088	% MN INIT:0.460	% S INIT:0.040
1	0	0	0	0	0
2	9	42	18	88	22
3	19	67	59	96	45
4	34	78	77	98	50

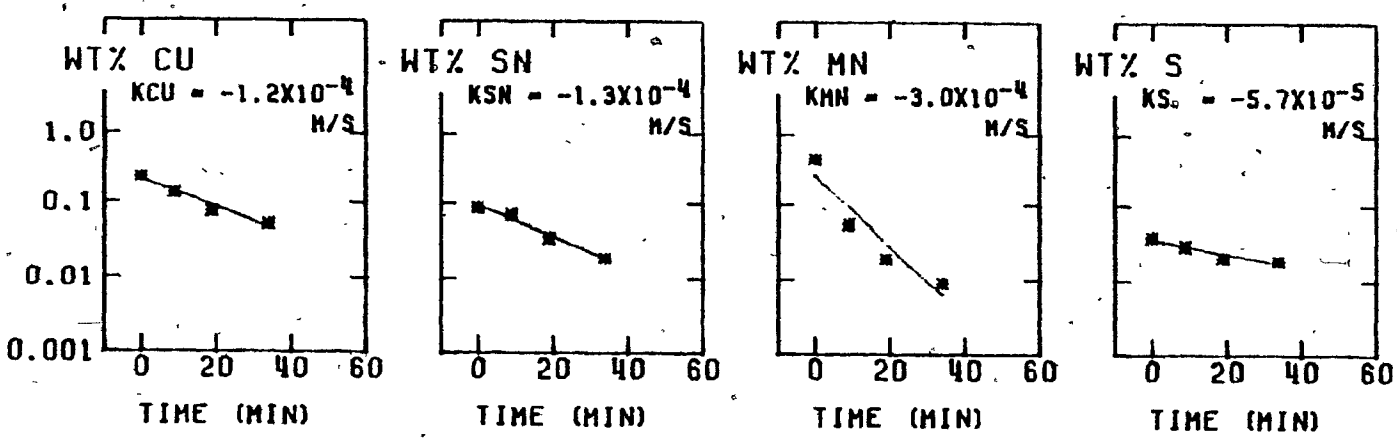

Figure 5.2.21. Values of experimental parameters, percentage copper, tin, manganese and sulphur eliminated at each sampling time and plots of natural logarithm of measured copper, tin, manganese and sulphur concentration against time for experiment 9A. The value of a rate coefficient for each measured solute are also given.

EXPERIMENT NUMBER : 9 B

MELT TEMPERATURE :2006±17K

CHAMBER PRESSURE :12.0±1.3PA

MELT MASS :34.4±0.5KG

CRUCIBLE DIAMETER :0.20M

CRUCIBLE DEPTH :0.20M

MELT AREA TO VOLUME :6.5±0.2/M

SAMPLE	TIME (MIN)	%CU ELIM'D	%SN ELIM'D	%MN ELIM'D	%S ELIM'D
		% CU INIT:0.181	% SN INIT:0.106	% MN INIT:0.016	% S INIT:0.018
1	0	0	0	0	0
2	8	29	25	75	28
3	16	55	34	13	28
4	26	74	57	81	39
5	35	81	60	50	44

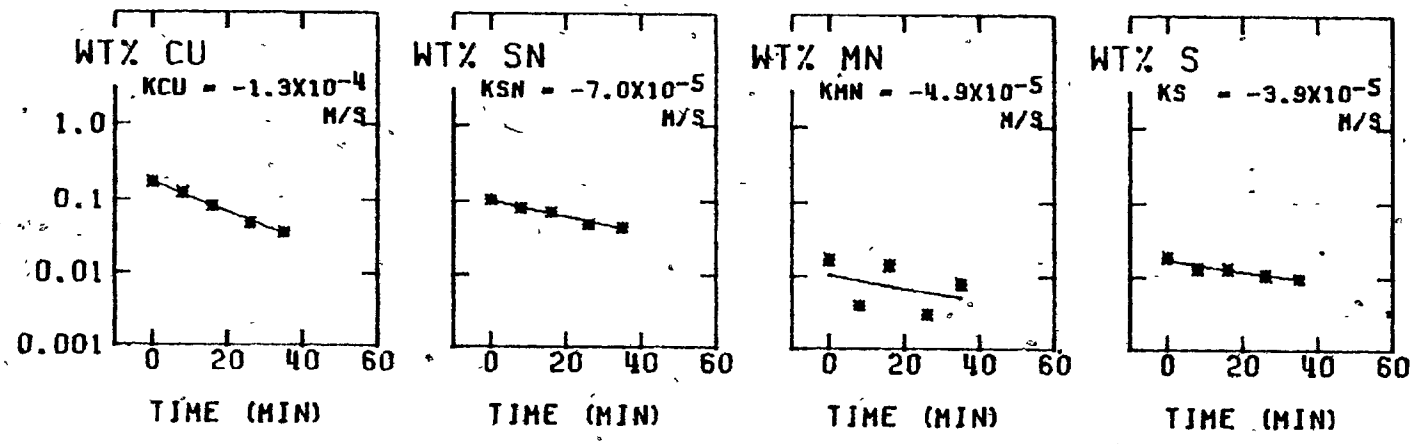

Figure 5.2.22. Values of experimental parameters, percentage copper, tin, manganese and sulphur eliminated at each sampling time and plots of natural logarithm of measured copper, tin, manganese and sulphur concentration against time for experiment 9B. The value of a rate coefficient for each measured solute are also given.

EXPERIMENT NUMBER : 9 C

MELT TEMPERATURE :1792±14K CRUCIBLE DIAMETER :0.20M

CHAMBER PRESSURE :8.7 ±2.0PA CRUCIBLE DEPTH :0.20M

MELT MASS :32.4±0.5KG MELT AREA TO VOLUME :6.9±0.2/M

SAMPLE	TIME (MIN)	%CU ELIM'D	%SN ELIM'D	%MN ELIM'D	%S ELIM'D
		% CU INIT:0.277	% SN INIT:0.135	% MN INIT:0.009	% S INIT:0.008
1	0	0	0	0	0
2	8	2	-1	0	-12
3	16	-1	-4	-111	-12
4	30	3	4	89	0

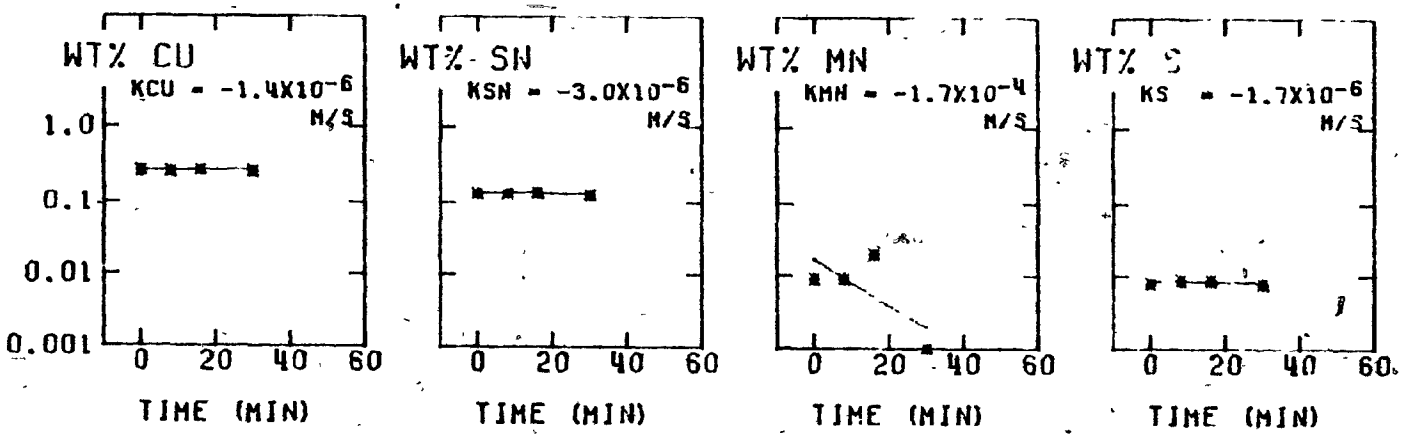

Figure 5.2.23. Values of experimental parameters, percentage copper, tin, manganese and sulphur eliminated at each sampling time and plots of natural logarithm of measured copper, tin, manganese and sulphur concentration against time for experiment 9C. The value of a rate coefficient for each measured solute are also given. Experiment deliberately carried out with slag covering.

EXPERIMENT NUMBER : 9 D

MELT TEMPERATURE : 1937±12K

CRUCIBLE DIAMETER : 0.20M

CHAMBER PRESSURE : 7.3 ±0.7PA

CRUCIBLE DEPTH : 0.20M

MELT MASS : 32.4±0.5KG

MELT AREA TO VOLUME : 6.9±0.2/M

SAMPLE	TIME (MIN)	%CU ELIM'D	%SN ELIM'D	%MN ELIM'D	%S ELIM'D
		% CU INIT:0.184	% SN INIT:0.132	% MN INIT:0.007	% S INIT:0.008
1	0	0	0	0	0
2	10	26	2	86	25
3	20	44	11	86	25
4	31	57	21	86	25

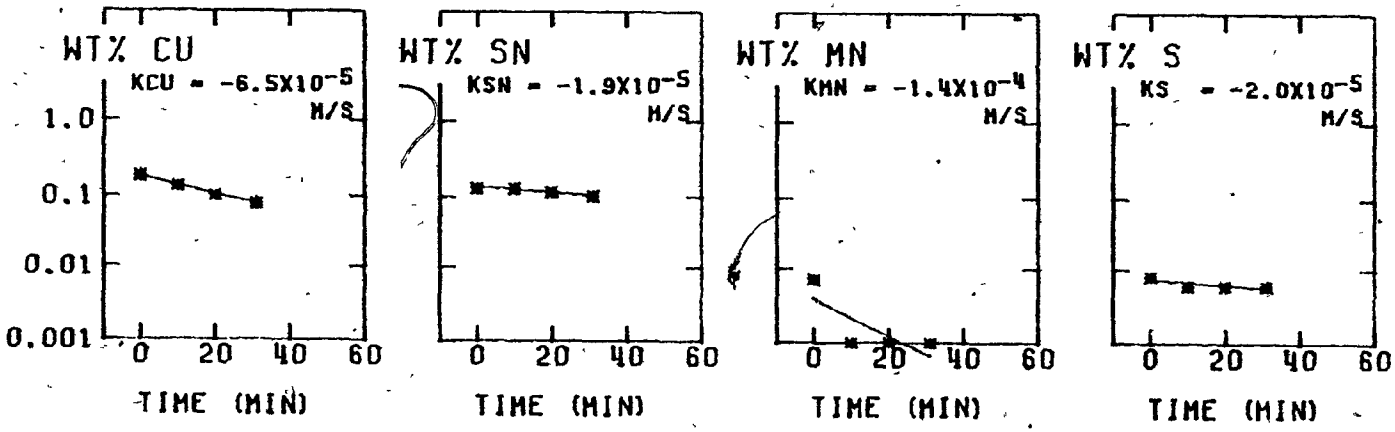

Figure 5.2.24. Values of experimental parameters, percentage copper, tin, manganese and sulphur eliminated at each sampling time and plots of natural logarithm of measured copper, tin, manganese and sulphur concentration against time for experiment 9D. The value of a rate coefficient for each measured solute are also given.

EXPERIMENT NUMBER : 10A

MELT TEMPERATURE : 1975±20K CRUCIBLE DIAMETER : 0.20M

CHAMBER PRESSURE : 14.6±1.5PA CRUCIBLE DEPTH : 0.20M

MELT MASS : 36.4±0.5KG MELT AREA TO VOLUME : 6.1±0.2/M

SAMPLE	TIME (MIN)	%CU ELIM'D	%SN ELIM'D	%MN ELIM'D	%S ELIM'D
		% CU INIT:0.205	% SN INIT:0.090	% MN INIT:0.450	% S INIT:*****
1	0	0	0	0	
2	11	25	18	66	
3	31	62	49	96	
4	41	70	65	94	
5	46	76	70	98	

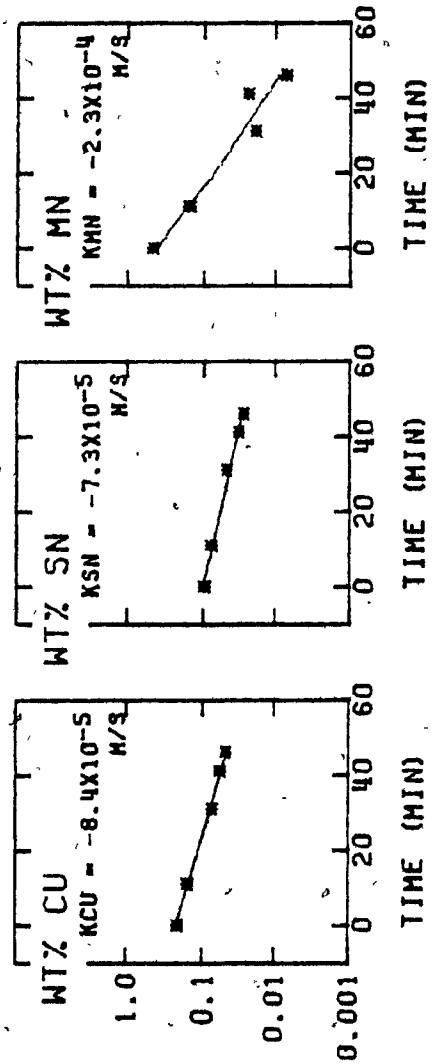

Figure 5.2.25. Values of experimental parameters, percentage copper, tin and manganese eliminated at each sampling time and plots of natural logarithm of measured copper, tin and manganese concentration against time for experiment 10A. The value of a rate coefficient for each measured solute are also given.

EXPERIMENT NUMBER : 10B

MELT TEMPERATURE : 1788±30K

CRUCIBLE DIAMETER : 0.20M

CHAMBER PRESSURE : 14.0±1.4PA

CRUCIBLE DEPTH : 0.20M

MELT MASS : 34.4±0.5KG

MELT AREA TO VOLUME : 6.5±0.2/M

SAMPLE	TIME (MIN)	%CU ELIM'D	%SN ELIM'D	%MN ELIM'D	%S ELIM'D
		% CU INIT:0.074	% SN INIT:0.083	% MN INIT:0.003	% S INIT:0.013
1	0	0	0	0	0
2	10	-1	-5	-300	-8
3	23	0	1	-100	-23
4	34	0	-1	33	-31

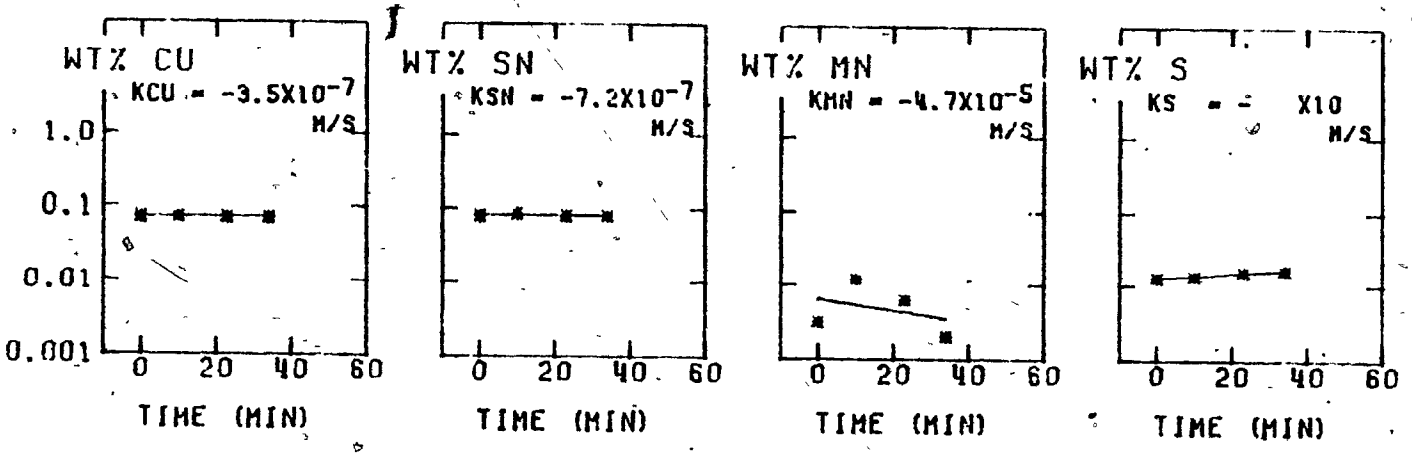

Figure 5.2.26. Values of experimental parameters, percentage copper, tin, manganese and sulphur eliminated at each sampling time and plots of natural logarithm of measured copper, tin, manganese and sulphur concentration against time for experiment 10B. The value of a rate coefficient for each measured solute are also given.

EXPERIMENT NUMBER : 11A

MELT TEMPERATURE :1984±23K

CRUCIBLE DIAMETER :0.20M

CHAMBER PRESSURE :7.0 ±0.7PA

CRUCIBLE DEPTH :0.20M

MELT MASS :34.4±0.5KG

MELT AREA TO VOLUME :6.5±0.2/M

SAMPLE	TIME (MIN)	%CU ELIM'D	%SN ELIM'D	%MN ELIM'D	%S ELIM'D
		% CU INIT:0.294	% SN INIT:0.034	% MN INIT:0.016	% S INIT:0.022
1	0	0	0	0	0
2	10	34	35	69	9
3	20	52	47	75	23
4	30	66	62	6	23

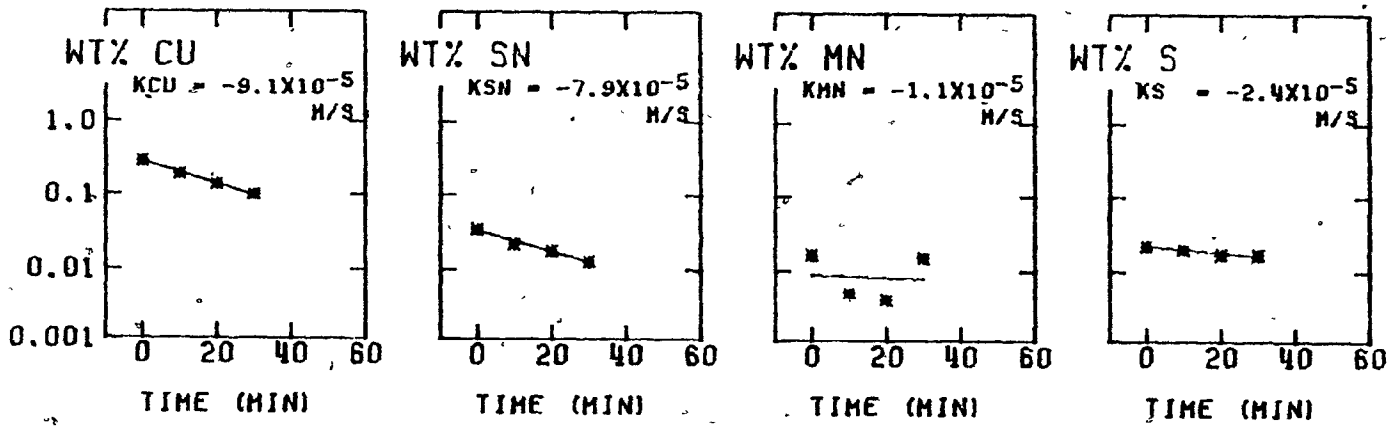

Figure 5.2.27. Values of experimental parameters, percentage copper, tin, manganese and sulphur eliminated at each sampling time and plots of natural logarithm of measured copper, tin, manganese and sulphur concentration against time for experiment 11A. The value of a rate coefficient for each measured solute are also given.

EXPERIMENT NUMBER : 11B

MELT TEMPERATURE : 1984±23K

CRUCIBLE DIAMETER : 0.20M

CHAMBER PRESSURE : 7.0 ±0.7PA

CRUCIBLE DEPTH : 0.20M

MELT MASS : 34.4±0.5KG

MELT AREA TØ VØLUME : 6.5±0.2/M

SAMPLE	TIME (MIN)	%CU ELIM'D	%SN ELIM'D	%MN ELIM'D	%S ELIM'D
		% CU INIT=0.294	% SN INIT=0.034	% MN INIT=0.016	% S INIT=0.022
1	0	0	0	0	0
2	10	34	35	69	9
3	20	52	47	75	23
4	30	66	62	6	23

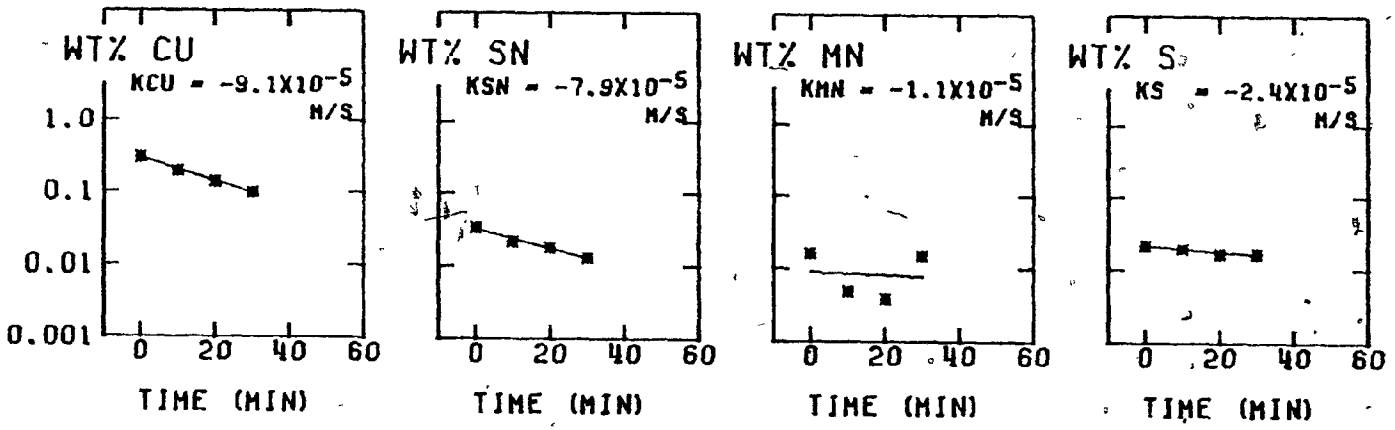

Figure 5.2.28. Values of experimental parameters, percentage copper, tin, manganese and sulphur eliminated at each sampling time and plots of natural logarithm of measured copper, tin, manganese and sulphur concentration against time for experiment 11B. The value of a rate coefficient for each measured solute are also given.

EXPERIMENT NUMBER : 12A

MELT TEMPERATURE :1992±17K

CHAMBER PRESSURE :10.0±3.3PA

MELT MASS :36.4±0.5KG

CRUCIBLE DIAMETER :0.20M

CRUCIBLE DEPTH :0.20M

MELT AREA TO VOLUME :6.1±0.2/M

SAMPLE	TIME (MIN)	%CU ELIM'D	%SN ELIM'D	%MN ELIM'D	%S ELIM'D
		% CU INIT:0.230	% SN INIT:0.095	% MN INIT:******	% S INIT:0.029
1	0	0	0		0
2	15	17	7		10

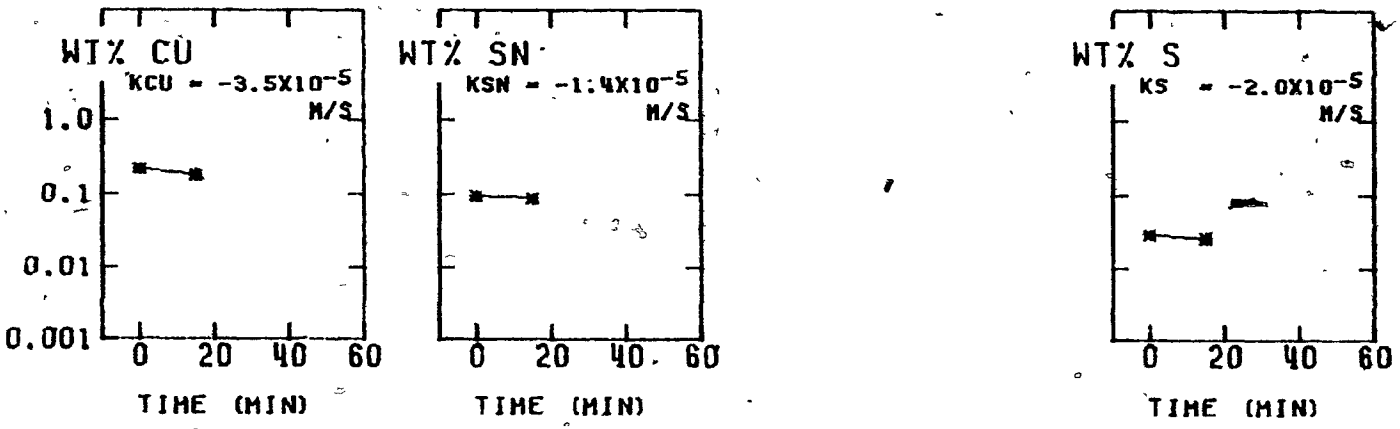

Figure 5.2.29. Values of experimental parameters, percentage copper, tin and sulphur eliminated at each sampling time and plots of natural logarithm of measured copper, tin and sulphur concentration against time for experiment 12A. The value of a rate coefficient for each measured solute are also given.

CHAPTER SIX

PHOTOGRAPHIC STUDIES

SECTION 6.1. : INTRODUCTION

This chapter presents photographs taken of the liquid metal under vacuum and of the flow of metal vapour in the chamber space above the induction furnace. Still 35 mm photographs and selected frames from 16 mm cine films are shown.

SECTION 6.2. : LIQUID METAL UNDER VACUUM

Three phenomena were photographed:

(a) slags and films on the liquid metal surface,

(b) melt turbulence due to induction stirring

and,

(c) gas bubble evolution and bursting due melt boiling.

6.2.1. : SLAGS AND SURFACE FILMS

The surface of the liquid steel was always covered by a bulky coherent slag at the time the steel charge was just fully molten. Figure 6.2.1 shows part of this slag. The pattern of

outward radiating lines was due to a jet of argon directed at the center of the charge during melting.

This bulky slag dissipated or was splashed off during the time the melt was being superheated to run temperature and left behind only a thin film on the liquid metal surface (Figure 6.2.2). This latter film broke up along the boundaries which can be seen in Figure 6.2.2. It receded towards the edge of the melt when the furnace power was on due to the convex shape of the melt surface caused by the induction field, Figure 6.2.3.

The film eventually broke up into small particles which moved about on the melt surface. With the furnace power on, they also remained near the melt edge and were disturbed only by induction stirring and bubble evolution. Figure 6.2.4 shows the nature of the film at this stage.

Figures 6.2.5 and 6.2.6 show the complete melt surface. The former shows about 30% clear surface and the latter shows 100% clear surface for evaporation which was the condition of the melt when additions of copper or copper and tin were made. This condition was maintained for the remainder of the quantitative elimination experiment. These photographs also indicate the manner in which metal vapour condensed on the crucible walls. They were taken during a preliminary run in which the crucible height had not been reduced.

Figure 6.2.1. Photograph of slag present on surface of liquid steel just after it had melted. Photograph taken through one of the observation ports atop the chamber. Black shadows are due to radiation shield obstructing view. Pattern in the slag was caused by a jet of argon impinging the surface at the upper left of the photograph (magnification: X 0.5).

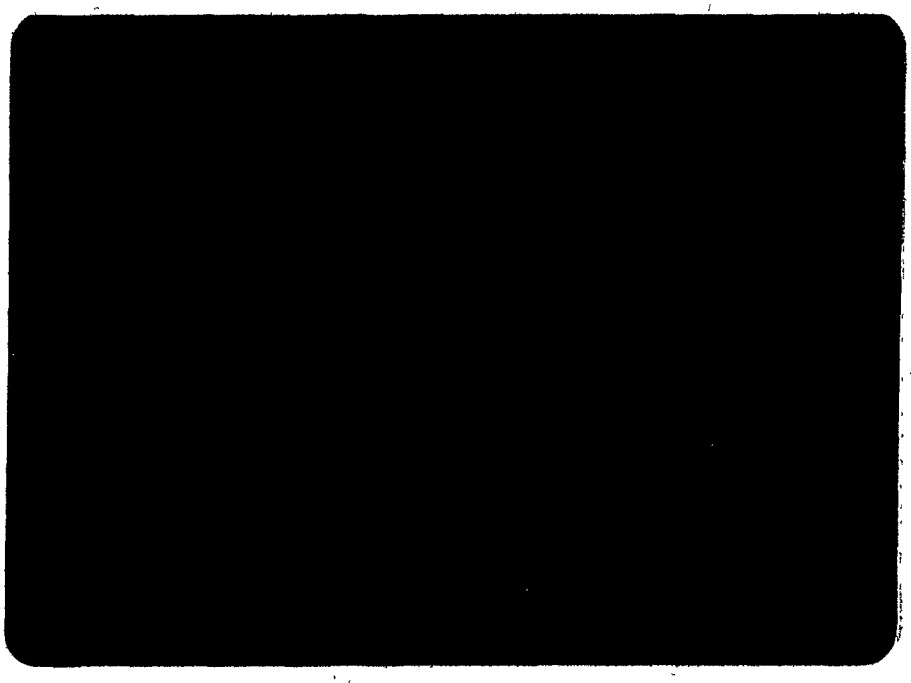

Figure 6.2.2. Part of the melt surface and a portion of the crucible wall. Points to note are the material which has splashed and frozen onto the crucible wall (top of photograph) and the thin film broken by many fissures on the melt surface (magnification: X 0.5).

Figure 6.2.3. Portion of the melt surface and part of the crucible wall. There had been very little splashing up to the time this photograph was taken, ie., the crucible wall is almost clean. The film on the melt surface can be seen to have broken up and receded to periphery of the melt (magnification: X 0.5).

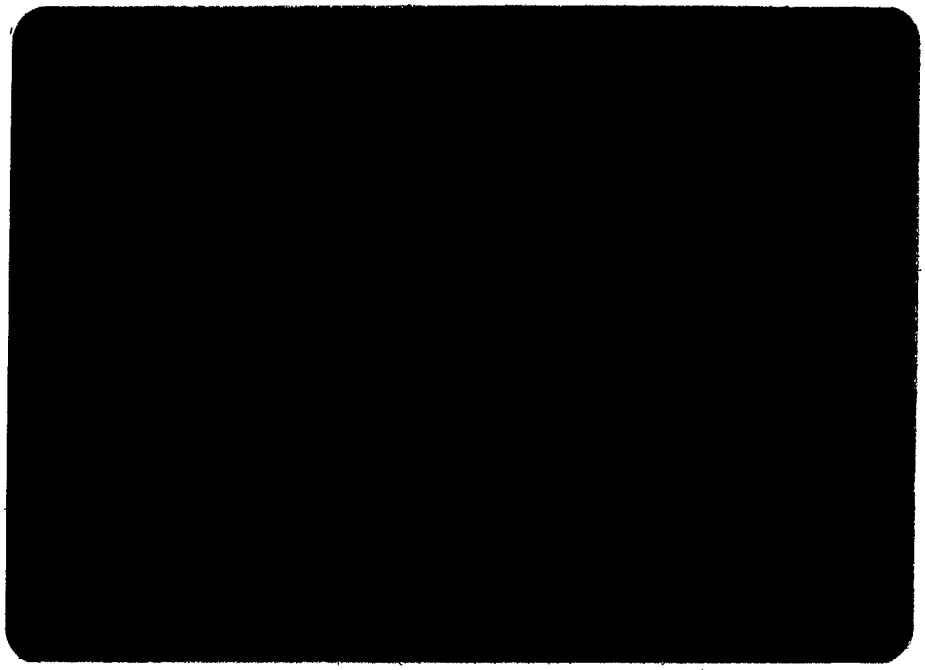

Figure 6.2.4. A portion of the melt surface. The film had fully broken up and lay around the melt edge. Melt turbulence, apparently due to gas bubble evolution, is visible at the top of the figure (magnification: X 0.5).

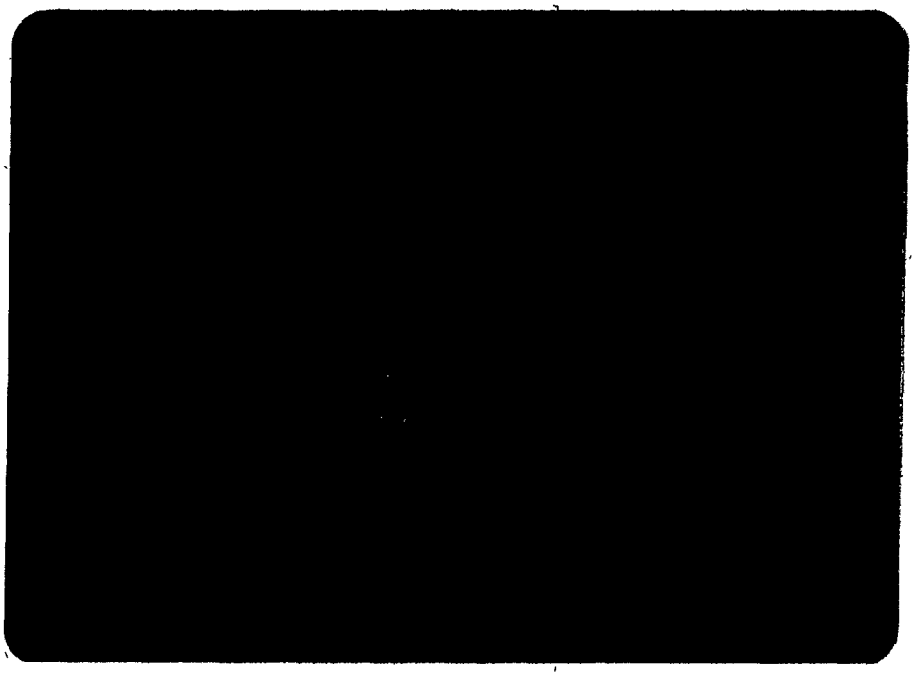

Figure 6.2.5. The entire melt surface as well as part of the crucible wall. About 30% of the melt was clear at this time. A point to note is the buildup of condensed material on the walls of the crucible, especially the right hand side. This photograph was taken during a preliminary run (magnification: X 0.3).

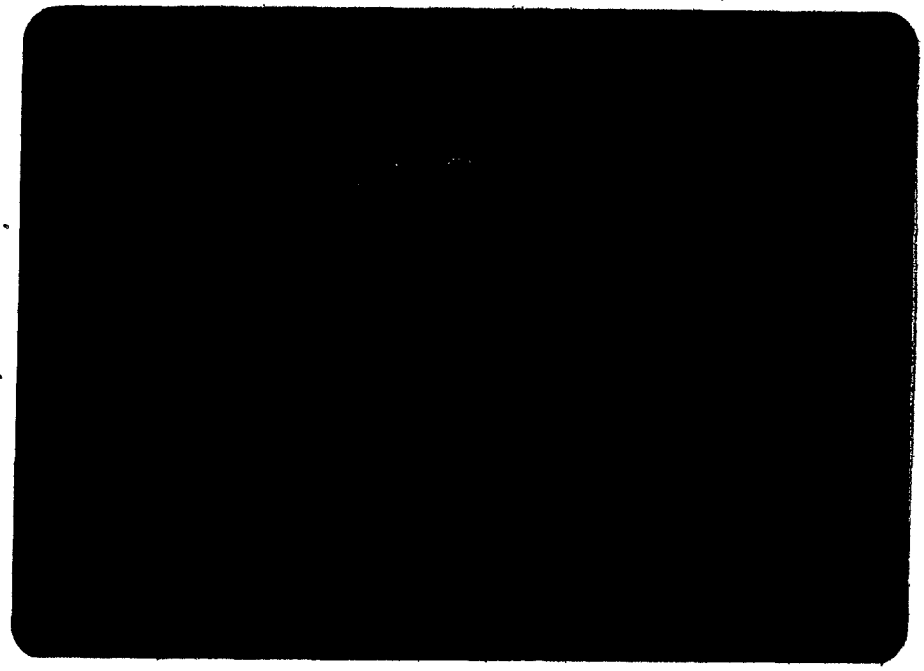

Figure 6.2.6. Condition of the melt surface typical of that during a qualitative vacuum distillation experiment. The buildup on the crucible wall can be seen once again (magnification: X 0.3).

6.2.2. : MELT TURBULENCE

The movement of the melt surface can be seen in Figure 6.2.4 as indicated by the blur of the particles on the melt surface. It was estimated that the surface was moving at 2 mm per 1/500 second (exposure time) in the vicinity of the gas bubble eruption which caused the movement in this instance.

A motor effect is generated in liquid metal which is directly heated by an induction field. In the present apparatus, this effect was so great that the forces generated by high power inputs on small melt masses physically lifted the liquid steel out of the crucible.

Figure 6.2.7 shows a sequence from a cine film of experiment 6C in which the melt depth was 2 cm and the furnace power was 60 kW at the time the photographs were taken. It can be seen that the liquid steel was levitated out of the crucible. Other photographs (not presented), showed that the liquid then fell back either into the liquid steel or onto the crucible walls washing the vapour which had condensed onto the crucible walls back into the melt. This example of condensate refluxing occurred only in experiments with very high melt area to volume ratios (approximately 40/m), ie., Experiments 5A to 6C.

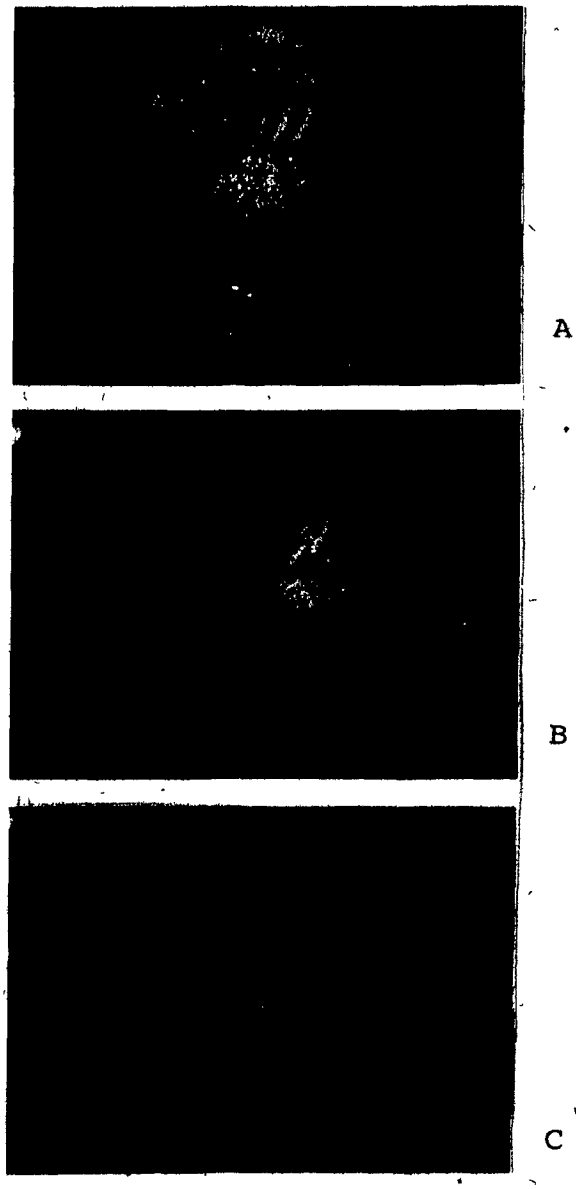

Figure 6.2.7. Series of frames taken from a cine film (500 frames per second) showing typical behaviour of a shallow melt. Under these conditions (2 cm depth, 50kW power input, Experiment 6C), liquid metal is levitated out of the the melt to a height of 25 cm (top of photograph). After a number of such eruptions the entire melt had been splashed out of the crucible (magnification: X 0.2).

6.2.3. : GAS BUBBLE EVOLUTION

Photographs presented in this section were taken from cine films of an experiment in which large bubbles formed on the melt surface and burst.

The films showed bubbles growing to a diameter of about 10 cm in about a tenth of a second. The last stages of the growth of a bubble and its rupture is presented in Figure 6.2.8. Dark spots where localized cooling occured are noticeable in the sequence. It can be seen that the bubble ruptured at the areas of localized cooling on the top portion of the bubble surface. Bubbles also ruptured at the liquid metal - bubble interface, however, it was not clear which of these locations predominated.

A second sequence, Figure 6.2.9, shows the induction furnace from the side and was taken at 100 frames per second through the observation port in the vacuum chamber door. Only large bubbles which protruded above the level of the induction furnace are visible from this view. In this sequence, it can be seen that rupture first occurred on the right hand side. A second rupture can be seen on the top left hand side in the second picture in the series.

Measurements taken from the cine films showed that the time for bubble rupture and dissipation was about 0.012 seconds. The volume of the bubbles was estimated to be 100 to 500 cm3 and the formation frequency to be about 4 per second.

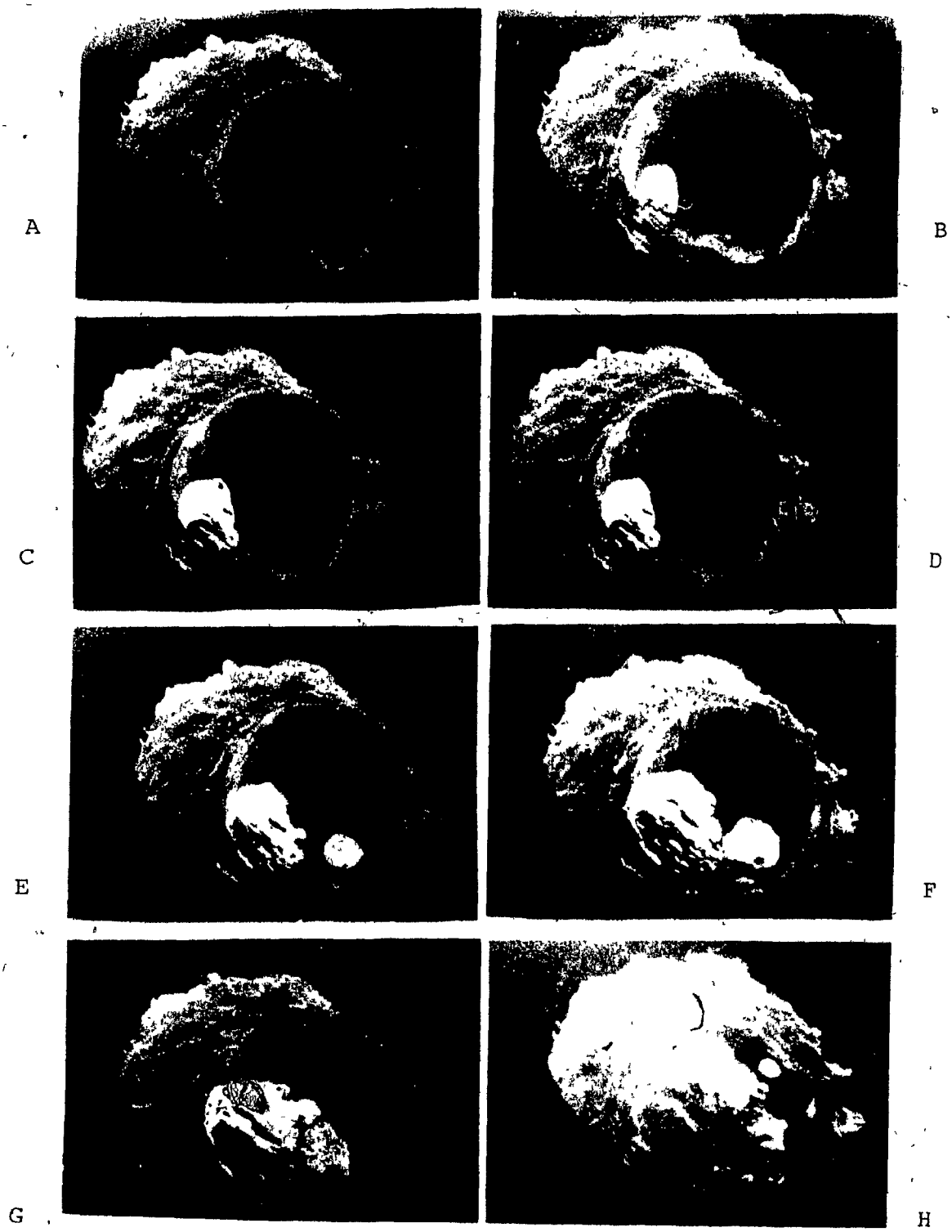

Figure 6.2.8. Sequence of frames 0.002 seconds apart showing a bubble bursting at the melt-vacuum surface (1900 K, 7 Pa chamber pressure). Rupture of the metal film covering the bubble is seen to originate at dark spots (perhaps areas of thinning) on the bubble surface, frames D, E and H. The bubble is thought to be due to melt boiling (magnification: X 0.2).

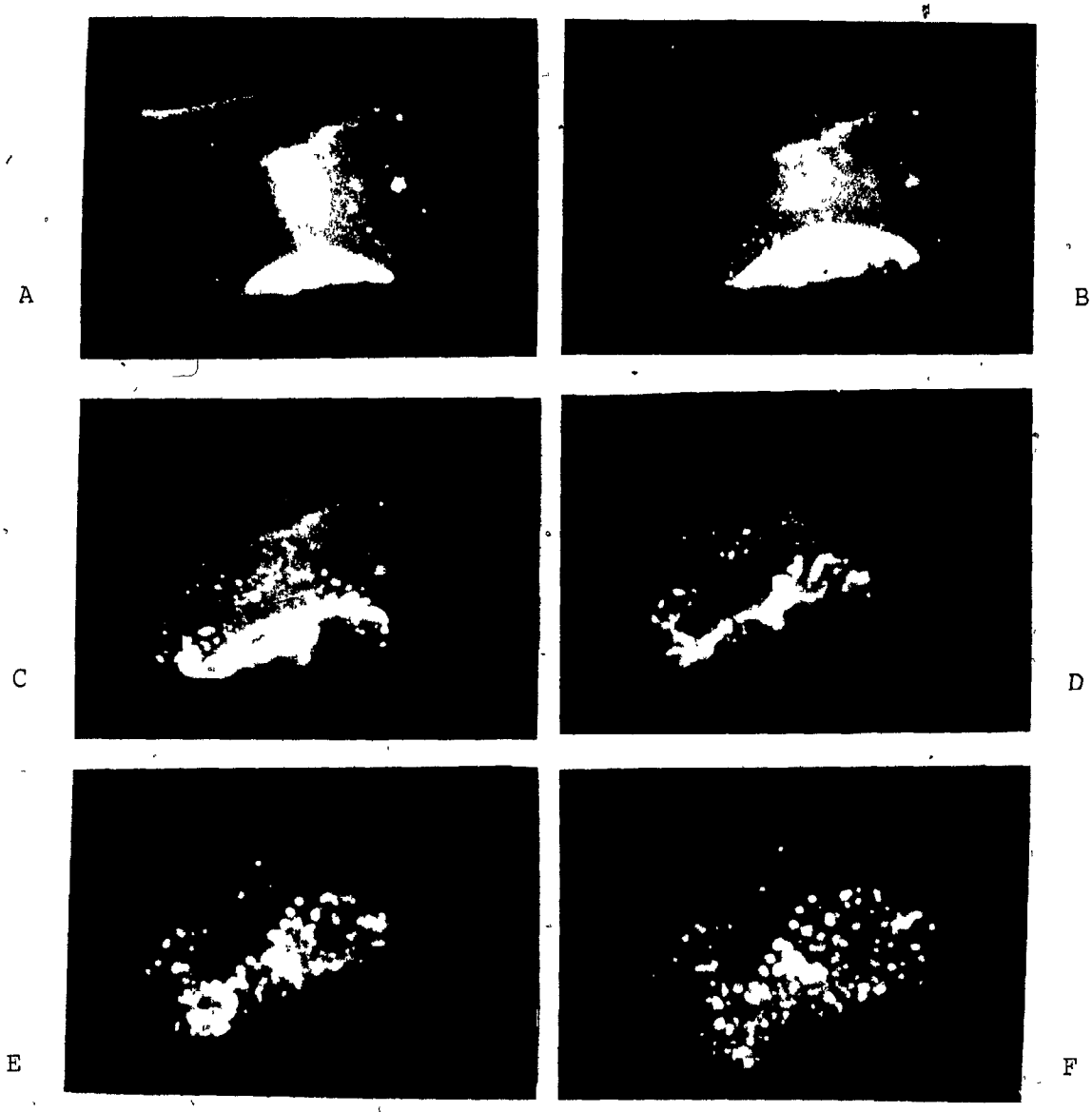

Figure 6.2.9. Disintegration of a large bubble extending above the level of the induction furnace housing. Metal droplets formed from the film of metal originally covering the bubble are readily seen (magnification: X 0.2).

SECTION 6.3. : METAL VAPOUR FLOW IN VACUUM

Photographs presented in this section were taken through the observation port in the chamber door. They show behaviour of material which evaporated from the liquid steel under various conditions of pressure, melt temperature, surface coverage and composition of the chamber atmosphere.

Chamber atmosphere which was initially clean argon (at about 1 atm.) became clouded with fume which evolved from the crucible contents during heating and melting the charge. The density of this fume decreased as the chamber was evacuated until the chamber gas space was completely transparent (Figure 6.3.1) in which slag fully covered the melt at the time of the photograph. As a result, there was very little material emanating from the crucible.

Superheating the melt under vacuum caused the surface film to dissipate and leave clean melt surface free for evaporation. Figure 6.3.2 shows streams of metal vapour evolving from the parts of the melt surface which had cleared at the time this photograph was taken. When the surface was completely clear the stream of metal vapour was uniform from the whole surface (Figures 6.3.3). These streams of vapour were seen under normal vacuum distillation conditions.

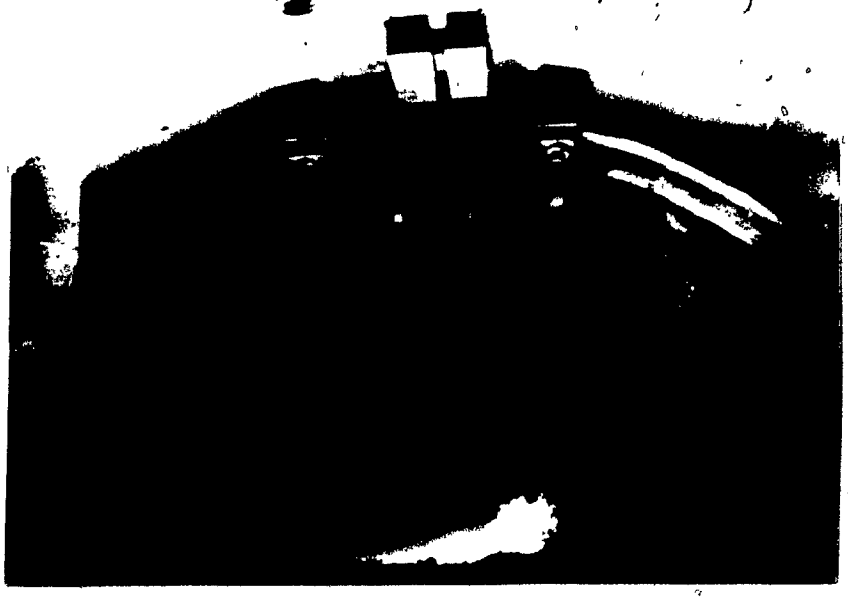

Figure 6.3.1. Interior of the vacuum chamber with experiment in progress. The conditions at the time were: (i) melt temperature = 1900 K, (ii) melt surface covered with slag and (iii) chamber pressure = 5 pascals. The furnace tilting mechanism can be seen at top center, the outlet to the pumps at center right, a thermocouple assembly in foreground and an additions shute at center left. The top of the induction furnace housing is shown at lower foreground center.

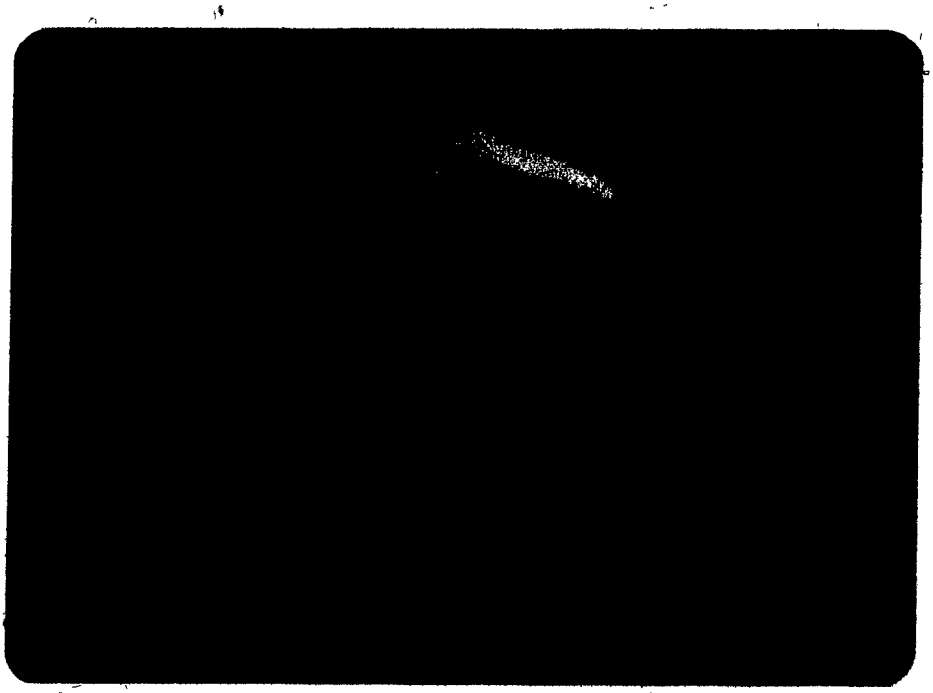

Figure 6.3.2. Interior of the chamber as it was set up for runs without the outlet extension in place. Metal vapour is streaming from a small patch of clear surface on the right of the melt surface (melt temperature 1950 K, chamber pressure less than 15 pascals).

Figure 6.3.3. Flow of metal vapour when the surface was clear of any film or slag. This form is typical of that observed during experiments in which melt temperatures were over 1950 K and chamber pressure was less than 15 pascals. This form of the vapour flow has been designated the 'EXTENDED MUSHROOM'.

Figure 6.3.4. Metal vapour flow had this form when (i) chamber pressure was about 14 pascals, (ii) the melt surface was fully clear and (iii) there was a small amount of air inleakage into the chamber. This shape of the metal vapour flow has been designated the 'SHORT MUSHROOM'. It was an intermediate form to the 'TALL MUSHROOM' (Figure 6.3.5) and the 'COMPRESSED MUSHROOM' (Figure 6.3.7).

At slightly higher chamber pressures (about 14 pascals) the stream did not reach the roof and a 'mushroom' shaped auroa formed (Figure 6.3.4). At an intermediate pressure the mushroom was taller but still did not reach the roof (Figure 6.3.5). At higher pressures (greater than 16 pascals), the mushroom was compressed below lip of the crucible and no longer visible. A different form of the metal vapour flow was seen at these pressures (Figure 6.3.6).

The transition from tall mushroom to no mushroom and back again is shown in Figures 6.3.7 and 6.3.8. Figure 6.3.7 shows the compression of the mushroom when a valve on the top of the chamber was opened admitting a small flow of air into the pumping system (raising chamber pressure from 13 pascals to 16 pascals). Figure 6.3.8 shows the effect of closing the valve.

The flow of metal vapour has the form shown in Figure 6.3.9 at much higher chamber pressures (- 1000 pascals). This photograph was taken when there was no pumping. The material evolving at this high pressure formed into stable vortices as it was removed from the chamber when the pumps were restarted (Figure 6.3.10). The material in the vortices was of a different nature to that observed close to the crucible at lower pressures, however, they were observed to coexist (Figure 6.3.11 - 15 pascals).

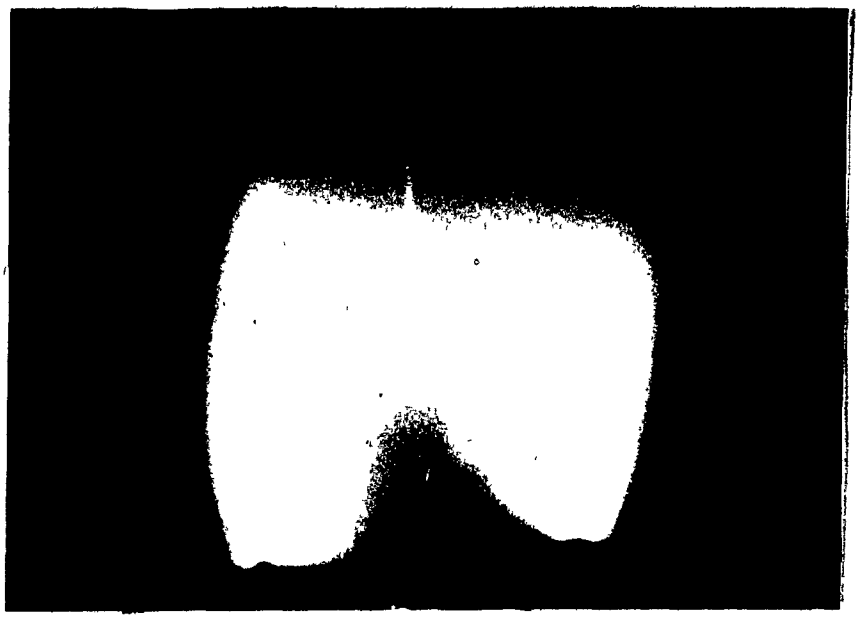

Figure 6.3.5. 'TALL MUSHROOM' vaporization mode. Melt temperature was 1950 K and chamber pressure was 13 pascals.

Figure 6.3.6. Form of vapour flow at higher pressures, around 16 pascals (melt temperature 1950 K).

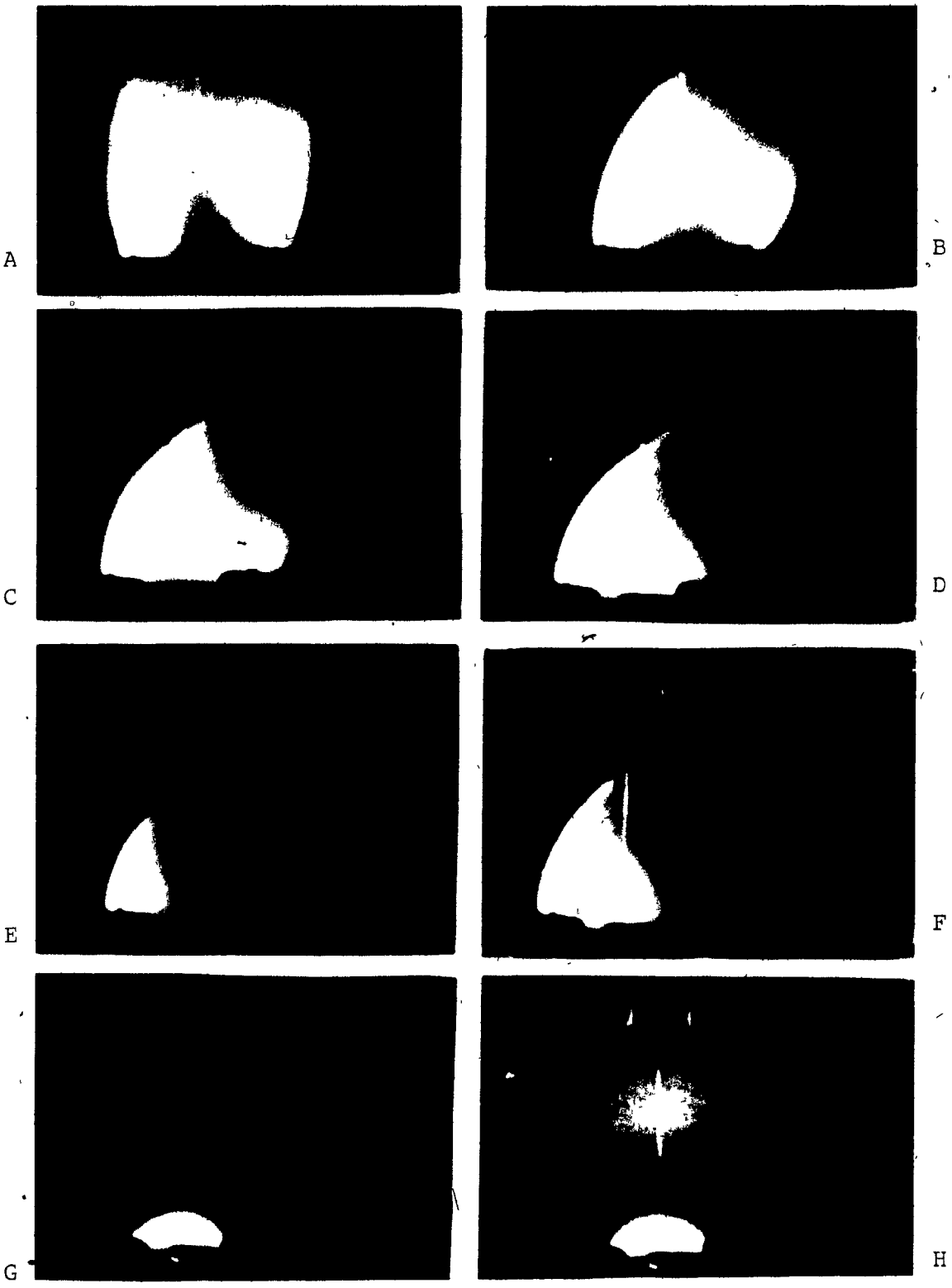

Figure 6.3.7. The tall mushroom type of metal vapour flow was compressed by slightly increasing the pressure in the chamber by injecting argon into the pumping system. When it was compressed fully ie., to below the rim of the crucible, a secondary form of the vapour flow appeared, frame H. Melt temperature was around 1950 K and chamber pressure increased from 13 pascals in the frame A to 16 pascals when the mushroom became fully compressed, frame H.

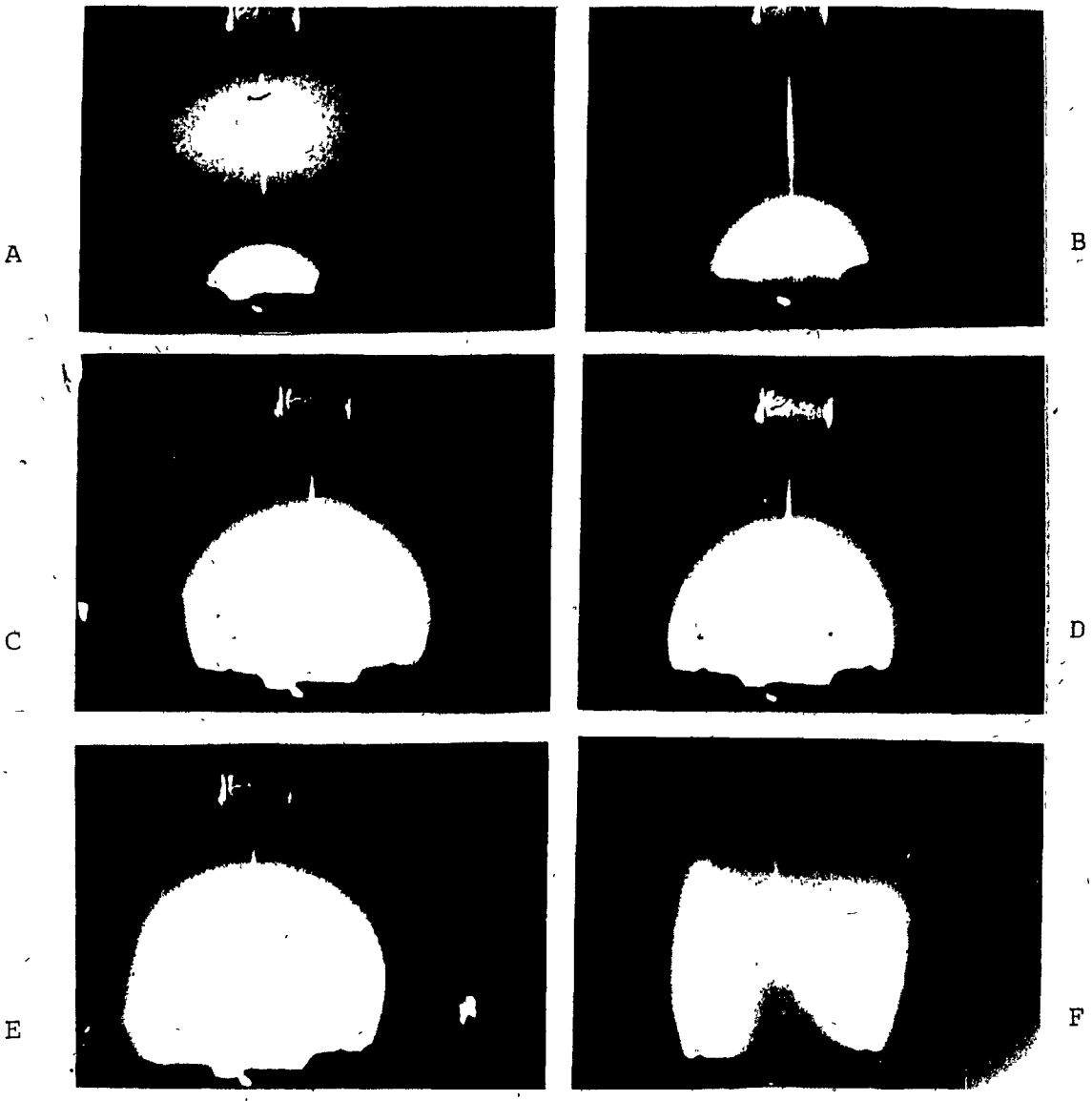

Figure 6.3.8. Regeneration of the tall mushroom as chamber pressure fell again when the small leak of argon was closed. The pressure dropped from 16 pascals in the first part of the sequence to 13 pascals at the end.

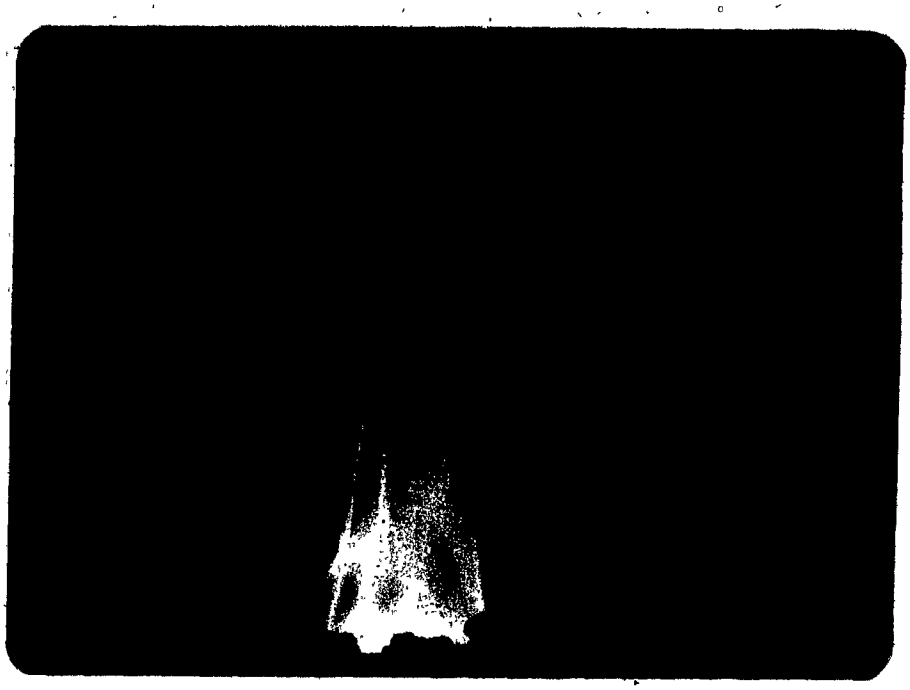

Figure 6.3.9. Form of the vapour flow at very high chamber pressures, in this case 1000 pascals. Lazy upward motion of the vapour is evident. Of interest are the bright droplets of steel which have splashed onto the gauze in the roof of the chamber (melt temperature 1950 K).

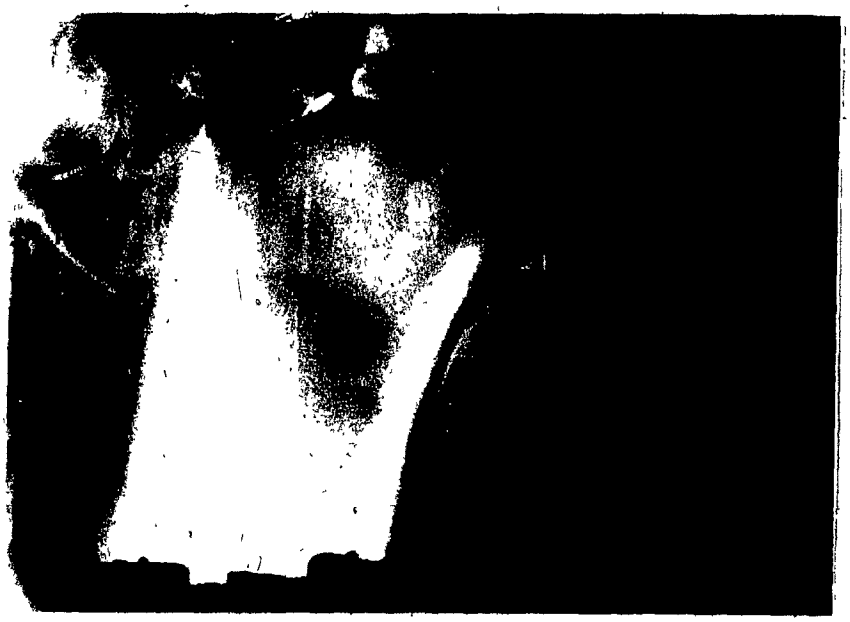

Figure 6.3.10. Two forms of vapour flow. Vortex type of flow can be seen funnelling down into the vacuum outlet and an extended tall mushroom type can be seen flowing from the crucible. It is thought that condensation occurs at the boundary of the mushroom and that the flow in the vortex is visible because of the presence of small drops of condensed vapour, (melt temperature around 1950 K and chamber pressure about 15 pascals).

In summary, the bright orange mushroom type behaviour of the vapour flow was not affected by the location of the pumping outlet, whereas, the white vortex forming material was strongly influenced by its position.

CHAPTER SEVEN

DISCUSSION

SECTION 7.1 : INTRODUCTION

The overall aim of this investigation was to determine rates of solute elimination from liquid steel. A second aim was to develop theoretical explanations for the rates and for the effects of experimental parameters on them.

The following discussion restates the experimental results and makes comparisons between the measured eliminations and theoretically predicted eliminations. It then discusses the limitations of the theoretical model and extends it to include all chamber pressure conditions.

The visual observations presented in the photographic studies chapter are then reviewed with regard to an explanation of condensation phenomena occurring in the gas space.

Finally bubble bursting is dicussed briefly.

SECTION 7.2. : VACUUM ELIMINATION RATES

The measured vacuum elimination data are summarized in Figure 7.2.1 which shows melt composition as a function of vacuum exposure time. The figure shows (i) that the initial composition of the melts was in the range 1.0 to 0.7 wt % copper, 0.3 to 0.14 wt % tin, 0.6 to 0.003 wt % manganese and 0.05 to 0.005 wt % sulphur, (ii) that the majority of experiments lasted 20 to 40 minutes and (iii) that the slope of wt % solute versus time plots decreases as initial solute concentration decreases. The third is a natural consequence of the elimination flux being dependant upon to solute concentration (Equation 3.22).

A more useful way of representing vacuum distillation data is to plot elimination as a percentage of the initial solute present at the commencement of refining. Figure 7.2.2 represents elimination of each of the solutes in terms of the measured solute content in the final sample expressed as a percentage of the solute content of the initial sample. The graphs show that in 30 minutes of vacuum refining: 40 to 90 % of the initial copper, 30 to 75 % of the initial tin, 60 to 100 % of the initial manganese and 20 to 40 % of the initial sulphur is eliminated.

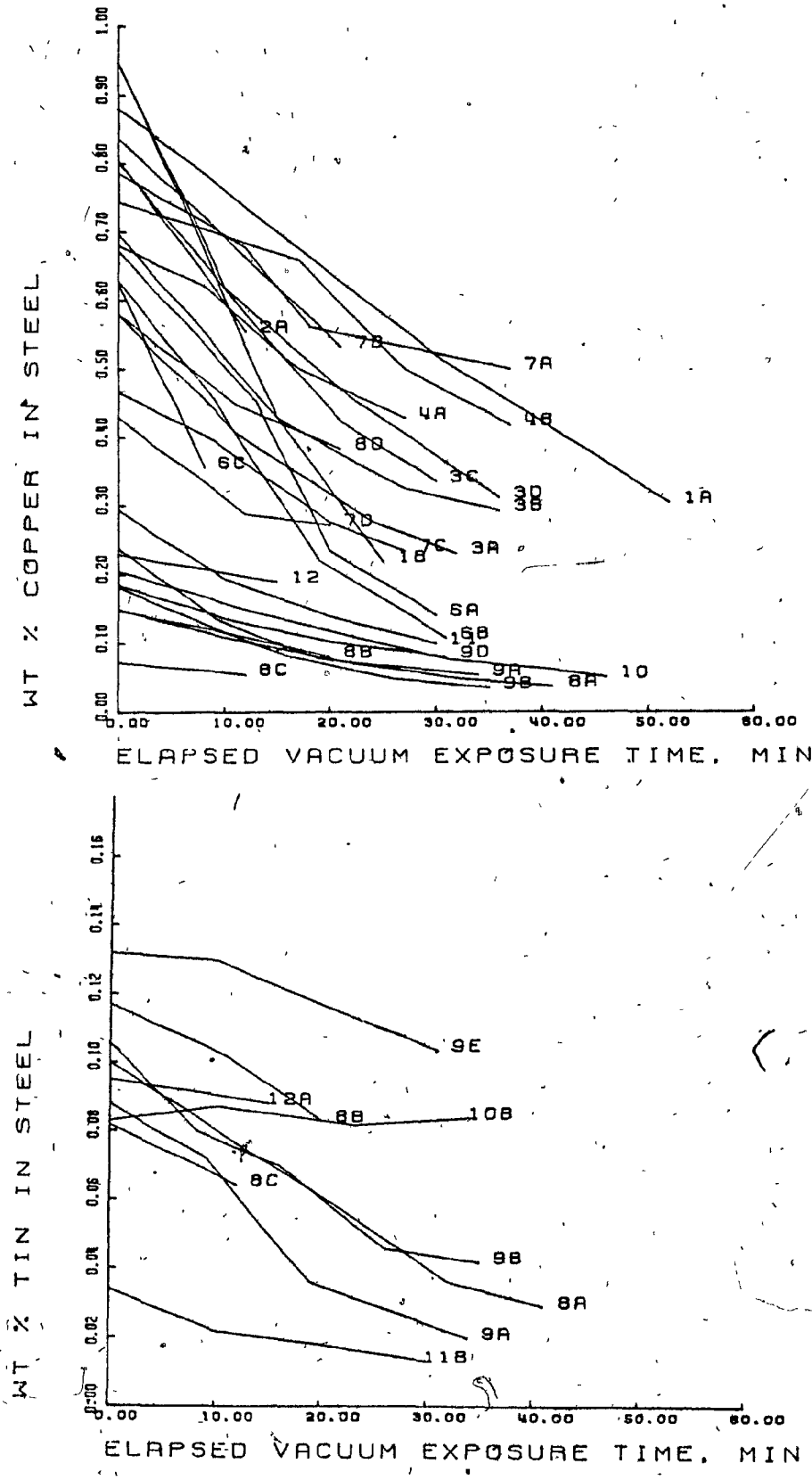

Figure 7.2.1 A and B. Measured weight percent copper and tin in liquid steel as a function of elapsed vacuum exposure time. Note scale of composition axis in each plot.

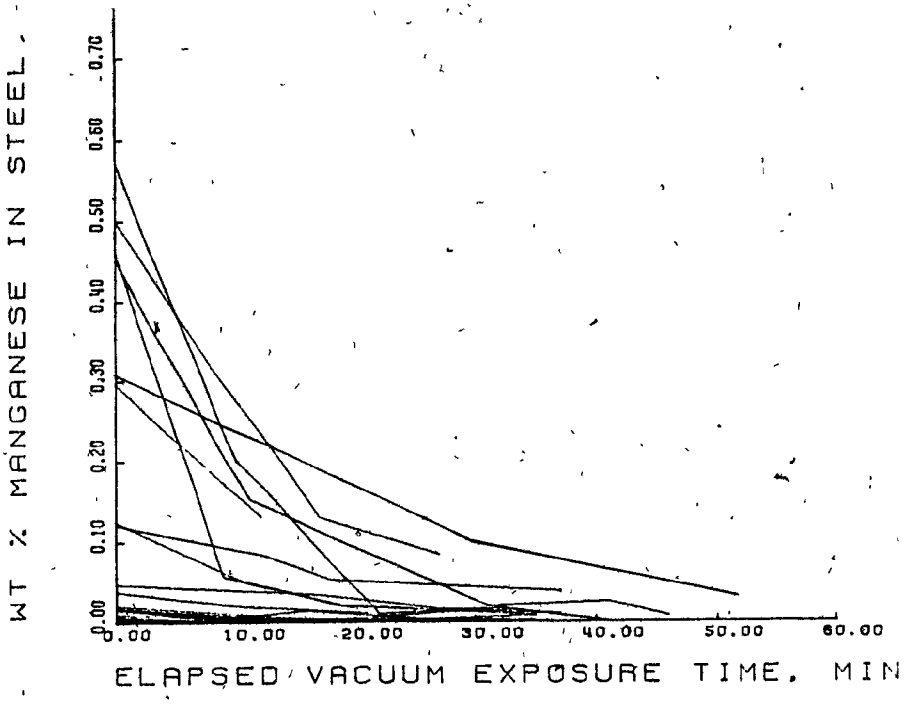

C

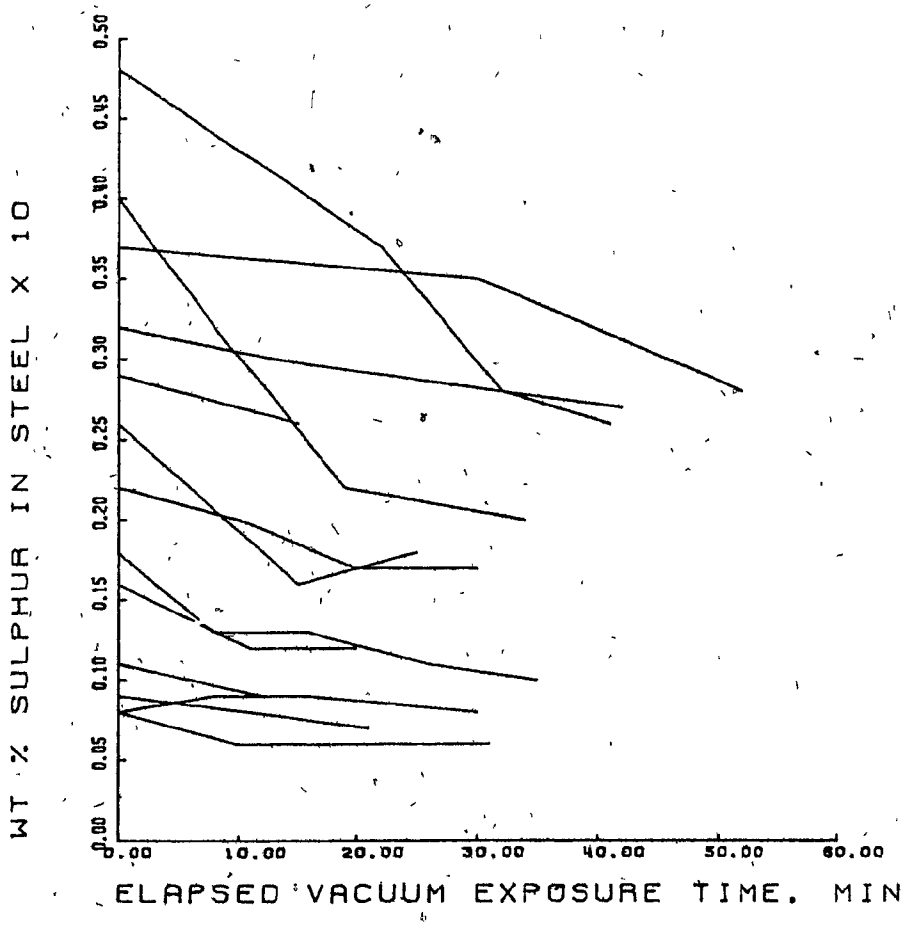

D

Figure 7.2.1 C and D. Measured weight percent manganese and sulphur in liquid steel as a function of elapsed vacuum exposure time. Note scale of composition axis in each plot.

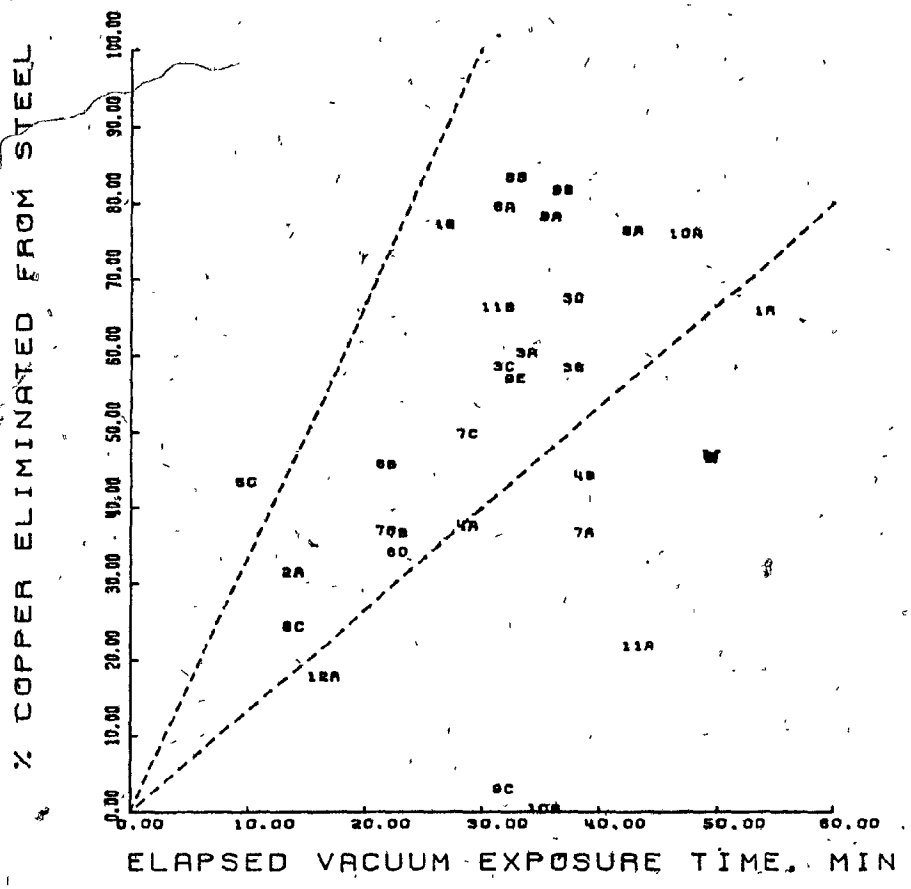

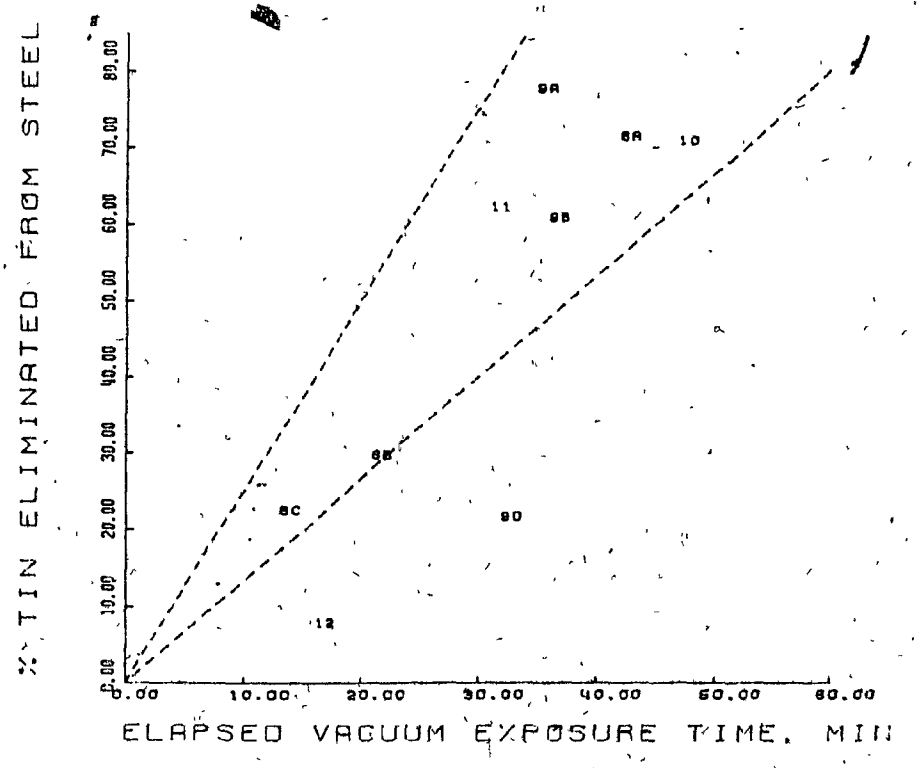

Figure 7.2.2. A and B. Percentage of initial copper concentration eliminated from melt at the time the final sample was taken.

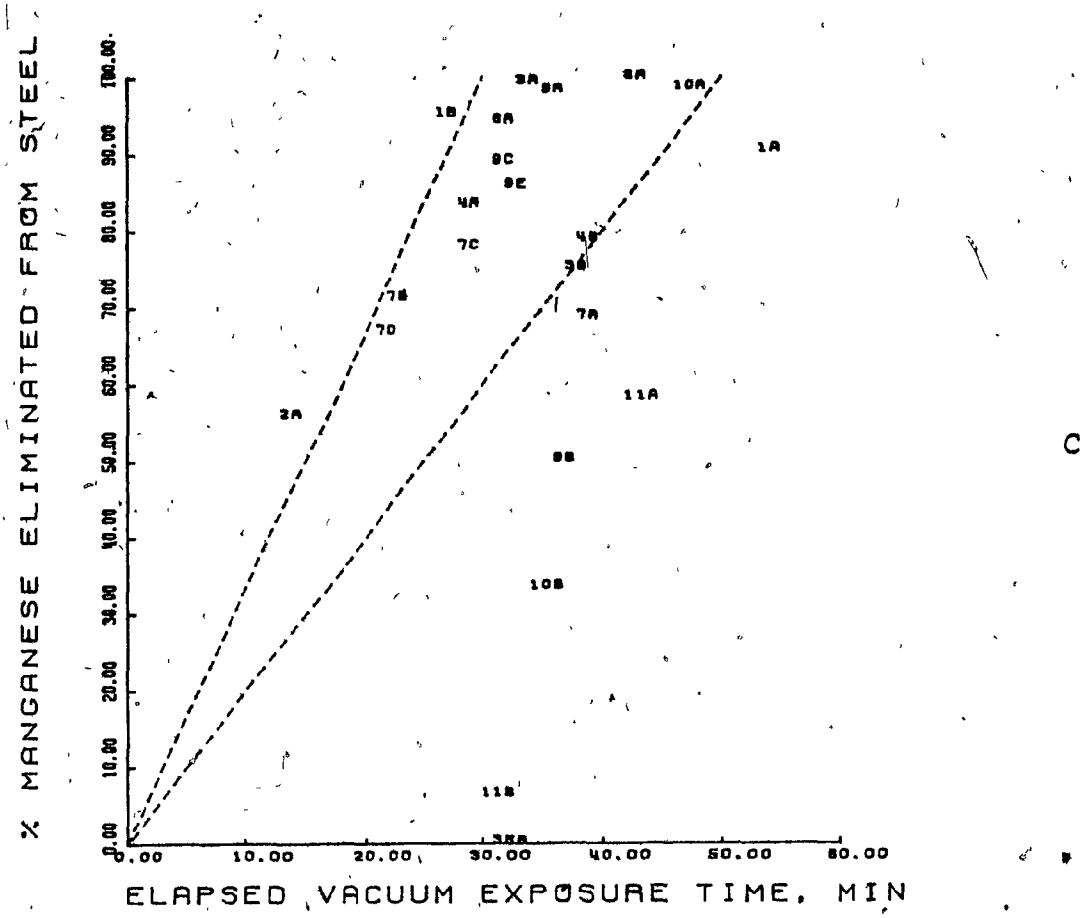

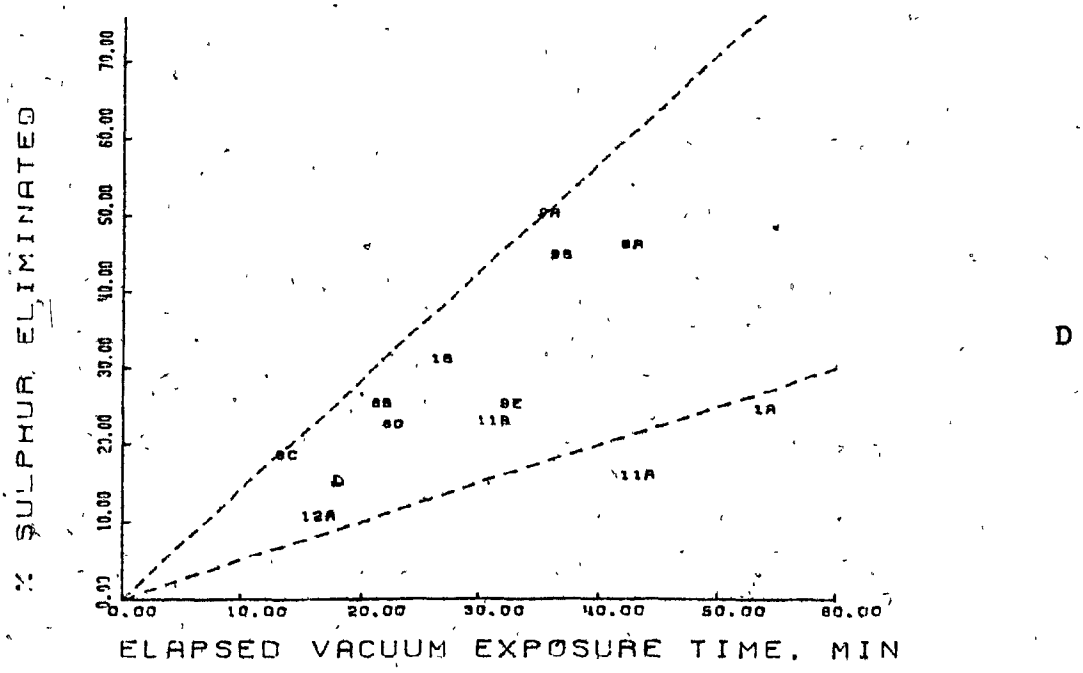

Figure 7.2.2. C and D. Percentage of initial tin and manganese concentrations eliminated from melt at the time the final sample was taken.

Previous pilot plant studies (26,31,33) measured copper elimination rates during vacuum distillation to be of the order of 20 % elimination in 30 minutes. This is considerably lower than the 40 to 90 % observed in the present investigation. Three reasons are suggested for the increased rates in the present work:

(a) increased melt temperatures,

(b) improved melt surface cleanliness,

and,

(c) reduced amount of condensate refluxing.

The first of these increases the elimination rate by increasing the equilibrium vapour pressure of the evaporating species. This increases the vapour pressure beneath the Langmuir plane and causes a resultant increase in the net flux across the plane. The second and third were discovered during visual observations of the experiments. Their retarding effects were seen to be a blocking of the evaporation for the former and a decreased net refining flux in the latter.

The rates measured in this study are the first pilot plant data which fulfil the industrial criterion that 80 % or more of the initial solute content be eliminated in 20 to 40 minutes. (This time is suggested on the basis of avoiding excessive temperature loss from the steel during treatment). Consequently, they are the first data which conclusively indicate that vacuum distillation can become a viable

industrial process.

In summary, it can be seen that sufficiently high vacuum distillation rates have been measured on a scale meaningful to full scale industrial processes. This clears the way for comprehensive steel scrap recycling with consequent lowering of raw material and energy demands for the steel industry. Table 7.2.1 shows the potential annual economic benefit of these reductions for the U.S.A. steel industry.

Value copper recovered / tonne scrap (0.5 % Cu at Can $2.50 / kg)	Can $12.50
Value tin recovered / tonne scrap (0.2 % Sn at Can $20 / kg)	Can $40
Savings (scrap compared to pigiron) (Scrap - $60/tonne, Pigiron - $200/tonne)	Can $130
TOTAL YEARLY BENIFIT (70,000,000 tonnes scrap replacement)	Can $13Billion

Table 7.2.1. Potential annual economic benefit for the United States steel industry assuming there is no accumulation of steel on the scrap stockpile.

SECTION 7.3. : COMPARISION OF EXPERIMENTAL RESULTS WITH THEORETICAL PREDICTIONS

A computer program (Section 3.10) based on a proposed model of vacuum distillation (Equation 3.22) was used to simulate vacuum distillation under conditions similar to those in each experiment of this study.

For the simulation, values of the experimental parameters which are input to the program to evaluate the terms in Equations 3.22a to 3.22d are those measured in each case and presented in Section 5.2.

A comparison is made between (i) theoretically predicted and (ii) observed melt composition at the time the final sample was taken. Figure 7.3.1 presents this comparison in the form of a plot for each solute element.

Elimination of sulphur was not simulated because of the uncertainty of its vapour pressures and activity coefficients at the temperatures of the melts in this work.

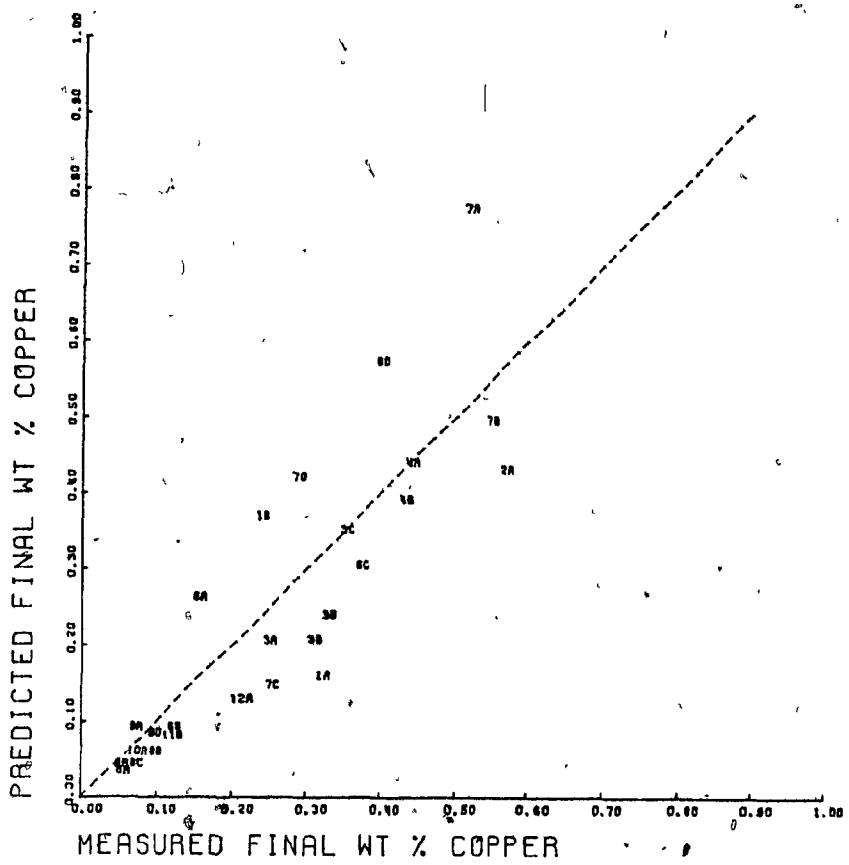

A

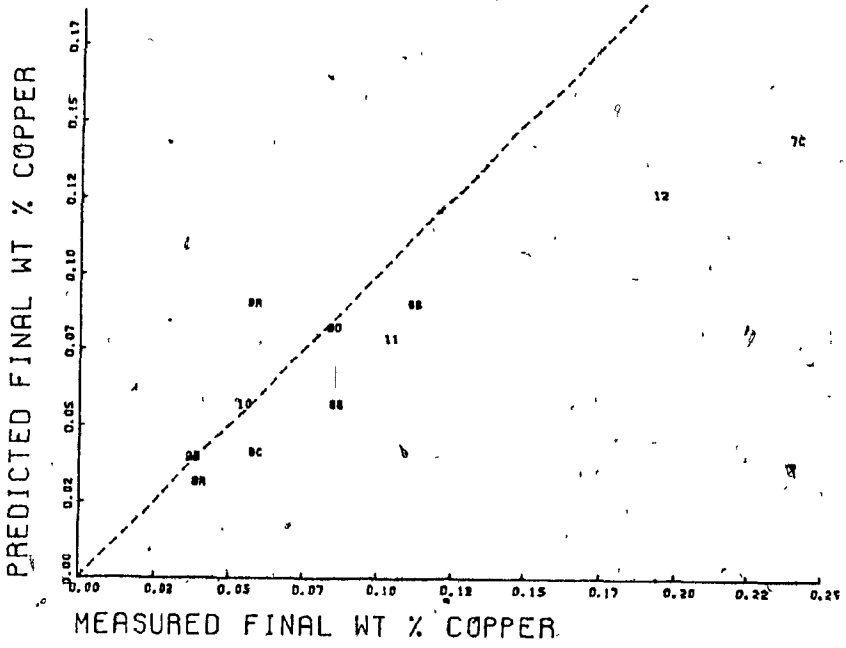

AA

Figure 7.3.1 A and AA. Comparison between theoretically predicted melt copper concentration and measured melt copper concentration at the time the final sample was taken. Figure A shows all the data, whereas, plot AA expands the 0 to 0.25 wt % copper range.

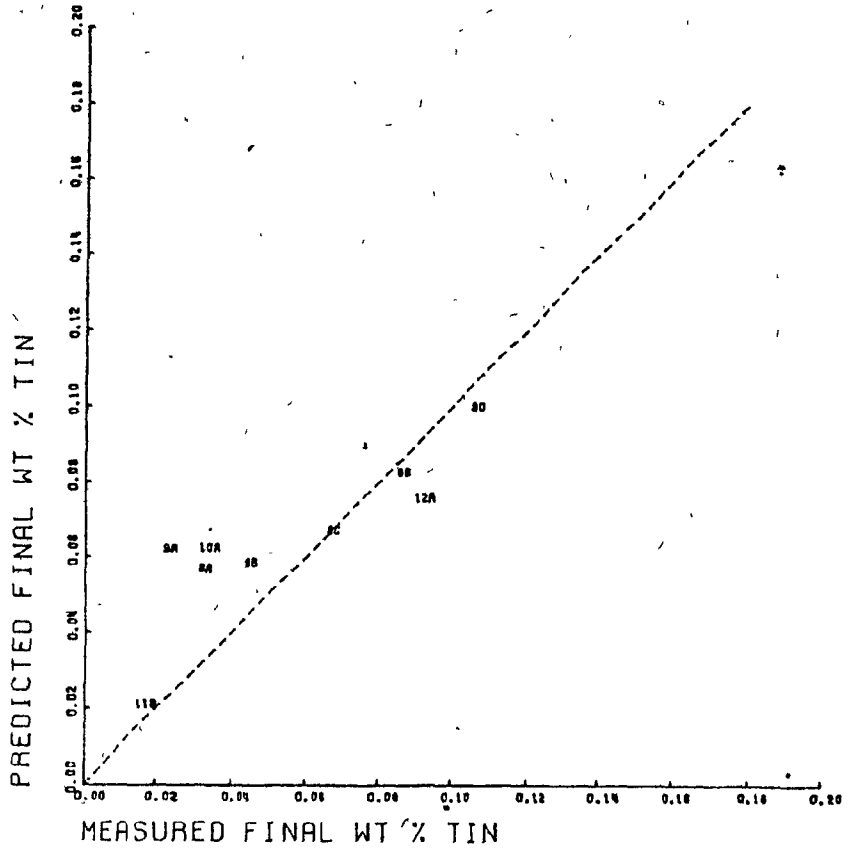

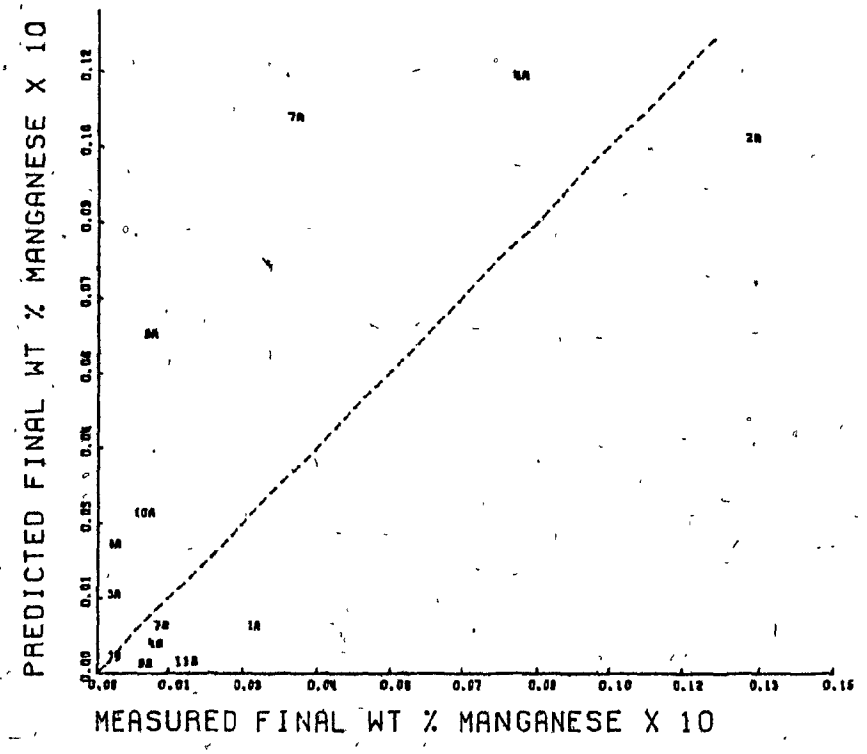

Figure 7.3.1 B and C. Comparison between theoretically predicted melt composition and observed melt composition at the time the final sample was taken. Figure A shows this for tin, Figure B shows it for manganese.

Figure 7.3.1 shows that the agreement between the theoretical predictions and the observed melt composition is excellent for copper and tin, but, quite poor for manganese. The excellent agreement for copper and tin indicates that the model accurately represents the observed vacuum elimination and also suggests that the sampling and analysis technique for both was very sound. The poor agreement for manganese is thought to be the result of poor precision in manganese analysis when the manganese contents of the samples were less than 0.01 wt %.

SECTION 7.4. : LIMITATIONS OF VACUUM DISTILLATION MODEL

7.4.1. : MASS TRANSFER IN THE LIQUID STEEL

The vacuum distillation model expresses the net flux from the bulk of the melt to the condensation location on the basis of predicted fluxes (i) in the melt, (ii) across the Langmuir plane and (iii) through the gas space.

The Machlin model (35) which was used to represent the flux in the liquid metal assumes that there is a flow of liquid from the bulk of the melt to the surface, radially outwards across the surface to the melt edge and from there back to the bulk of the melt. This behaviour was observed under ideal conditions in the present experiments.

However, the evolution of gas or vapour bubbles in the melt (Section 6.2.3) severely disrupts this flow. A second factor which disrupts the ideal flow is application of a large power input to a shallow melt. As was shown in Figure 6.2.7, for example, 50 kW power input to a 2 cm deep melt completely destroyed any of the flow patterns suggested by Machlin. Fortunately, this was not the normal mode of operation and there was seldom melt bubbling. Consequently, it appears that in most cases the Machlin model suitably describes the liquid phase flux.

7.4.2. : MASS TRANSFER ACROSS THE LANGMUIR PLANE

The concept of the Langmuir plane immediately above the melt surface is based on atomic ie., non empirical, theory. It is believed to accurately represent the gas phase flux adjacent to the liquid surface as long as the melt surface area exposed to vacuum is constant with time.

7.4.3. : MASS TRANSFER THROUGH THE GAS PHASE

Further limitations of the vacuum distillation model may lie in the assumptions made in developing an expression for gas phase mass transfer of the evaporated vapour (Section 3.9).

A quick glance at the photograph of the apparatus (Figure 4.3.2) shows that the first assumption (gas space cross-sectional area constant and equal to the melt surface area) does not always hold. However, the maximum rates of solute elimination are attained when the vapour flow in the chamber clearly reached the chamber roof (ie., the extended mushroom), Figure 6.3.3. It can be see that the sideways expansion of the vapour flow under these conditions is small compared to the vertical flow. Hence, the constant area assumption appears to be valid for predicting the gas phase flux under normal vacuum distillation conditions.

The second assumption (isothermal system) is true under normal vacuum distillation conditions when the vapour flow reaches the chamber roof before condensing.

The third assumption (all evaporated vapour condenses at the condensation location) holds because the vapour pressure of the evaporated vapour is negligible over the solid condensate (51).

The fourth assumption (chamber pressure uniformity) is a natural consequence of the large dimensions of the apparatus.

The last assumption (no generation or consumption of vapour in the gas space) is based on the fact that the vapour loses heat and condenses only at the condensation location.

In summary, it has been shown that under most of the experimental conditions of this work (normal vacuum distillation conditions): (i) the Machlin expression accurately represents the flux in the melt phase, (ii) the Langmuir plane theory accurately represents the net flux evaporating and (iii) the expression developed for the flux in the gas phase represents it accurately.

SECTION 7.5. : EXTENSION OF VACUUM DISTILLATION MODEL

The vacuum distillation model was developed for normal vacuum distillation conditions, ie., chamber pressure is less than the sum of the equilibrium vapour pressures of the evaporating species in the surface. Under these conditions there is always a bulk flow of vapour away from the melt surface to the condensation location.

The model can be extended to apply to all chamber pressures by rewriting the expression for the flux of evaporated vapour across the gas space in its entirety:

$$\dot{n}''_{i,gas} = \frac{-D}{R.T} \cdot \frac{\partial P_{i,x,t}}{\partial x} + v \cdot P_{i,x,t} \quad \ldots\ldots 7.1$$

where all terms have the meanings defined in Equation 3.15.

Equation 7.2 was used to evaluate the flux at the commencement of vacuum distillation for conditions given as an insert on Figure 7.5.1. This figure plots the predicted flux against the chamber pressure and shows that the flux becomes negligible at chamber pressures close to the equilibrium vapour pressure of the melt surface. This is very close to the prediction of the original model (flux equal to zero under these conditions). Consequently, it appears that the model accurately describes the evaporation process for all chamber pressures.

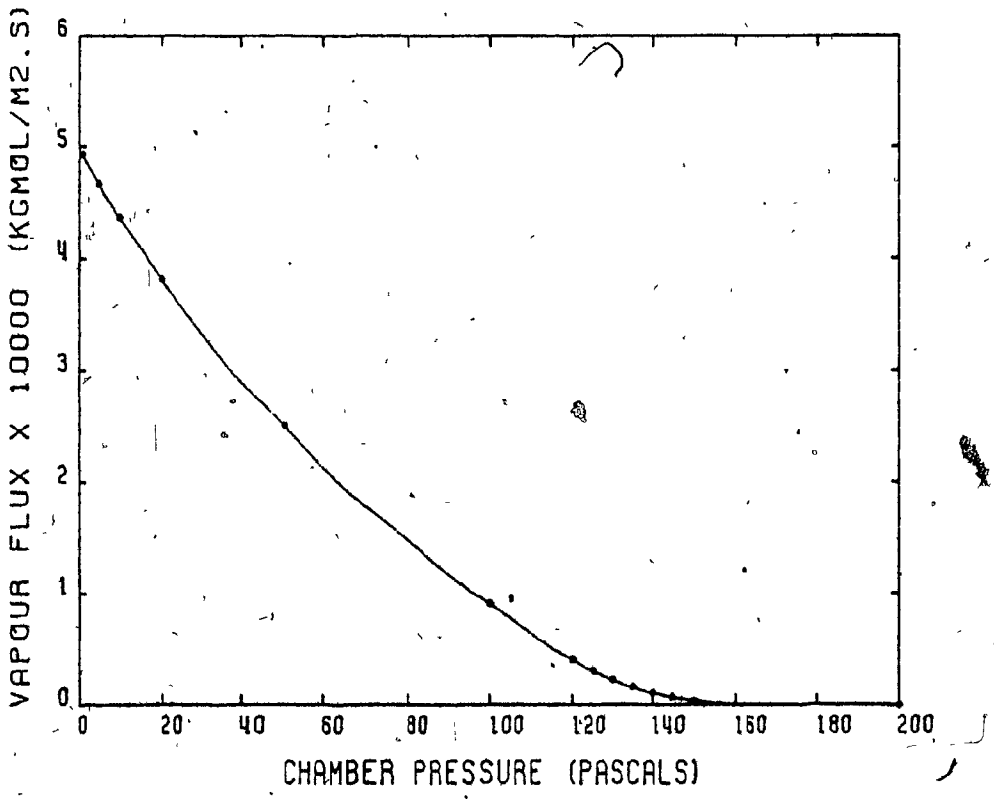

Figure 7.5.1. Evaporation flux evaluated at commencement of distillation under typical vacuum distillation conditions. The flux can be seen to be almost zero at chamber pressure approximately equal to equilibrium vapour pressure of the melt (120 pascals).

SECTION 7.6. : DISCUSSION OF PHOTOGRAPHIC STUDIES

A significant breakthrough in this work was the experimental practice of clearing the melt surface of slags or films before beginning a quantitative refining experiment. This practice was adopted because visual observations showed clearly that when the melt surface was covered with slag or film there was very little vapour evolution from the melt, Figure 6.3.1. It was the removal of the surface film that significantly increased elimination rates in this study above those of similar studies in the same apparatus at similar melt temperatures (18,28,30). Experiment 9C was deliberately carried out with a film on the melt surface to confirm or deny this behaviour. The result was that in 30 minutes exposure to vacuum only 3 % of the initial copper or tin was eliminated.

The photographic studies also led to an understanding of the limitations of the Machlin model in describing melt phase mass transfer in shallow melts at high power inputs. They also showed that the assumption of constant plane area by the Langmuir plane theory is incorrect when the melt is bubbling or boiling.

Perhaps the most useful application of the photographic studies was in the development of the gas phase mass transfer model. Photographs under normal vacuum distillation conditions (Figures 6.3.2 and 6.3.3) clearly showed the vapour rushing from the crucible to the chamber roof and stimulated the ideas

behind the gas phase mass transport model developed in Section 3.9.

Figures 6.3.4 and 6.3.5 show that the flow of vapour in the gas space did not reach the roof when chamber pressure was just slightly less than the equilibrium vapour pressure of the melt.

It is believed that this behaviour is the result of gravity slowing the upwards velocity of the vapour to zero. This is possible when its initial velocity is small enough, for example, less than 4.5 m/s.

Under such circumstances, there would probably be homogeneous nucleation of very small droplets of liquid or solid condensate particles or of metal oxide due to (i) the increased concentration of vapour atoms at the point the vapour stops, (ii) cooling of the vapour by heat transfer to the non-condensible gas present at this point (52-55) or (iii) reaction with oxygen which may have leaked into the chamber (30).

Consequently, the boundary that can be seen in the photographs is the plane at which the vapour velocity away from the melt surface has fallen to zero and nucleation of condensate or oxide has occurred. In terms of the overall picture of vacuum distillation, the transition pressure range in which the flow of vapour was seen to not extend all the way

to the chamber was quite narrow, ie., +/- 2 pascals.

Gravity does not reduce the elimination rate because the bulk velocity of the vapour just above the melt surface is unaltered. Homogeneous nucleation does not alter the validity of the model either, because, the assumptions made in Section 3.9 and discussed here apply to the case of homogeneously condensing vapours as well. They are also valid for the situation in which the vapour reacts to form an oxide.

Figure 6.3.6 shows beautifully the form on the vapour flow when the chamber pressure is higher than the equilibrium vapour pressure of the melt. It shows that there is no rush of vapour from the crucible and diffusion is the means of mass transfer in the gas space. It can also be seen that sideways expansion is exaggerated compared to the lower pressure photographs. Under such conditions however, the refining rate is quite small. Figures 6.3.7 and 6.3.8 show quite clearly the transition back and forth through the pressure range in which this behaviour was observed.

Photographs of the material evolving from the crucible were also taken at much high chamber pressure (≈ 1000 pascals Figure 6.3.9). The material in the gas space shown in this figure is thought to be iron fume formed by reaction with oxygen which entered in the chamber as air inleakage. Although, the amount of material in the gas space appears considerable, the elimination rate is negligible because its

velocity is very small compared that of the vapour under normal vacuum distillation conditions.

The last part of the photographic study to be discussed here is the melt bubbling shown in Figures 6.2.8 and 6.2.9. The bubbles are believed to be melt boiling which is possible when the vapour pressure of the liquid below the surface exceeds the static pressure at that point. This is the case at very small depths when there is a high concentration of highly volatile impurities (0.5 wt% manganese for example), or when the melt superheat is very high (300 K).

The bubbles are thought not to be carbon monoxide as melt oxygen was low due to the aluminium killing at the commencement of the experiment.

In the photographs (Figure 6.2.8 B, E and H), the bubbles can be seen to rupture at dark spots which grow and become darker on the film of metal covering the bubble. These spots are thought to be areas of localized cooling which possibly freeze and fracture. Other unchanging dark spots on the bubble surface are possibly due to reflection of the chamber's interior or dirt in the camera's optical path.

Figure 6.2.9 is a sequence of spectacular photographs showing the rupture and dispersion of a bubble from the side. It shows that the film which was covering the bubble peeled off in one direction and gave the resultant droplets of steel

trajectories in the same direction.

In summary, the photographic studies have given invaluable assistance to the understanding of the experimental phenomena. Without them, the work in this thesis would not have been as fruitful as it has been.

SECTION 7.7. : COMMENT ON THE USE OF RATE CONSTANTS

In previous studies (25,26,28-33), vacuum distillation data have been represented in the form of an average rate constant (m/s) evaluated for the time during which the melt composition was measured. In this study, however, it has been shown that the multiplier in the expression for the overall flux during vacuum distillation (Equation 3.22) is not constant with respect to time and as a result the use of a rate constant is not suitable. Nevertheless, it is possible to evaluate a pseudo rate constant by a numerical fit to the measured data (Appendix 3) and these values are reported for each experiment on Figures 5.2.1 to 5.2.29.

The pseudo rate constant has not been used because percentage elimination of initial solute content appears to be more useful industrially and experimentally.

SECTION 7.8. : FUTURE WORK.

Theoretical investigations which appear to be most promising for the immediate future are:

(a) a technological feasibility study of applying vacuum distillation to industrial electric furnace practice, and,

(b) an economic cost and benefit analysis of the process, while promising future industrial studies are:

(c) full scale tests on Finkl-Mohr vacuum units (56), and,

(b) pilot scale tests on Ruhrstahl Hattingen vacuum degassing units (56).

On a pilot plant scale, promising suggestions for future investigations are:

(a) inert gas purging through the melt to increase melt turbulence and perhaps the bulk flow of gas away from the liquid surface,

(b) manganese and sulphur elimination,

(c) vacuum distillation of non-ferrous systems, for example, elimination of arsenic, antimony, lead and bismuth from copper matte or blister copper,

(d) vacuum distillation in dynamic systems in which the metal flows from one container to another, and,

(e) continuous spray vacuum distillation.

CHAPTER EIGHT

CONCLUSIONS

Experiments have shown that 40 to 90 % of the initial copper, 30 to 75 % of the initial tin, 60 to 100 % of the initial manganese and 20 to 40 % of the initial sulphur are eliminated by 30 minutes of vacuum distillation.

These results indicate that vacuum distillation can become a viable industrial process.

The elimination rates measured in this study were higher than those observed in previous studies. This is due to:

(a) higher melt temperatures,

(b) cleaner melt surfaces,

(c) lesser degree of condensate refluxing

and,

(d) lower chamber pressures

in the present experiments.

A theoretical model has been developed to describe vacuum distillation elimination in terms of fluxes in the melt, across the Langmuir plane and through the gas space. The model

accurately predicts copper and tin elimination but it is somewhat less accurate for manganese and sulphur.

Photographic studies showed that:

(a) surface films critically block evaporation,

(b) induction stirring turbulence limits the applicability of the Machlin induction stirred melt mass transfer model,

(c) melt bubbling limits the use of the Langmuir plane theory,

and,

(d) vapour flow patterns are very sensitve to chamber pressures when these pressures are approximately the same as the melt equilibrium vapour pressure.

CHAPTER NINE

CONTRIBUTION

The following items are claimed as original contributions to knowledge:

(a) a technique has been developed to melt steel scrap under vacuum and attain a clean surface for evaporation,

(b) techniques have been developed for reproducible melt sampling and accurate temperature measurement without breaking vacuum,

(c) rates of copper, tin, manganese and sulphur elimination by vacuum distillation have been measured and techniques developed for maximizing the rates, in particular: (i) cleaner melt surfaces, (ii) higher melt temperatures and (iii) lesser degree of condensed vapour refluxing,

(d) a theoretical model describing the mechanism of vacuum distillation has been developed based upon (i) melt phase diffusion, (ii) evaporation across the Langmuir plane and (iii) convective mass transport in the gas phase and a precise correlation has been shown between (i) predictions of the theoretical model, (ii) quantitative experimental measurements and (iii) visual

observations,

(e) a photographic record of the vacuum distillation process has been obtained, leading to a much fuller understanding of the process,

and,

(f) an evaluation of the potential role of vacuum distillation in the steelmaking cycle has been made showing that it will most likely become a common and essential component of electric steelmaking.

BIBLIOGRAPHY

1. Yearbook, Facts, Inst. Scrap Iron and Steel Inc., 36th. Edition, 1978.

2. Anon., 'The Horn of Plenty Keeps Overflowing', Phoenix Quarterly, Vol. 9, No. 3, 1971, pp.3-7.

3. Peacey, J.G. and Davenport, W.G. The Iron Blast Furnace. Permagon, Oxford, 1979, p. 62

4. Koros, P.J., Shoenberger, L.R. and Silver, J., 'The utilization of bundled auto scrap and its relation to sheet steel quality', Pittsburg Regional Tech. Meet., Am. Iron and Steel Inst., 1969, pp. 1-32.

5. Hundy, B.B., 'Residual elements in iron and steel', I.S.I Special Report 114, 1968, pp. 75-89.

6. Blickwede, D.J., 'Committee Correspondence - Survey on Residual April 1977', Bethlehem Steel Corporation, Homer Research Laboratories, Bethlehem, U.S.A., 1977.

7. Sachs, K., 'Residuals in engineering steels', Metals Tehnology, Jan. 1979, pp. 33-37.

8. Copeland, M.I., 'Reducing surface hot shortness of copper-containing steels using silicon additions and controlled reheating conditions', Bureau of Mines, United States Department of the Interior, Report of Investigations 7936.

9. Cox, A.R. and Winn, J.M., 'Scaling of plain and complex copper steels', JISI, Feb. 1965, pp. 175-179.

10. Foster, G.G. and Gillhrist, J.K., 'The influence of copper, nickel and tin on the hot working properties of mild steel', Metallurgia, May 1952, pp. 225-230.

11. Melford, D.A., 'Influence of antimony and arsenic on surface hot shortness in copper-containing mild steels. JISI, May 1966, pp. 495-496.

12. Melford, D.A., 'Surface hot shortness in mild steel', JISI, April 1962, pp. 290-299.

13. Nicholson, A. and Murray, J.D. 'Surface hot shortness in low carbon steel', JISI, Oct. 1965, pp. 1007-1017.

14. Penning, J:, Dept, F. and Vidts, J., 'The mechanism of Proc. ICSTIS, Suppl. Trans. ISIJ, Vol. 11, 1971, pp. 1053-1055.

15. Salter, W.J.M., 'Effect of chromium on solubility of copper in mild steel', JISI, Nov. 1967, pp. 1156-1160.

16. Salter, W.J.M., 'Effects of alloying element on solubility and surface energy of copper in mild steel', JISI, May 1966, pp. 478-488.

17. Brimacombe, J.K., 'Formation of longnitudinal, mid-face cracks in strand-cast slabs', 108th Ann. Meet. A.I.M.E., New Orleans, 1979.

18. Anon.,'The effect of contaminants in scrap on steel and steelmaking', Steel Furnace Monthly, Oct. 1971, pp. 412-414.

19. Salomon-De-Friedberg, H., 'Residual copper in steel: Significance, vacuum removal', Master's of Engineering Thesis, McGill University, 1976.

20. Brochu, M., 'Scrap metal recycling: Profitable junk', Science Dimension, Vol. 4, 1978, pp. 4-7.

21. Leak, V.G., Fine, M.M. and Dolezac, H., 'Separating Cu from scrap by preferential melting: Laboratory and economic evaluation', Rep. Invest. 7809, U.S. Bureau of Mines, Wash., D.C., 1973.

22. Safiah, A.R. and Sale, F.R., 'Influence of carbon on the removal of copper from iron melts with sulphide slags', JISI, Jan. 1972, pp. 52-56.

23. Makar, H.V. and Brown, R.C., 'Copper removal from molten ferrous scrap: A pilot plant study', Rep. Invest. 7914, U.S. Bureau of Mines, Wash., D.C., 1974.

24. Gill, G.M., Inveson, E. and Wesley-Austin, G., 'The behaviour of various elements in vacuum steelmaking', JISI, Feb. 1959, pp. 172-175.

25. Olette, M., 'Vacuum distillation of minor elements from liquid ferrous alloys', Physical Chemistry of Process Metallurgy - Part 2 Interscience, New York, 1961, pp. 1065-1087.

26. Ward, R.G. 'Evaporative losses during vacuum induction melting', JISI, Jan. 1963, pp. 11-15.

27. Fischer, V.H. and Derenbach, M., 'Contribution to the question of evaporation in melts of iron alloys in a vacuum: Part 1. Theoretical investigations on binary alloys of iron with arsenic, manganese, copper and tin', Arch. Eisen, Vol. 35, No. 4, 1964, pp. 307-316.

28. Smith, P.N. and Ward, R.G., 'The evaporation of liquid iron alloys under vacuum', Can. Met. Q., Vol. 5, Feb. 1966, pp. 77-92.

29. Ohno, R. and Ishida, T., 'Rate of evaporation of manganese, copper, tin, chromium and sulphur from molten iron under vacuum', JISI, Vol. 206, 1968, pp. 904-908.

30. Fischer, W.A. and Janke, D., 'The evaporation of copper, maganese and chromium from melts of steel X5 Cr Ni 18 9 under reduced pressure', Arch. Eisen, Vol. 45, 1974, pp. 361-365.

31. Salomon-De-Frieberg, H. and Davenport, W.G., 'Vacuum removal of copper from melted steel scrap', Met. Soc. CIM. Ann.Vol., 1977, pp. 225-231.

32. Ohno, R., 'Kinetics of evaporation of manganese, copper and sulphur from iron alloys in vacuum induction melting', Trans. Iron and Steel Inst. of Japan, Vol. 17, 1977, pp. 732-741.

33. Harris, R. and Davenport, W.G., 'Pilot plant scale vacuum distillation of liquid steel to remove copper', Can. Met. Q., Vol. 18, 1979, pp. 303-311.

34. Ohno, R. Liquid Metals Chemistry and Physics, Beer, S.Z., ed., Marcel and Decker, N.Y., 1972, pp. 38-79.

35. Machlin, E.S., 'Kinetics of vacuum induction melting-theory', Trans AIME, Vol. 218, 1960, pp. 314-326.

36. Davenport, W.G., Wakelin, D.H. and Bradshaw, A.V., 'Interaction of both bubbles and jets with liquids', Heat and Mass Transfed in Process Metallurgy., ed. by Hills, A.W.D., Inst. Mining and Metallurgy, London, 1967, pp. 207-240.

37. Irons, G.A., Chang, C.W., Guthrie, R.I.L. and Szekely, J., 'The measurement and prediction of the vaporization of magnesium from an inductively stirred melt', Met. Trans. B, Vol. 9B, March 1978, pp. 151-154.

38. Szekely, J., Chang, C.W. and Johnson, W.E., 'Experimental measurement and prediction of melt surface velocities in a 30,000 lb. inductively stirred melt', Met. Trans. B., Vol. 8B, Sept. 1977, pp. 514-517.

39. Richardson, F.D., Physical Chemistry of Melts in Metallurgy, Vols. I and II, Academic Press, New York, 1974, pp.

40. Langmuir, I., 'The dissociation of hydrogen into atoms: Part I', J. Am. Chem. Soc., Vol. 36, 1914, pp. 1708-

41. Langmuir, I., 'The dissociation of hydrogen into atoms: Part II', J. Am. Chem. Soc., Vol. 37, 1915, pp. 415.

42. Langmuir, I., 'The dissociation of hydrogen into atoms: Part III', J. Am. Chem. Soc., Vol. 38, 1916, pp. 1145-1155.

43. Knacke, O.T. and Stranski, I.N., 'The mechanism of evaporation', Progress in Metal Physics, Chalmers, B. and King, R., eds., Pergamon Press, New York, Vol. 16, 1956, pp. 181-233.

44. Knudsen, M. Ann. Physic., Vol. 31, p. 205; Vol. 32, p. 890; Vol. 33, p. 14; Vol. 35, p. 1910.

45. Maxwell, J.C., Phil. Trans. Roy. Soc., Vol. 170, pp. 332-

46. Roth, A. Vacuum Technology, Northland, New York, 1976, 16-146.

47. Szekely, J. and Themelis, N.J. Rate Phenomena in Process Metallurgy, Wiley-Interscience, New York, 1971, pp. 365-

48. Geiger, G.H. and Poirier, D.R. Transport Phenomena in Metallurgy, Addison-Wesley, Reading, Mass. 1973, a-47; b-464.

49. Bird, R.B., Stewart, W.E. and Lightfoot, E.N. Transport Phenomena, John Wiley & Sons, New York, 1960, pp. 556.

50. Ozberk, E., Master's of Engineering Thesis, McGill University, 1980.

51. Kubaschewski, O.K., Evans, E.L. and Alcock, C.B. Metallurgical Thermochemistry, Pergamon Press, New York, 1972.

52. Freund, H.J. and Bauer, S.H., 'Homogeneous nucleation of metal vapours, 2. Dependence of the heat of condensation on cluster size', Jour. Phys. Chem.,Vol. 81, No. 10, 1977, pp. 994-1000.

53. Frurip, D.J. and Bauer, S.H., 'Homogeneous nucleation of metal vapours, 3. Temperature dependence of the critical supersaturation ratio for iron lead and bismuth', Jour. Phy. Chem., Vol. 81, No. 10, 1977, pp. 1001-1006.

54. Frurip, D.J. and Bauer, S.H., 'Homogeneous nucleation in metal vapours. 4. Cluster growth rates from light scattering', Jour. Phys. Chem., Vol. 81, No. 10, 1977, pp. 1077-1015.

55. Bauer, S.H. and Frurip, D.J., 'Homogeneous nucleation in metal vapours. 5. A self-consistent kinetic model', Jour. Phys. Chem., Vol. 81, No. 10, 1977, pp. 1015-1024.

56. Winkler, O. and Bakish, R. Vacuum Metallurgy, Elsevier, Amsterdam, 1971, pp. 343.

APPENDIX ONE

VACUUM DISTILLATION SIMULATION

The following is a listing of the Fortran computer program which simulates vacuum distillation on the basis of Equation 3.22.

```
      REAL NCU,NSN,NMN,NFE,K1,K2,K3,K2CU,K2SN,K2MN,
     +K2FE,MCU,MSN,MMN,MFE,MM,
     +CU(250),SN(250),MN(250),TI(250),
     +MNK,MNFIN
C
C
C     THE PROGRAM INTERACTIVELY REQUESTS INPUT INITIAL DATA
C
C
    1 WRITE(9,300)
  300 FORMAT(' ENTER THE DIFFUSION COEFF. IN LIQUID STEEL(M2/S)')
      READ(9,*)DLIQ
      WRITE(9,301)
  301 FORMAT(' ENTER THE VELOCITY OF THE LIQUID SURFACE(M/S)')
      READ(9,*)VELS
      WRITE(9,302)
  302 FORMAT(' ENTER MELT TEMPERATURE(K), MASS(KG) AND DIAMETER(M)')
      READ(9,*)T,MM,CD
      WRITE(9,303)
  303 FORMAT(' ENTER CHAMBER PRESSURE(PASCALS)')
      READ(9,*)PCH
      WRITE(9,304)
  304 FORMAT(' ENTER WT% CU, WT% SN, WT% MN AND WT% FE')
      READ(9,*)WTCU,WTSN,WTMN,WTFE
C
C     PROMPTING ASKS FOR A SIMULATION TIME LESS THAN 25000(SECS)
C
      WRITE(9,305)
  305 FORMAT(' ENTER CALCULATION STOPPING TIME(SECS)')
      READ(9,*)TSTOP
C
C     PROMPTING ASKS FOR A DISPLAY TIME LIMIT (½ CALC.STOP TIME)
C
      WRITE(9,306)
  306 FORMAT(' ENTER DISPLAY STOPPING TIME(SECS)')
      READ(9,*)DSTOP
C
C     PROMPTING ASKS IF ALL RESULTS ARE TO BE PRINTED
```

```
C
      WRITE(9,308)
  308 FORMAT(' DO YOU WANT THE DISPLAY DEPRESSED ? 1 - YES : 2 - NO')
      READ(9,*) IDSDPR
C
C
C     VARIOUS VARIABLES ARE NOW INITIALLIZED OR COMPUTED
C
C
  307 MCU=63.54
      MSN=118.69
      MMN=54.95
      MFE=55.85
      NCU=WTCU*1.228
      NSN=WTSN*0.657
      NMN=WTMN*1.419
      NFE=WTFE*1.397
      DEN=7.8E3
      DELTAT=10.0
      TIME=DELTAT
      J=1
      A=3.14159*CD*CD/4.0
      VOL=MM/DEN
      K1=SQRT(8.0*DLIQ*VELS/(3.14159*(CD/2.0)))
      K2=SQRT(1.0/(2.0*3.14159*8.314E3*T))
      K2CU=K2*SQRT(1.0/MCU)
      K2SN=K2*SQRT(1.0/MSN)
      K2MN=K2*SQRT(1.0/MMN)
      K2FE=K2*SQRT(1.0/MFE)
      P0CU=EXP(((-17520/T)-0.5254*ALOG(T)+15.334)*2.303)
      P0SN=EXP(((-15500/T)+10.354)*2.303)
      P0MN=EXP(((-14520/T)-1.311*ALOG(T)+21.364)*2.303)
      P0FE=EXP(((-19710/T)-0.5515*ALOG(T)+15.394)*2.303)
      GAMACU=10.0
      GAMASN=3.0
      GAMAMN=1.0
      GAMAFE=1.0
      ACU=GAMACU*P0CU*MFE/DEN
      ASN=GAMASN*P0SN*MFE/DEN
      AMN=GAMAMN*P0MN*MFE/DEN
      AFE=GAMAFE*P0FE*MFE/DEN
C
C
C     AN INITIAL VALUE OF TOTAL FLUX IS COMPUTED ASSUMMING
C     ZERO GAS PHASE TRANSPORT RESISTANCE
C
C
      F1CU=NCU/((1/K1)+(1/(K2CU*ACU)))
      F1SN=NSN/((1/K1)+(1/(K2SN*ASN)))
      F1MN=NMN/((1/K1)+(1/(K2MN*AMN)))
      F1FE=NFE*K2FE*AFE
      SIGF1=F1CU+F1SN+F1MN+F1FE
      K3=SIGF1/PCH
C
C     LOOP CONTROL PARAMETERS ARE EVALUATED
C
```

```
      ICSTOP=TSTOP/100
      ISTP=DSTOP/100
C
C
C     THE TRUE SIMULATION STARTS ITERATIVELY
C
C
      DO 200 I=1,ICSTOP
      DO 199 L=1,10
C
C     A FLUX FOR EACH SOLUTE IS CALCULATED
C
      FCU=NCU/((1/K1)+(1/(K2CU*ACU))+(1/(K3*ACU)))
      FSN=NSN/((1/K1)+(1/(K2SN*ASN))+(1/(K3*ASN)))
      FMN=NMN/((1/K1)+(1/(K2MN*AMN))+(1/(K3*AMN)))
      FFE=NFE/((1/(K2FE*AFE))+(1/(K3*AFE)))
C
C     USING THE EVALUATED FLUOES THE MELT COMPOSITION
C     AND MASS IS READJUSTED
C
      SIGV=(FCU*MCU+FSN*MSN+FMN*MMN+FFE*MFE)*A*DELTAT/DEN
      SIGF=FCU+FSN+FMN+FFE
      NCU=((NCU*VOL)-(FCU*A*DELTAT))/(VOL-SIGV)
      NSN=((NSN*VOL)-(FSN*A*DELTAT))/(VOL-SIGV)
      NMN=((NMN*VOL)-(FMN*A*DELTAT))/(VOL-SIGV)
      NFE=((NFE*VOL)-(FFE*A*DELTAT))/(VOL-SIGV)
      WTCU=NCU/1.224
      WTSN=NSN/0.657
      WTMN=NMN/1.419
      WTFE=NFE/1.397
      SIGWT=WTCU+WTSN+WTMN+WTFE
      SIGP=ACU*NCU+ASN*NSN+AMN*NMN+AFE*NFE
C
C     A NEW VALUE OF GAS PHASE RESISTANCE IS EVALUATED
C
      K3=SIGF/PCH
      TIME=TIME+DELTAT
  199 CONTINUE
C
C     OUTPUT IS CONTROLLED
C
      IF(IDSDPR.EQ.1.AND.I.GT.1.AND.I.LT.ISTP)GO TO 201
      IF(I.GT.ISTP.AND.I.LT.ICSTOP)GO TO 200
      TM=TIME-10.0
      WRITE(9,1001)TM
      WRITE(9,1000)WTCU,WTSN,WTMN,WTFE
 1000 FORMAT(8E12.3)
 1001 FORMAT('0',F10.0,F10.2,E12.2)
  201 IF(I.GT.ISTP)GO TO 202
C
C     RESULTS OF SIMULATION ARE STORED FOR EVALUATION OF
C     RATE CONSTANTS AND REGRESSION COEFFICIENTS
C
      CU(I)=WTCU
      SN(I)=WTSN
      MN(I)=WTMN
```

```
      TI(I)=TIME-10.0
  202 IF(I.LT.ICSTOP)GO TO 200
      CUFIN=WTCU
      SNFIN=WTSN
      MNFIN=WTMN
  200 CONTINUE
C
C     RESULTS ARE CONVERTED TO LOGS AND REGRESSION FOLLOWS
C
      DO 50 I=1,ISTP
      CU(I)=ALOG(CU(I))
      SN(I)=ALOG(SN(I))
      MN(I)=ALOG(MN(I))
   50 CONTINUE
C
C     REGRESSION VARIABLES ARE INITIALIZED
C
      SX=0.0
      SXCU=0.0
      SXSN=0.0
      SXMN=0.0
      SXYCU=0.0
      SXYSN=0.0
      SXYMN=0.0
      SXXCU=0.0
      SXXSN=0.0
      SXXMN=0.0
      SYY=0.0
      SY=0.0
C
C
C     REGRESSION OF RESULTS TO EVALUATE RATE CONSTANTS
C
C
  203 DO 500 I=1,ISTP
      SXYCU=SXYCU+CU(I)*TI(I)
      SXYSN=SXYSN+SN(I)*TI(I)
      SXYMN=SXYMN+MN(I)*TI(I)
      SXCU=SXCU+CU(I)
      SXSN=SXSN+SN(I)
      SXMN=SXMN+MN(I)
      SXXCU=SXXCU+CU(I)*CU(I)
      SXXSN=SXXSN+SN(I)*SN(I)
      SXXMN=SXXMN+MN(I)*MN(I)
      SY=SY+TI(I)
      SYY=SYY+(TI(I)*TI(I))
  500 CONTINUE
      TOPCU=SXYCU-(SXCU*SY/ISTP)
      TOPSN=SXYSN-(SXSN*SY/ISTP)
      TOPMN=SXYMN-(SXMN*SY/ISTP)
      BOT=SYY-(SY*SY/ISTP)
      BOTCU=SXXCU-(SXCU*SXCU/ISTP)
      BOTSN=SXXSN-(SXSN*SXSN/ISTP)
      BOTMN=SXXMN-(SXMN*SXMN/ISTP)
      CUK=TOPCU*VOL/(BOT*A)
      SNK=TOPSN*VOL/(BOT*A)
```

```
      MNK=TOPMN*VOL/(BOT*A)
      WRITE(9,1996)
 1996 FORMAT('0','    KCU          KSN          KMN')
      WRITE(9,1000)CUK,SNK,MNK
 1999 FORMAT('0',8E12.3)
C
C     REGRESSION COEFFICIENTS ARE EVALUATED
C
      RCU=SQRT((TOPCU*TOPCU)/(BOT*BOTCU))
      RSN=SQRT((TOPSN*TOPSN)/(BOT*BOTSN))
      RMN=SQRT((TOPMN*TOPMN)/(BOT*BOTMN))
      WRITE(9,1995)
 1995 FORMAT('0',' REGRESSION COEFFICIENTS')
      WRITE(9,1997)RCU,RSN,RMN
 1997 FORMAT(8E12.4)
C
C     A SECOND REGRESSION IS PERFORMED
C
      IF(J.EQ.2)GO TO 2000
      J=J+1
C
C     NEW REGRESSION VALUES ARE STORED IN THE COMPOSITION ARRAYS
C
      DO 501 I=1,ISTP
      CU(I)=ALOG(EXP(CU(I))-CUFIN)
      SN(I)=ALOG(EXP(SN(I))-SNFIN)
      MN(I)=ALOG(EXP(MN(I))-MNFIN)
  501 CONTINUE
      GO TO 50
C
C
C     MORE CALCULATION IS REQUESTED AND THE INPUT FORMAT IS
C     REQUESTED
C
C
 2000 WRITE(9,2001)
 2001 FORMAT('0',' MORE CALCULATION ? 1 - YES : 2 - NO')
      READ(9,*)CAL
      IF(CAL.EQ.2)STOP
      WRITE(9,2002)
 2002 FORMAT('0',' ABBREVIATED PROMPTING ? 1 - YES ; 2 - NO')
      READ(9,*)AP
      IF(AP.EQ.1)GO TO 3000
      GO TO 1
C
C     THE MODIFIED FORM OF THE DATA INPUT FOLLOWS
C
 3000 WRITE(9,3001)
 3001 FORMAT(' DIFF. COEFF? : SURF VEL ')
      READ(9,*)DLIQ,VELS
      WRITE(9,3002)
 3002 FORMAT(' MELT T, MASS, DIAM. ?')
      READ(9,*)T,MM,CD
      WRITE(9,3005)
 3005 FORMAT(' PRESS. ?')
      READ(9,*)PCH
```

```
      WRITE(9,3003)
3003  FORMAT(' MELT COMP. ?')
      READ(9,*)WTCU,WTSN,WTMN,WTFE
      WRITE(9,3004)
3004  FORMAT(' CALC. STOP TIME : DISP. STOP TIME ?')
      READ(9,*)TSTOP,DSTOP
      WRITE(9,3006)
3006  FORMAT(' DISPLAY DEPRESSED ?')
      READ(9,*)IDSDPR
      GO TO 307
      END
```

APPENDIX TWO

The following is a list of equipment, materials and their associated manafacturers and suppliers.

Furnace: 150 kW, 3000 hz, 'Tocco' induction furnace: coil diameter, 35 cm; maximum capacity, 180 kg steel. Manufactured by Inductotherm Inc., Rancocas, N.J. Supplied by Deltec Systems Inc., Primrose, PA. (Bankrupt).

Power Supply: Motor generator: 3000 hz, 150 kW, 800 V, 188 A. Manufactured by Reliance Electrical, Cleveland, Ohio. Supplied by Deltec Systems Inc.

Vacuum Chamber: Cylindrical; volume, 2.25 m3; dimensions, 1.5 m in diameter x 1.8 m in length. Manufactured and supplied by Deltec Systems Inc.

Pumping System: two stages:

a) Stokes mechanical pump (nominal capacity, 0.142 m3 s-1)

b) Roots Blower (nominal capacity, 0.614 m3.s-1). The blower could only be activated at manifold pressures below 2.7 x 10**3 pascal.

Supplied by Deltec Systems Inc.

Pressure Measuring Devices:

a) Standard 'McLeod' gauge, 0 to 270 pascal.

Supplied by Fischer Scientific Co., Montreal, Quebec.

Temperature Measuring Devices:

a) Pt/Pt-13% Rh 'Dip-Tip Type R' thermocouples mounted on the temperature measurement probe. Manufactured and supplied by Leeds and Northrup, Elliport, PA.

b) digital voltmeter, 0 to 200 mV range; 10 mV accuracy. Manufactured and supplied by John Fluke Mfg. Co. Inc., Mississauga, Ontario.

Crucibles: 'Hycor Alumina', nominal composition, wt.%:

Al_2O_3	88.3	TiO_2	0.10
SiO_2	11.2	K_2O	0.03
Fe_2O_3	0.15	MgO	0.03
NaO_2	0.12	CaO	0.02

Manafactured ans supplied by Engineered Ceramics, Gilliberts, Illinios.

Locam Hispeed Camera: Model 50. Supplied by Photographic Analysis Ltd., Toronto, Ontario.

Perkin Elmer Flame Atomic Absorption Spectrometer. Manufactured and supplied by Perkin Elmer, Norwalk, Connecticut.

Baird Atomic Vacuum Spark Atomic Absorption Spectrometer. Manufactured and supplied by Baird Atomic, Boston, Mass.

Steel: 6 m x 4 cm x 4 cm; hot rolled bar; A36 grade. Supplier analysis: C 0.17; Mn 0,72; S 0.03; Si 0.039; P 0.016. Steel supplied by A.E. Leslie, Montreal, Quebec.

Steel: Scrap off-cuts from Dept. of Metallurgical Engineering Workshop, McGill University, Montreal, Quebec.

Copper: Electrolytic tough pitch copper off-cuts. Copper supplied by Noranda Mines Ltd., Pointe Claire, Quebec.

Aluminium: Commercial grade ingots (2S grade). Aluminium supplied by Alcan Limited, Montreal, Quebec.

Graphite: Commercial grade graphite rod, machined to specification. Graphite supplied by Union Carbide Ltd., Lachine, Quebec.

Gas: Commerical grade argon in cylinders; capacity 7 m3, 298 K, 1 atm. Gas supplied by Welding Products Ltd., Montreal, Quebec.

APPENDIX THREE

RATE CONSTANTS

A pseudo rate constant may be evaluated for experimentally measured vacuum distillation data by assuming that, for the time the melt composition was measured, the proportionality constant in Equation 3.22 is constant with respect to time, ie.,

$$n''_i = K_i \cdot n'''_{i,b} \qquad \text{.... A.1}$$

where, K_i is constant with respect to time.

Equation A.1 can then be rearranged and integrated to yeild:

$$\ln\left[\frac{n'''_{i,final}}{n'''_{i,initial}}\right] = K_i \cdot \frac{A}{V} \cdot t \qquad \text{.... A.2}$$

where, A/V is the area to volume ratio of the melt.

Equation A.2 shows that K_i can be determined from the slope of the best fitting straight line plotted through the natural logarithm of melt composition versus time.